

EFFICIENT AND ACCURATE NUMERICAL METHODS FOR TWO CLASSES
OF PDES WITH APPLICATIONS TO QUASICRYSTALS

A Dissertation

Submitted to the Faculty

of

Purdue University

by

Duo Cao

In Partial Fulfillment of the

Requirements for the Degree

of

Doctor of Philosophy

May 2020

Purdue University

West Lafayette, Indiana

THE PURDUE UNIVERSITY GRADUATE SCHOOL
STATEMENT OF DISSERTATION APPROVAL

Dr. Jie Shen, Chair

Department of Mathematics

Dr. Min Chen

Department of Mathematics

Dr. Guang Lin

Department of Mathematics

Dr. Suchuan Dong

Department of Mathematics

Approved by:

Dr. Plamen Stefanov

Associate Head of the Department Graduate Program

I dedicate this dissertation, to my beloved family for their unconditional support.

ACKNOWLEDGMENTS

I would like to express the deepest gratitude to my Ph.D. advisor Professor Jie Shen for his kind and patient academic guidance. His broad knowledge, unconditionally supports and ubiquitous encouragement greatly enlighten my path to the degree and the subject. He guides me how to approach a problem, how to think like a researcher and how to deal with a complicated mathematics question. It has been a great honor and a privilege for me to become one of his students.

Next, I owe my sincere thanks to my other committee member Prof. Guang Lin, Prof. Min Chen and Prof. Steven Dong for the time and patience reading and commenting on my manuscript of this thesis. I would also like to thank Prof. Jie Xu at the Laboratory of Scientific and Engineering Computing, Dr. Changtao Sheng, Dr. Sheng Chen, Dr. Yingwei Wang, Dr. Yiqi Gu and Prof. Leevan Ling at Hong Kong Baptist University who offered great help and advice on my thesis.

In addition, there are many friends of mine that make my six years at Purdue University colorful, but I will only mention Shiwei Liu, Xinyu Liu, Lingfei Li, Jimmy Vogel, Zeyu Zhang for sharing this wonderful time with me.

Finally, at this point, I would like to thank my parents for their continuous support spiritually and materially. Without their education and help, this work could never be possible.

TABLE OF CONTENTS

	Page
LIST OF FIGURES	vii
ABSTRACT	ix
1 EFFICIENT SPECTRAL METHODS FOR PDES WITH FRACTIONAL LAPLACIAN	1
1.1 Introduction	1
1.2 Algorithms	4
1.2.1 Fourier-like basis functions	5
1.2.2 Spectral method for fractional Laplacian equation	7
1.2.3 Space-time spectral method	8
1.3 Error analysis	10
1.3.1 Approximation of fractional Laplacian	10
1.3.2 Error bounds for (1.17)	15
1.3.3 Error bounds for (1.25)	18
1.4 Numerical results for linear fractional equations	22
1.5 Application to nonlinear fractional equations	26
1.5.1 Fractional FitzHugh-Nagumo model	27
1.5.2 Fractional Allen-Cahn equation	29
1.6 Stochastic pde with fractional laplacian	33
1.6.1 Formulation	33
1.6.2 Numerical Examples	35
1.7 Conclusion	35
2 EFFICIENT NUMERICAL SCHEME FOR COMPUTING STABILITY OF QUASI-CRYSTALLINE INTERFACE	38
2.1 Introduction	38
2.2 Model and numerical algorithms	42
2.2.1 Lifshitz–Petrich model and quasicrystal solutions	42
2.2.2 General setting for the interface system	45
2.2.3 SAV approach	50
2.2.4 Spatial discretization	52
2.2.5 Discretization in the x -direction	56
2.2.6 Outline of the numerical method	59
2.3 Numerical simulations	60
2.3.1 Dirichlet boundary condition	60
2.3.2 Periodic boundary condition	67

	Page
2.4 Conclusion	78
REFERENCES	87

LIST OF FIGURES

Figure	Page
1.1 (a). $H^{\frac{\alpha}{2}}$ -error in semi-log scale of (1.1) with $u(x) = \varphi_k(x)$; (b). $H^{\frac{\alpha}{2}}$ -error in semi-log scale of (1.1) with $u(x, y) = \varphi_k(x)\varphi_k(y)$	23
1.2 (a). $H^{\frac{\alpha}{2}}$ -error, in log-log scale, of our method for (1.1) with right hand side term $f(x) = 1$; (b). $H^{\frac{\alpha}{2}}$ -error, in log-log scale, of Fourier spectral method in [1] for (1.1) with right hand side term $f(x) = 1$	24
1.3 L^2 -error, in log-log scale, of our method for (1.1) with right hand side term $f(x) = 1$	24
1.4 Numerical solution of fractional heat equation (1.71) for different α : (a) initial data: $e^{-25x^2/(1-x^2)}$; (b) initial data: $\tanh(25x/\sqrt{1-x^2})$	25
1.5 L^2 -error for (1.71) at $T = 0.1$ for different α ; (a) initial data $u_0 = e^{-25x^2/(1-x^2)}$; (b). initial data $u_0 = \tanh(25x/\sqrt{1-x^2})$	26
1.6 Spiral wave in FitzHugh-Nagumo model for various α and K_u ; top: $K_u = 10^{-4}$; bottom: $\alpha = 1.7$	28
1.7 Solution transitions in Allen-Cahn equation with $t \in [0, 3000]$ for various α	30
1.8 Initial transition of the Allen-Cahn equation with $t \in [0, 10]$	30
1.9 (a) Interfacial layers with different α ; (b) Layer width L against ϵ for different values of α	31
1.10 Evolution of solution of fractional Allen-Cahn equation with initial condition (1.77) for various fractional order α	32
1.11 Temporal evolution of circular domain for various α	34
1.12 Radius of the circular domain as a function of time obtained with different fractional order α using time step $\Delta t = 0.5$	34
1.13 Stochastic solution of fractional PDE	36
2.1 Three patterns formed under LP model.	46
2.2 Setting of the interface problem	47
2.3 Laminar flow interface steady state with small and big rotation angle θ	62
2.4 Interfacial transition and energy dissipation of two crystals with $\theta = \arctan \frac{\sqrt{3}}{4}$	64

Figure	Page
2.5 Interfacial transition with various θ	65
2.6 Interfacial transition with big-small crystals	66
2.7 Quasicrystal interfacial transition with $\theta = \arctan\frac{\sqrt{3}}{4}$	68
2.8 Crystal-Quasicrystal interfacial transition and energy dissipation.	69
2.9 6-fold symmetry crystal equilibrium state	70
2.10 12-fold and 10-fold symmetry quasicrystal phases	71
2.11 Order parameters obtained from minimization of free energy model	74
2.12 Modified non-local model steady state with different σ	75
2.13 Energy dissipation plots of non-local model	76
2.14 Interface problem for 6-fold symmetry crystal	77
2.15 Interface problem for 12-fold symmetry	79
2.16 Interface problem for 10-fold symmetry	80
2.17 Interface problem for 6-fold symmetry with big-small crystals	81
2.18 Interface problem for 12-fold symmetry under Multi-phase model	82
2.19 Interface problem for 10-fold symmetry under Multi-phase model	83
2.20 Interface problem for 12-fold symmetry in non-local model	84
2.21 Interface problem for 10-fold symmetry in non-local model	85

ABSTRACT

Cao Duo Ph.D., Purdue University, May 2020. Efficient and Accurate Numerical Methods for Two Classes of PDEs With Applications to Quasicrystals. Major Professor: Jie Shen Professor.

This dissertation is a summary of the graduate study in the past few years. In first part, we develop efficient spectral methods for the spectral fractional Laplacian equation and parabolic PDEs with spectral fractional Laplacian on rectangular domains. The key idea is to construct eigenfunctions of discrete Laplacian (also referred to Fourier-like basis) by using the Fourierization method. Under this basis, the non-local fractional Laplacian operator can be trivially evaluated, leading to very efficient algorithms for PDEs involving spectral fractional Laplacian. We provide a rigorous error analysis for the proposed methods, as well as ample numerical results to show their effectiveness.

In second part, we propose a method suitable for the computation of quasiperiodic interface, and apply it to simulate the interface between ordered phases in Lifschitz–Petrich model, which can be quasiperiodic. The function space, initial and boundary conditions are carefully chosen such that it fix the relative orientation and displacement, and we follow a gradient flow to let the interface find its optimal structure. The gradient flow is discretized by the scalar auxiliary variable (SAV) approach in time, and spectral method in space using quasiperiodic Fourier series and generalized Jacobi polynomials. We use the method to study interface between striped, hexagonal and dodecagonal phases, especially when the interface is quasiperiodic. The numerical examples show that our method is efficient and accurate to successfully capture the interfacial structure.

1. EFFICIENT SPECTRAL METHODS FOR PDES WITH FRACTIONAL LAPLACIAN

1.1 Introduction

We consider in this part numerical approximation of the spectral fractional Laplacian equation

$$(-\Delta)^{\frac{\alpha}{2}}v = f, \quad \forall \mathbf{x} \in \Omega, \quad (1.1)$$

with suitable boundary conditions, and parabolic PDEs with spectral fractional Laplacian:

$$v_t + \epsilon(-\Delta)^{\frac{\alpha}{2}}v + \mathcal{N}(v, t) = 0, \quad \forall(\mathbf{x}, t) \in D := \Omega \times (0, T], \quad (1.2)$$

with suitable initial and boundary conditions. In the above, Ω is a bounded domain, $(-\Delta)^{\frac{\alpha}{2}}$ is the spectral fractional Laplacian operator defined by the spectral decomposition

$$(-\Delta)^{\frac{\alpha}{2}}u(\mathbf{x}) = \sum_n \tilde{u}_n \lambda_n^{\frac{\alpha}{2}} \phi_n(\mathbf{x}), \quad \alpha \in (0, 2), \quad (1.3)$$

where $\{\lambda_n, \phi_n\}_{n \geq 0}$ are the eigenvalues and eigenfunctions of the Laplace operator $-\Delta$ with given Dirichlet boundary conditions.

Approximation of spectral fractional Laplacian (1.3) has been the subject of many investigations recently. For problems with periodic boundary conditions, it is natural and effective to use Fourier spectral methods e.g., [1–3]. For non-periodic boundary conditions, there are essentially four different approaches:

- Use space spanned by eigenfunctions of Laplacian operator as approximation space. An one-dimensional example is considered in [4]. However, since the eigenfunctions of Laplacian, $\sin c_k x$ or $\cos c_k x$, have very poor approximation properties for non-periodic functions, the convergence of such method is very slow, even if the solution is smooth.

- Use space spanned by eigenfunctions of discrete Laplacian operator as approximation space. In [5], a spectral-element method is used to construct discrete eigenfunctions which are then used to approximate the fractional Laplacian operator.
- Use the Caffarelli-Silvestre extension [6,7]. This approach was first considered in [8] using a finite-element method followed by extension to space-time parabolic fractional PDEs in [9] and improvements with tensor product finite elements and adaptivity in [10]. A spectral method for the extended problem is presented in [11]. A different approach using the Caffarelli-Silvestre extension is given in [12].
- Use the Dunford-Taylor formula. This formula can be viewed as a semi-analytic solution of the Caffarelli-Silvestre extension in which the extended direction is analytically represented by an integral formula. This approach was first adopted in [13] with a finite-element method in space.

For more detailed presentation on numerical methods for fractional Laplacians (in spectral form and integral form) and up-to-date references, we refer to two excellent recent review papers [14, 15].

In this part, we focus on the numerical approximation of spectral fractional Laplacian (1.3) with non-periodic boundary conditions. We adopt the second approach. More precisely, we use space spanned by eigenfunctions of **discrete** Laplacian operator where the discretization is done by a Legendre-Galerkin method [16].

It is well-known that only a portion of the discrete eigenpairs are good approximation of the corresponding exact eigenpairs, so a main question in using the second approach is whether to use all discrete eigenpairs or only those who are good approximations of the exact ones. Numerical results in [5] indicated that better results can be obtained by using all discrete eigenpairs, but no theoretical justification is available on why spurious discrete eigenpairs should be included in the approximation space.

A main purpose of this paper is to provide a theoretical justification by carrying out a delicate error analysis.

A main bottleneck in using the second approach is that computing and storing all discrete eigenpairs in multidomains is usually prohibitively expensive. So another purpose of this paper is to develop a robust and efficient method to compute discrete eigenpairs. To this end, we restrict our attention in this paper to rectangular domains, with the expectation that the method developed here can be extended to more generally domain using the recently developed novel spectral methods for complex domains in [17]. Following the idea in [18], we construct eigenfunctions of **discrete** Laplacian operator in the Legendre-Galerkin formulation using the so called Fourier-like basis functions. The benefits of such choice are significant: the construction of Fourier-like basis functions only involves finding all the eigenpairs of a symmetric positive definite penta-diagonal matrix, and thanks to the orthonormality of the Fourier-like basis functions in the underlying inner products, the linear system for approximating (1.1) is diagonal so its solution can be obtained very efficiently.

We also construct a space-time spectral method for (1.2) by using the approximation based on the discrete eigenpairs in space and a dual-Petrov Galerkin method in time. For linear parabolic systems, this method leads to a sequence of one-dimensional tridiagonal systems that can be easily solved, and nonlinear parabolic systems can also be solved very efficiently with a preconditioned iterative procedure using a suitable linear parabolic system as a preconditioner.

We highlight below the main advantages of the proposed methods and main contributions of the paper:

- Accuracy: the space spanned by the eigenfunctions of **discrete** Laplacian operator with Legendre-Galerkin method has excellent approximation properties: it leads to exponential convergence for smooth functions, and can double the convergence rate of finite-element methods for problems with corner singularities which are present in problems with spectral fractional Laplacian.

- Efficiency: Unlike the approaches based on the Caffarelli-Silvestre extension and Dunford-Taylor formula which involve an extra-dimension, the presence of the nonlocal fractional Laplacian operator does not introduce any additional computational complexity so the cost of our proposed methods are essentially the same as the very efficient spectral-Galerkin method for the Poisson type equations [16] and dual-Petrov Galerkin method for parabolic type equations [18].
- We derived error bounds between the discrete fractional Laplacian $(-\Delta_M)^{\frac{\alpha}{2}}$ and the fractional Laplacian $(-\Delta)^{\frac{\alpha}{2}}$, which in particular justifies the use of all discrete eigenfunctions. This approach (results in Section 3.1) can also be used to other discretization methods such as finite differences and finite-elements.
- We established error analysis of our proposed methods for fractional Laplacian equation and linear fractional reaction-diffusion equation.

The rest of the paper is organized as follows. In the next section, we construct the Fourier-like basis functions as the discrete eigenfunctions of fractional Laplacian operator. In Section 3, we provide a complete error analysis of the proposed methods for fractional Poisson equation and fractional PDE. Numerical experiments for boundary value problem involving spectral fractional Laplacian are carried out in Section 4. In Section 5 we develop efficient methods for space fractional reaction-diffusion equations. Some concluding remarks are given in the last section.

1.2 Algorithms

We construct below the Fourier-like basis functions which are the eigenfunctions of discrete fractional Laplacian, and present spectral algorithms for fractional Laplacian equation and a space-time spectral method for linear parabolic PDEs with spectral fractional Laplacian on rectangular domains.

Let us first introduce some notations.

- Let \mathbb{R} (resp. \mathbb{N}) be the set of all real numbers (resp. non-negative integers), and let $\mathbb{N}_0 = \mathbb{N} \cup \{0\}$.
- We use boldface lowercase letters to denote d -dimensional multi-indexes, vectors and multi-variables, e.g., $\mathbf{j} = (j_1, \dots, j_d)$, $\mathbf{k} = (k_1, \dots, k_d)$ and $\mathbf{x} = (x_1, \dots, x_d)$. Also, let $\mathbf{1} = (1, 1, \dots, 1) \in \mathbb{N}^d$, $e_i = (0, \dots, 1, \dots, 0)$ be the i -th unit vector in \mathbb{R}^d , and use the following conventions

$$\boldsymbol{\alpha} \geq \mathbf{k} \Leftrightarrow \forall_{1 \leq j \leq d}, \alpha_j \geq k_j.$$

- Denote by $|\boldsymbol{\xi}|_1, |\boldsymbol{\xi}|_2, |\boldsymbol{\xi}|_\infty$ be the l^1, l^2, l^∞ norm of $\boldsymbol{\xi}$ in \mathbb{R}^d , respectively.

1.2.1 Fourier-like basis functions

We consider the following general homogeneous boundary conditions:

$$a_j^\pm v(\pm 1) + b_j^\pm v_x(\pm 1) = 0 \quad 1 \leq j \leq d. \quad (1.4)$$

To ensure the well-posedness, we assume that for any $0 \leq j \leq d$, the constants a_j^\pm and b_j^\pm satisfy the following conditions

$$(i) a_j^\pm \geq 0; \quad (ii) (a_j^-)^2 + b_j^- \neq 0, a_j^- b_j^- \leq 0; \quad (iii) (a_j^+)^2 + b_j^+ \neq 0, a_j^+ b_j^+ \geq 0. \quad (1.5)$$

We first define the one-dimensional spatial approximation space as

$$V_M = \{v \in \mathcal{P}_M : a_\pm v(\pm 1) + b_\pm v_x(\pm 1) = 0\}, \quad (1.6)$$

and denote

$$h_k(x) = L_k(x) + a_k L_{k+1}(x) + b_k L_{k+2}(x), \quad 0 \leq k \leq M-2, \quad (1.7)$$

where $L_k(x)$ is the Legendre polynomial of degree k . It is shown in [19] that, for boundary conditions in form of (1.4), there exists a unique set $\{a_k, b_k\}$ such that $h_k \in V_{k+2}$.

We recall below the construction of the Fourier-like basis functions [18]. Denote by \mathbf{M} (with entries $m_{pq} = (h_p, h_q)$) and \mathbf{S} (with entries $s_{pq} = -(h_p'', h_q)$) be the mass matrix and stiffness matrix, respectively. Let $\mathbf{E} := (e_{pq})_{p,q=0,\dots,M-2}$ be the matrix formed by the orthonormal eigenvectors of generalized eigenvalue problem of \mathbf{M} and \mathbf{S} , and $\mathbf{\Lambda} = \text{diag}(\lambda_{M,i})$ be the diagonal matrix with main diagonal being the corresponding eigenvalues, i.e.,

$$\mathbf{S}\mathbf{E} = \mathbf{M}\mathbf{E}\mathbf{\Lambda}, \quad \mathbf{E}^T\mathbf{S}\mathbf{E} = \mathbf{\Lambda}, \quad \mathbf{E}^T\mathbf{M}\mathbf{E} = \mathbf{I}_{M-1}. \quad (1.8)$$

Then, the Fourier-like basis is given by

$$\phi_{M,n}(x) = \sum_{j=0}^{M-2} e_{jn} h_j(x), \quad 0 \leq n \leq M-2. \quad (1.9)$$

Thank to (1.8), it is easy to verify that

$$\begin{aligned} (\phi_{M,p}, \phi_{M,q}) &= \sum_{k,j=0}^{M-2} e_{kp} e_{jq} (h_k, h_j) = \sum_{k,j=0}^{M-2} e_{jq} m_{jk} e_{kp} = (\mathbf{E}^T \mathbf{M} \mathbf{E})_{pq} = \delta_{pq}, \\ (-\Delta \phi_{M,p}, \phi_{M,q}) &= - \sum_{k,j=0}^{M-2} e_{kp} e_{jq} (h_k'', h_j) = \sum_{k,j=0}^{M-2} e_{jq} s_{jk} e_{kp} = (\mathbf{E}^T \mathbf{S} \mathbf{E})_{pq} = \lambda_{M,q} \delta_{pq}. \end{aligned} \quad (1.10)$$

Let us define d -dimensional tensorial eigenfunctions and eigenvalues

$$\phi_{M,\mathbf{n}}(\mathbf{x}) = \prod_{j=1}^d \phi_{M,n_j}(x_j), \quad \mathbf{x} \in \Omega := (-1, 1)^d, \quad \text{and} \quad \boldsymbol{\lambda}_{M,\mathbf{n}} = (\lambda_{M,n_1}, \dots, \lambda_{M,n_d})^T,$$

and the d -dimensional approximation space

$$V_M^d := \text{span}\{\phi_{M,\mathbf{n}}(\mathbf{x}) : \mathbf{n} \in \Upsilon_M, \mathbf{x} \in \Omega\}, \quad (1.11)$$

where the index set

$$\Upsilon_M := \{n = (n_1, \dots, n_d) : 0 \leq n_j \leq M-2, 1 \leq j \leq d\}. \quad (1.12)$$

One verifies by using (1.10) that

$$(\phi_{M,\mathbf{n}}, \phi_{M,\mathbf{m}}) = \delta_{\mathbf{m}\mathbf{n}}, \quad (-\Delta \phi_{M,\mathbf{n}}, \phi_{M,\mathbf{m}}) = |\boldsymbol{\lambda}_{M,\mathbf{n}}|_1 \delta_{\mathbf{m}\mathbf{n}}, \quad (1.13)$$

where $\mathbf{m}, \mathbf{n} \in \Upsilon_M$ and

$$\delta_{mn} = \prod_{j=0}^d \delta_{m_j n_j}, \quad |\boldsymbol{\lambda}_{M,\mathbf{n}}|_1 = \lambda_{M,n_1} + \cdots + \lambda_{M,n_d}. \quad (1.14)$$

Indeed, the discrete Laplacian operator $-\Delta_M : V_M^d \rightarrow V_M^d$ can be interpreted as $-\Delta|_{V_M^d}$, which satisfies

$$\langle -\Delta_M \boldsymbol{\phi}_{M,\mathbf{n}}, \boldsymbol{\phi}_{M,\mathbf{m}} \rangle = -(\Delta \boldsymbol{\phi}_{M,\mathbf{n}}, \boldsymbol{\phi}_{M,\mathbf{m}}) = |\boldsymbol{\lambda}_{M,\mathbf{n}}|_1 \delta_{mn}, \quad \forall \boldsymbol{\phi}_{M,\mathbf{n}}, \boldsymbol{\phi}_{M,\mathbf{m}} \in V_M^d.$$

Then, we arrive at following definition of discrete spectral fractional Laplacian.

Definition 1.2.1 Let $\{\boldsymbol{\lambda}_{M,\mathbf{n}}, \boldsymbol{\phi}_{M,\mathbf{n}}\}_{\mathbf{n} \in \Upsilon_M}$ be the discrete eigenpairs of the Laplacian operator $-\Delta_M$ on V_M^d . For any $u \in \mathcal{D}(-\Delta)$, the discrete spectral fractional Laplacian is given by

$$(-\Delta_M)^{\frac{\alpha}{2}} \Pi_M u(x) = \sum_{\mathbf{n} \in \Upsilon_M} \tilde{u}_{\mathbf{n}} |\boldsymbol{\lambda}_{M,\mathbf{n}}|_1^{\frac{\alpha}{2}} \boldsymbol{\phi}_{M,\mathbf{n}}(\mathbf{x}). \quad (1.15)$$

where $\Pi_M : \mathcal{D}(-\Delta) \rightarrow V_M^d$ denote the orthogonal projection. Moreover, for any $u_M \in V_M^d$, namely, $u_M(x) = \sum_{\mathbf{n} \in \Upsilon_M} \tilde{u}_{\mathbf{n}} \boldsymbol{\phi}_{M,\mathbf{n}}(\mathbf{x})$, the spectral fractional Laplacian is given by

$$(-\Delta_M)^{\frac{\alpha}{2}} u_M(x) = \sum_{\mathbf{n} \in \Upsilon_M} \tilde{u}_{\mathbf{n}} |\boldsymbol{\lambda}_{M,\mathbf{n}}|_1^{\frac{\alpha}{2}} \boldsymbol{\phi}_{M,\mathbf{n}}(\mathbf{x}). \quad (1.16)$$

1.2.2 Spectral method for fractional Laplacian equation

We consider (1.1) with (1.4). Then, our spectral Galerkin method using the Fourier-like basis functions is as follows:

Find $u_M \in V_M^d$ such that

$$((-\Delta_M)^{\frac{\alpha}{2}} u_M, v)_{\Omega} = (f, v)_{\Omega} \quad \forall v \in V_M^d. \quad (1.17)$$

We write

$$u_M(\mathbf{x}) = \sum_{\mathbf{m} \in \Upsilon_M} \tilde{u}_{\mathbf{m}} \boldsymbol{\phi}_{M,\mathbf{m}}(\mathbf{x}). \quad (1.18)$$

Substituting (1.18) into (1.17) and taking $v = \boldsymbol{\phi}_{M,\mathbf{n}}(\mathbf{x})$, the scheme (1.25) becomes

$$\sum_{\mathbf{m} \in \Upsilon_M} \tilde{u}_{\mathbf{m}} ((-\Delta_M)^{\frac{\alpha}{2}} \boldsymbol{\phi}_{M,\mathbf{m}}, \boldsymbol{\phi}_{M,\mathbf{n}})_{\Omega} = (f, \boldsymbol{\phi}_{M,\mathbf{n}})_{\Omega}. \quad (1.19)$$

By the orthogonality (1.13) and (1.16), we obtain

$$\tilde{u}_{\mathbf{n}} = |\lambda_{M,\mathbf{n}}|^{-\frac{\alpha}{2}} \tilde{f}_{\mathbf{n}}, \quad \forall \mathbf{n} \in \Upsilon_M,$$

where

$$\tilde{f}_{\mathbf{n}} = (f, \phi_{M,\mathbf{n}})_{\Omega}.$$

Finally, the numerical solutions of (1.17) can be obtained from (1.18).

1.2.3 Space-time spectral method

We shall start by considering a special case of (1.2) with $\mathcal{N}v = \beta v - g$:

$$v_t + \epsilon(-\Delta)^{\frac{\alpha}{2}}v + \beta v = g, \quad \forall (\mathbf{x}, t) \in D = \Omega \times (0, T], \quad (1.20)$$

with the initial condition $v(\mathbf{x}, 0) = u_0(\mathbf{x})$ and boundary conditions (1.4). We shall extend the algorithm to the general case of (1.2) in Section 5.

We propose below a space-time spectral method for (1.20) based on the Fourier-like basis in space and a dual-Petrov Legendre-Galerkin formulation in time.

We first decompose the solution $v(\mathbf{x}, t)$ into two parts as

$$v(\mathbf{x}, t) = u(\mathbf{x}, t) + u_0(\mathbf{x}), \quad (1.21)$$

with $u(\mathbf{x}, 0) = 0$. Hence, by (1.21), the equation (1.20) is equivalent to the following equation

$$u_t + \epsilon(-\Delta)^{\frac{\alpha}{2}}u + \beta u = f, \quad \forall (\mathbf{x}, t) \in D, \quad (1.22)$$

where

$$f(\mathbf{x}, t) = g(\mathbf{x}, t) - \epsilon(-\Delta)^{\frac{\alpha}{2}}u_0(\mathbf{x}) - \beta u_0(\mathbf{x}),$$

with

$$u(\mathbf{x}, 0) = 0, \quad \forall \mathbf{x} \in \Omega, \quad (1.23)$$

and the boundary conditions (1.4).

Since (1.20) or (1.22) has first order derivative in time, it is suitable to use the dual-Petrov Legendre-Galerkin method in time direction [18, 20]. To simplify the presentation, we first scale the time interval from $(0, T)$ to $(-1, 1)$, and define a pair of “dual” approximation spaces (in time):

$$S_N = \{u \in \mathcal{P}_N : u(-1) = 0\}, \quad S_N^* = \{u \in \mathcal{P}_N : u(1) = 0\}. \quad (1.24)$$

Then, after scaling the time interval to $(-1, 1)$, the space-time spectral approximation of (1.22) is: Find $u_L \in V_M^d \otimes S_N$ such that

$$(\partial_t u_L, v)_D + \epsilon((-\Delta_M)^{\frac{\alpha}{2}} u_L, v)_D + \beta(u_L, v)_D = (f, v)_D, \quad \forall v \in V_M^d \otimes S_N^*. \quad (1.25)$$

We now describe the numerical implementation of (1.25). An obvious choice for V_M^d in space is the Fourier-like basis function $\{\phi_{M,k}\}_{k \in \Upsilon_M}$. As for S_N and S_N^* in time, we set

$$\psi_n(t) = L_n(t) + L_{n+1}(t), \quad \psi_q^*(t) = L_q(t) - L_{q+1}(t), \quad (1.26)$$

and write

$$u_L(\mathbf{x}, t) = \sum_{m \in \Upsilon_M} \sum_{n=0}^{N-1} \tilde{u}_{n,m} \phi_{M,m}(\mathbf{x}) \psi_n(t). \quad (1.27)$$

Substituting (1.27) into (1.25) and taking $v = \phi_{M,p}(\mathbf{x}) \psi_q^*(t)$, the scheme (1.25) becomes

$$\begin{aligned} \sum_{m \in \Upsilon_M} \sum_{n=0}^{N-1} \tilde{u}_{n,m} \left\{ (\phi_{M,m}, \phi_{M,p})_{\Omega} (\partial_t \psi_n, \psi_q^*)_I + \epsilon((-\Delta_M)^{\frac{\alpha}{2}} \phi_{M,m}, \phi_{M,p})_{\Omega} (\psi_n, \psi_q^*)_I \right. \\ \left. + \beta(\phi_{M,m}, \phi_{M,p})_{\Omega} (\psi_n, \psi_q^*)_I \right\} = (f, \phi_{M,p} \psi_q^*)_D. \end{aligned} \quad (1.28)$$

Denote

$$\begin{aligned} u_{\mathbf{m}} &= (\tilde{u}_{0,\mathbf{m}}, \tilde{u}_{1,\mathbf{m}}, \dots, \tilde{u}_{N-1,\mathbf{m}})^T, \\ s_{qn}^t &= (\partial_t \psi_n, \psi_q^*)_I, \quad m_{qn}^t = (\psi_j, \psi_i^*)_I, \\ \mathbf{S}^t &= (s_{qn}^t)_{0 \leq q, n \leq N-1}, \quad \mathbf{M}^t = (m_{qn}^t)_{0 \leq q, n \leq N-1}, \\ \tilde{f}_{q,p} &= (f, \phi_{M,p} \psi_q^*)_D, \quad \mathbf{f}_{\mathbf{m}} = (\tilde{f}_{0,\mathbf{m}}, \tilde{f}_{1,\mathbf{m}}, \dots, \tilde{f}_{N-1,\mathbf{m}})^T. \end{aligned} \quad (1.29)$$

One may verify that [18]

$$s_{qn}^t = (\partial_t \psi_n, \psi_q^*) = 2\delta_{qn}, \quad m_{qn}^t = (\psi_n, \psi_q^*) = 0, \quad \text{if } |q - n| > 1. \quad (1.30)$$

Then, from (1.29) and (1.30), we find that (1.25) is equivalent to the following

$$(2\mathbf{I} + (\epsilon|\lambda_{M,m}|^{\frac{\alpha}{2}} + \beta)\mathbf{M}^t)u_m = \mathbf{f}_m, \quad \mathbf{m} \in \Upsilon_M. \quad (1.31)$$

Since \mathbf{M}^t is tri-diagonal, the above systems can be efficiently solved.

Finally, we obtain the numerical solutions of (1.25) by (1.27).

1.3 Error analysis

The aim of this section is to perform error analysis for the two spectral algorithms (1.17) and (1.25) described in the previous section. For the sake of brevity, we shall restrict ourselves to the cases with homogeneous Dirichlet boundary conditions.

Throughout this section, we assume that $\alpha \in (0, 2)$, $s = \frac{\alpha}{2}$ and $\alpha \neq 1$.

1.3.1 Approximation of fractional Laplacian

We first recall some results in [21], which play a very important role in the forthcoming analysis.

Definition 1.3.1 (see, e.g., [21, Appendix]) *Let $(\mathcal{X}, \|\cdot\|_X)$ and $(\mathcal{Y}, \|\cdot\|_Y)$ be two Banach spaces. A linear operator $A : \mathcal{D}(A) \subset \mathcal{X} \rightarrow \mathcal{Y}$ with operator norm*

$$\|A\|_{\mathcal{L}(\mathcal{X}, \mathcal{Y})} = \sup_{0 \neq x \in \mathcal{X}} \frac{\|Ax\|_Y}{\|x\|_X}$$

is said to be of type (ω, K) , if

1. *A is densely defined and closed;*
2. *the resolvent set of $-A$ contains the sector $|\arg \lambda| < \pi - \omega$, $0 < \omega < \pi$, and $\lambda(\lambda + A)^{-1}$ is uniformly bounded in each smaller sector $|\arg \lambda| < \pi - \omega - \varepsilon$, $\varepsilon > 0$ with $\|\lambda(\lambda + A)^{-1}\|_{\mathcal{L}(\mathcal{Y}, \mathcal{X})} \leq K$ for $\lambda > 0$.*

The following Corollary can be found in [21, Appendix].

Corollary 1.3.1 *If A is of type $(\frac{\pi}{2}, K)$, then we have*

$$\|(\mu + A)^{-1}Au\|_X \leq (1 + K)\|u\|_X, \quad \|(\mu + A)^{-1}\|_{\mathcal{L}(\mathcal{Y}, X)} \leq K\mu^{-1}. \quad (1.32)$$

For $u \in \mathcal{D}(-\Delta) := H^2(\Omega) \cap H_0^1(\Omega)$, the operator $-\Delta : H^2(\Omega) \rightarrow L^2(\Omega)$ can be defined via a bilinear form $\mathcal{A}(\cdot, \cdot) : H_0^1(\Omega) \times H_0^1(\Omega) \rightarrow \mathbb{R}$, namely

$$\mathcal{A}(u, v) := \langle -\Delta u, v \rangle = (\nabla u, \nabla v), \quad \text{for } u, v \in H_0^1(\Omega), \quad (1.33)$$

which satisfies continuity and coercivity.

For $u_M, v_M \in V_M^d$, the operator $-\Delta_M$ can be defined by the following bilinear form

$$\langle -\Delta_M u_M, v_M \rangle = (\nabla u_M, \nabla v_M), \quad u_M, v_M \in V_M^d, \quad (1.34)$$

which satisfies continuity and coercivity.

Because of the continuity and coercivity, we immediately get the following lemma.

Lemma 1 *The operator $-\Delta$ is of type $(\frac{\pi}{2}, 1)$. Moreover, the operator $-\Delta_M$ is also of type $(\frac{\pi}{2}, 1)$.*

Proof According to [21, 22], the operator Δ is a closed and maximal accretive operator. On the other hand, we have the following equivalence (see, e.g., [21])

- the operator $-\Delta$ in Ω is a closed and maximal accretive operator;
- the operator $-\Delta$ is of type $(\frac{\pi}{2}, 1)$;

which will automatically lead to the desired results. Note that $-\Delta_M = -\Delta|_{V_M^d}$, so the operator $-\Delta_M$ is also of type $(\frac{\pi}{2}, 1)$ (see, e.g., [21]). ■

We now turn to fractional Laplacian operator $(-\Delta)^{\frac{\alpha}{2}}$.

For $u \in \mathcal{D}((-\Delta)^{\frac{\alpha}{2}}) := \{u : (-\Delta)^{\frac{\alpha}{2}}u \in L^2(\Omega), u \in H_0^{\frac{\alpha}{2}}(\Omega)\}$, the operator $(-\Delta)^{\frac{\alpha}{2}}$ can also be defined via a bilinear form

$$\mathcal{A}^{\frac{\alpha}{2}}(u, v) := \langle (-\Delta)^{\frac{\alpha}{2}}u, v \rangle = ((-\Delta)^{\frac{\alpha}{4}}u, (-\Delta)^{\frac{\alpha}{4}}v), \quad \text{for } u, v \in H_0^{\frac{\alpha}{2}}(\Omega). \quad (1.35)$$

By density, the operator $(-\Delta)^{\frac{s}{2}}$ can be extended to the Hilbert space

$$\mathbb{H}^s(\Omega) = \left\{ u = \sum_{k=1}^{\infty} u_k \phi_k \in L^2(\Omega) : \|u\|_{\mathbb{H}^s(\Omega)}^2 = \sum_{k=1}^{\infty} |u_k|^2 \lambda_k^s < \infty \right\}. \quad (1.36)$$

The theory of Hilbert scales presented in Chap. 1 of [23] shows that

$$[H_0^1(\Omega), L^2(\Omega)]_{\theta} = \mathcal{D}((-\Delta)^{\frac{s}{2}}), \quad \text{with } \theta = 1 - s. \quad (1.37)$$

This implies the following characterization of the space $\mathbb{H}^s(\Omega)$

$$\mathbb{H}^s(\Omega) = \begin{cases} H^s(\Omega) = [H^1(\Omega), L^2(\Omega)]_{1-s}, & s \in (0, \frac{1}{2}), \\ H_{00}^{\frac{1}{2}}(\Omega) = [H_0^1(\Omega), L^2(\Omega)]_{\frac{1}{2}}, & s = \frac{1}{2}, \\ H_0^s(\Omega) = [H_0^1(\Omega), L^2(\Omega)]_{1-s}, & s \in (\frac{1}{2}, 1), \end{cases} \quad (1.38)$$

where $H^s(\Omega)$ and $H_0^s(\Omega)$, $s \neq \frac{1}{2}$, are the classical fractional Sobolev spaces, and $H_{00}^{\frac{1}{2}}$ denote the Lions-Magenes space, which can be characterized as

$$H_{00}^{\frac{1}{2}} = \left\{ u \in H^{\frac{1}{2}}(\Omega) : \int_{\Omega} \frac{u^2(y)}{\text{dist}(y, \partial\Omega)} dy < \infty \right\}.$$

If the boundary of Ω is Lipschitz, we have $H_0^s(\Omega) = H^s(\Omega)$ for $s \in (0, \frac{1}{2}]$; and $H_0^s(\Omega)$ is strictly contained in $H^s(\Omega)$ for $s \in (\frac{1}{2}, 1)$. In particular, we have the strict inclusion $H_{00}^{\frac{1}{2}}(\Omega) \subsetneq H_0^{\frac{1}{2}}(\Omega) = H^{\frac{1}{2}}(\Omega)$.

Lemma 2 For $v \in H_0^{\frac{\alpha}{2}}(\Omega)$, $\alpha \neq 1$ we have

$$|(-\Delta)^{\frac{\alpha}{4}} v| \cong |v|_{H^{\frac{\alpha}{2}}(\Omega)}. \quad (1.39)$$

Proof One derives immediately from (1.38) that the equality holds. ■

Using the first equality of (1.39), we deduce the following:

$$\begin{aligned} |\mathcal{A}^{\frac{\alpha}{2}}(u, v)| &\lesssim \|u\|_{H^{\frac{\alpha}{2}}(\Omega)} \|v\|_{H^{\frac{\alpha}{2}}(\Omega)}, \quad \text{for } u, v \in H_0^{\frac{\alpha}{2}}(\Omega), \\ |\mathcal{A}^{\frac{\alpha}{2}}(u, u)| &\gtrsim \|u\|_{H^{\frac{\alpha}{2}}(\Omega)}, \quad \text{for } u \in H_0^{\frac{\alpha}{2}}(\Omega). \end{aligned} \quad (1.40)$$

From Definition 1.2.1, for any $u_M, v_M \in V_M^d$, the operator $(-\Delta_M)^{\frac{\alpha}{2}} : V_M^d \rightarrow V_M^d$ can be defined via following bilinear form

$$\langle (-\Delta_M)^{\frac{\alpha}{2}} u_M, v_M \rangle = ((-\Delta_M)^{\frac{\alpha}{4}} u_M, (-\Delta_M)^{\frac{\alpha}{4}} v_M). \quad (1.41)$$

The following Lemma can be found in [22, Lemma 4.1].

Lemma 3 For $0 \leq s \leq \frac{1}{2}$, there is a constant C , such that for any $v_M \in V_M^d$,

$$\|(-\Delta)^s v_M\| \leq C \|(-\Delta_M)^s v_M\|. \quad (1.42)$$

For $0 \leq s \leq 1$, there is a constant C , such that for any $v_M \in V_M^d$,

$$\|(-\Delta_M)^s v_M\| \leq C \|(-\Delta)^s v_M\|. \quad (1.43)$$

Therefore, we deduce from Lemma 2 and Lemma 3 that

$$\begin{aligned} |((-\Delta_M)^{\frac{\alpha}{4}} u_M, (-\Delta_M)^{\frac{\alpha}{4}} v_M)| &\lesssim \|(-\Delta_M)^{\frac{\alpha}{4}} u_M\|_{L^2(\Omega)} \|(-\Delta_M)^{\frac{\alpha}{4}} v_M\|_{L^2(\Omega)} \\ &\lesssim \|(-\Delta)^{\frac{\alpha}{4}} u_M\|_{L^2(\Omega)} \|(-\Delta)^{\frac{\alpha}{4}} v_M\|_{L^2(\Omega)} \\ &\lesssim \|u_M\|_{H^{\frac{\alpha}{2}}(\Omega)} \|v_M\|_{H^{\frac{\alpha}{2}}(\Omega)}, \quad \text{for } u_M, v_M \in V_M^d, \quad (1.44) \\ |((-\Delta_M)^{\frac{\alpha}{4}} u_M, (-\Delta_M)^{\frac{\alpha}{4}} u_M)| &\gtrsim \|(-\Delta_M)^{\frac{\alpha}{4}} u_M\|_{L^2(\Omega)}^2 \\ &\gtrsim \|(-\Delta)^{\frac{\alpha}{4}} u_M\|_{L^2(\Omega)}^2 \gtrsim \|u_M\|_{H^{\frac{\alpha}{2}}(\Omega)}^2, \quad \text{for } u_M \in V_M^d. \end{aligned}$$

Next, we define negative norms by

$$\|u\|_{-s} = \sup \left\{ \frac{(u, v)}{\|v\|_{H^s}}; v \in H^s \right\}, \quad \text{for } s \geq 0. \quad (1.45)$$

The following Lemma plays a key role in the error analysis.

Lemma 4 For any $0 < s < 1$ and $u \in H_0^1(\Omega) \cap H^{2-s}(\Omega)$, we have

$$\|(-\Delta)^s u - (-\Delta_M)^s \Pi_M u\|_{H^{-s}(\Omega)} \leq c_{u,s} \|(-\Delta)u - (-\Delta_M)\Pi_M u\|_{H^{-s}(\Omega)}^s.$$

where $c_{u,s} = c(s) (\|\Pi_M u\|_{H^{-s}(\Omega)} + \|u\|_{H^{-s}(\Omega)})^{1-s}$.

Proof By virtue of $-\Delta_M$ is of type $(\frac{\pi}{2}, 1)$ and $(-\Delta_M)^{-1}$ is bounded, we follow the procedure used in [21], the operator $(-\Delta_M)^s$ can be defined indirectly by

$$(-\Delta_M)^s \Pi_M u = \frac{\sin(\pi s)}{\pi} \int_0^\infty \mu^{s-1} (\mu + (-\Delta_M))^{-1} (-\Delta_M) \Pi_M u \, d\mu. \quad (1.46)$$

Subtracting from (1.46) a similar expression with M replaced by M' , $M \leq M'$, we have

$$\begin{aligned}
& (-\Delta_M)^s \Pi_M u - (-\Delta_{M'})^s \Pi_{M'} u \\
&= \frac{\sin(\pi s)}{\pi} \left[\int_0^\delta \mu^{s-1} (\mu + (-\Delta_M))^{-1} (-\Delta_M) \Pi_M u \, d\mu - \int_0^\delta \mu^{s-1} (\mu + (-\Delta_{M'}))^{-1} (-\Delta_{M'}) \Pi_{M'} u \, d\mu \right. \\
&\quad \left. + \int_\delta^\infty \mu^s (\mu + (-\Delta_M))^{-1} (\mu + (-\Delta_{M'}))^{-1} \left((-\Delta_M) \Pi_M u - (-\Delta_{M'}) \Pi_{M'} u \right) d\mu \right].
\end{aligned} \tag{1.47}$$

Moreover, we can derive from (1.32) with $K = 1$ and the norm of linear operators (see, e.g., [24, p102]) upon H^{-s} that

$$\|(\mu + (-\Delta_M))^{-1} (-\Delta_M) \Pi_M u\|_{H^{-s}} \stackrel{(1.32)}{\leq} 2 \|\Pi_{M'} u\|_{H^{-s}(\Omega)}$$

and

$$\begin{aligned}
& \|(\mu + (-\Delta_M))^{-1} (\mu + (-\Delta_{M'}))^{-1} \left((-\Delta_M) \Pi_M u - (-\Delta_{M'}) \Pi_{M'} u \right)\|_{H^{-s}(\Omega)} \\
&\stackrel{(1.32)}{\leq} \|(\mu + (-\Delta_M))^{-1} (\mu + (-\Delta_{M'}))^{-1}\|_{\mathcal{L}(V_M^d, V_{M'}^d)} \|(-\Delta_M) \Pi_M u - (-\Delta_{M'}) \Pi_{M'} u\|_{H^{-s}(\Omega)} \\
&\stackrel{(1.32)}{\leq} \mu^{-2} \|(-\Delta_M) \Pi_M u - (-\Delta_{M'}) \Pi_{M'} u\|_{H^{-s}(\Omega)}.
\end{aligned}$$

This, along with equation (1.47), yields

$$\begin{aligned}
& \|(-\Delta_M)^s \Pi_M u - (-\Delta_{M'})^s \Pi_{M'} u\|_{H^{-s}(\Omega)} \\
&\leq \frac{\sin(\pi s)}{\pi} \left[2(\|\Pi_M u\|_{H^{-s}(\Omega)} + \|\Pi_{M'} u\|_{H^{-s}(\Omega)}) \int_0^\delta \mu^{s-1} d\mu \right. \\
&\quad \left. + \|(-\Delta_M) \Pi_M u - (-\Delta_{M'}) \Pi_{M'} u\|_{H^{-s}(\Omega)} \int_\delta^\infty \mu^{s-2} d\mu \right] \\
&= \frac{\sin(\pi s)}{\pi} \left[2s^{-1} \delta^s (\|\Pi_M u\|_{H^{-s}(\Omega)} + \|\Pi_{M'} u\|_{H^{-s}(\Omega)}) \right. \\
&\quad \left. + (1-s)^{-1} \delta^{s-1} \|(-\Delta_M) \Pi_M u - (-\Delta_{M'}) \Pi_{M'} u\|_{H^{-s}(\Omega)} \right].
\end{aligned}$$

Taking $\delta = \|(-\Delta_M) \Pi_M u - (-\Delta_{M'}) \Pi_{M'} u\|_{H^{-s}(\Omega)} / (\|\Pi_M u\|_{H^{-s}(\Omega)} + \|\Pi_{M'} u\|_{H^{-s}(\Omega)})$, we deduce that

$$\begin{aligned}
& \|(-\Delta_M)^s \Pi_M u - (-\Delta_{M'})^s \Pi_{M'} u\|_{H^{-s}(\Omega)} \\
&\leq c(s) (\|\Pi_M u\|_{H^{-s}(\Omega)} + \|\Pi_{M'} u\|_{H^{-s}(\Omega)})^{1-s} \|(-\Delta_M) \Pi_M u - (-\Delta_{M'}) \Pi_{M'} u\|_{H^{-s}(\Omega)}^s.
\end{aligned}$$

Finally, letting $M' \rightarrow \infty$ leads to the desired results. ■

1.3.2 Error bounds for (1.17)

To fix the idea, we restrict our attention to $\Omega = \Lambda^d$, $\Lambda = (-1, 1)$. To derive the error bounds, we take $\Pi_M = \Pi_M^{2,d}$ where $\Pi_M^{2,d} : H^2(\Omega) \rightarrow \mathcal{P}_M^d$ satisfy

$$\Pi_M^{2,d} u|_{\partial\Omega} = u|_{\partial\Omega}, \quad \frac{\Pi_M^{2,d} u}{\partial \mathbf{n}} = \frac{u}{\partial \mathbf{n}}. \quad (1.48)$$

To measure the truncation error $\Pi_M^{2,d} u - u$, let us denote

$$\chi^r(\mathbf{x}) = \prod_{j=1}^d \chi^{r_j}(x_j) = \prod_{j=1}^d (1 - x_j^2)^{r_j},$$

and introduce the non-uniformly weighted Sobolev space \tilde{B}^r with semi-norm and norm:

$$|u|_{\tilde{B}^r(\Omega)} = \left(\sum_{j=1}^d \sum_{\mathbf{r} \in \tilde{\Upsilon}_j} \|\partial_{\mathbf{x}}^{\mathbf{r}} u\|_{\chi^{(\mathbf{r}_j - 2)\mathbf{e}_j}}^2 \right)^{\frac{1}{2}}, \quad \|u\|_{\tilde{B}^r(\Omega)} = \left(\|u\|^2 + |u|_{\tilde{B}^r(\Omega)}^2 \right)^{\frac{1}{2}}.$$

where the index sets

$$\tilde{\Upsilon}_j = \left\{ \mathbf{r} \in \mathbb{N}_0^d : d \leq r_j \leq r; r_i \in \{0, 2\}, i \neq j; \sum_{k=1}^d r_k = r \right\}, \quad \forall 1 \leq j \leq d. \quad (1.49)$$

The approximation property of $\Pi_M^{2,d}$ stated below:

Lemma 5 *If $u \in H^2(\Omega)$ and $u \in \tilde{B}^r(\Omega)$ with $\max(d, 2) \leq r \leq M + 1$ then we have*

$$\|\Pi_M^{2,d} u - u\|_{H^\mu(\Omega)} \lesssim M^{\mu-r} (\|u\|_{H^2(\Omega)} + |u|_{\tilde{B}^r(\Omega)}), \quad \mu \in [0, 2]. \quad (1.50)$$

Proof Let $\Pi_M^2 : H^2(\Lambda) \rightarrow \mathcal{P}_M$ be the H^2 -orthogonal projection on $\Lambda = (-1, 1)$ such that

$$\Pi_M^2 u(\pm 1) = u(\pm 1), \quad (\Pi_M^2 u)'(\pm 1) = u'(\pm 1).$$

According to [25, Theorem 4.2], for any $u \in H^2(\Lambda)$ and $\partial_x^r u \in L_{\chi^{r-2}}^2(\Lambda)$ with $2 \leq r \leq M + 1$, we have

$$\|\Pi_M^2 u - u\|_{H^\mu} \leq c M^{\mu-r} (\|u\|_{H^2} + \|\partial_x^r u\|_{\chi^{r-2}}), \quad \mu \in [0, 2], \quad (1.51)$$

where c is a positive constant independent of M and u . In view of (1.48), we have

$$\Pi_M^{2,d} := \Pi_M^{2,(1)} \circ \dots \circ \Pi_M^{2,(d)} \quad \text{with} \quad \Pi_M^{2,(j)} = \Pi_M^2, \quad j = 1, \dots, d. \quad (1.52)$$

For clarity, we only prove the results with $d = 3$, as it is straightforward to extend the results to the case with $d > 3$. Using integration by parts, we have

$$\begin{aligned} \|\Delta(\Pi_M^{2,3}u - u)\|^2 &= \sum_{j=1}^3 \|\partial_{x_j}^2(\Pi_M^{2,3}u - u)\|^2 + \sum_{\substack{i,j=1 \\ i \neq j}}^3 \int_{\Lambda^3} \partial_{x_i}^2(\Pi_M^{2,3}u - u) \partial_{x_j}^2(\Pi_M^{2,3}u - u) d\mathbf{x} \\ &= \sum_{j=1}^3 \|\partial_{x_j}^2(\Pi_M^{2,3}u - u)\|^2 + \sum_{\substack{i,j=1 \\ i \neq j}}^3 \|\partial_{x_i} \partial_{x_j}(\Pi_M^{2,3}u - u)\|^2 := I_1 + I_2. \end{aligned} \quad (1.53)$$

By virtue of (1.51) and (1.52), we obtain that

$$\begin{aligned} I_1 &\leq 2 \left(\|\partial_{x_1}^2(\Pi_M^{2,(1)}u - u)\|^2 + \|\partial_{x_1}^2 \Pi_M^{2,(1)} \circ (\Pi_M^{2,(2)} \circ \Pi_M^{2,(3)}u - u)\|^2 \right. \\ &\quad + \|\partial_{x_2}^2(\Pi_M^{2,(2)}u - u)\|^2 + \|\partial_{x_2}^2 \Pi_M^{2,(2)} \circ (\Pi_M^{2,(1)} \circ \Pi_M^{2,(3)}u - u)\|^2 \\ &\quad \left. + \|\partial_{x_3}^2(\Pi_M^{2,(3)}u - u)\|^2 + \|\partial_{x_3}^2 \Pi_M^{2,(3)} \circ (\Pi_M^{2,(1)} \circ \Pi_M^{2,(2)}u - u)\|^2 \right) \\ &\leq cM^{2(2-r)} \left(\|u\|_{H^2}^2 + \sum_{j=1}^d \|\partial_{x_j}^r u\|_{\chi^{(r-2)e_j}}^2 \right) + 2\|\Pi_M^{2,(2)} \circ \Pi_M^{2,(3)}(\partial_{x_1}^2 u) - (\partial_{x_1}^2 u)\|^2 \\ &\quad + 2\|\Pi_M^{2,(1)} \circ \Pi_M^{2,(3)}(\partial_{x_2}^2 u) - (\partial_{x_2}^2 u)\|^2 + 2\|\Pi_M^{2,(1)} \circ \Pi_M^{2,(2)}(\partial_{x_3}^2 u) - (\partial_{x_3}^2 u)\|^2. \end{aligned} \quad (1.54)$$

Hence, it remains to estimate the last three terms in (1.54), and we only need to consider the last term as they are similar to each other. Then, we can derive from (1.54) and (1.51) with $\mu = 0$ that

$$\begin{aligned} \|\Pi_M^{2,(1)} \circ \Pi_M^{2,(2)}(\partial_{x_3}^2 u) - (\partial_{x_3}^2 u)\| &\leq \|\Pi_M^{2,(2)}(\partial_{x_3}^2 u) - (\partial_{x_3}^2 u)\| \\ &\quad + \|\Pi_M^{2,(1)}(\partial_{x_3}^2 u) - (\partial_{x_3}^2 u)\| + \|(\mathcal{I} - \Pi_M^{2,(2)})(\Pi_M^{2,(1)}(\partial_{x_3}^2 u) - (\partial_{x_3}^2 u))\| \\ &\leq cM^{2-r} \left(\|u\|_{H^2} + \|\partial_{x_2}^{r-2} \partial_{x_3}^2 u\|_{\chi^{(r-4)e_2}} + \|\partial_{x_1}^{r-2} \partial_{x_3}^2 u\|_{\chi^{(r-4)e_1}} \right) + cM^{-2} \|\Pi_M^{2,(1)}(\partial_{x_2}^2 \partial_{x_3}^2 u) - (\partial_{x_2}^2 \partial_{x_3}^2 u)\| \\ &\leq cM^{2-r} \left(\|u\|_{H^2} + \|\partial_{x_2}^{r-2} \partial_{x_3}^2 u\|_{\chi^{(r-4)e_2}} + \|\partial_{x_1}^{r-2} \partial_{x_3}^2 u\|_{\chi^{(r-4)e_1}} + \|\partial_{x_1}^{r-4} \partial_{x_2}^2 \partial_{x_3}^2 u\|_{\chi^{(r-6)e_1}} \right). \end{aligned}$$

Applying this argument repeatedly leads to

$$\begin{aligned}
I_1 \leq & cM^{2(2-r)} \left(\|u\|_{H^2}^2 + \sum_{j=1}^3 \|\partial_{x_j}^r u\|_{\mathcal{X}^{(r-2)e_j}}^2 + \sum_{\substack{i,j=1 \\ i \neq j}}^3 \|\partial_{x_i}^{r-2} \partial_{x_j}^2 u\|_{\mathcal{X}^{(r-4)e_i}}^2 \right. \\
& \left. + \sum_{\substack{i,j,k=1 \\ i \neq j \neq k}}^3 \|\partial_{x_i}^{r-4} \partial_{x_j}^2 \partial_{x_k}^2 u\|_{\mathcal{X}^{(r-6)e_i}}^2 \right). \tag{1.55}
\end{aligned}$$

Now, we turn to estimate I_2 . Similarly, we only consider $i = 1, j = 2$ in I_2 , since the other terms in I_2 can be derived in a similar fashion. Then, we obtain from (1.52) and the triangle inequality that

$$\begin{aligned}
\|\partial_{x_1} \partial_{x_2} (\Pi_M^{2,3} u - u)\| & \leq \|\partial_{x_1} \partial_{x_2} (\Pi_M^{2,(1)} \circ \Pi_M^{2,(2)} u - u)\| + \|\partial_{x_1} \partial_{x_2} \Pi_M^{2,(1)} \circ \Pi_M^{2,(2)} (\Pi_M^{2,(3)} u - u)\| \\
& \leq cM^{2-r} \left(\|u\|_{H^2} + \|\partial_{x_1}^{r-2} \partial_{x_2}^2 u\|_{\mathcal{X}^{(r-4)e_1}} + \|\partial_{x_1}^2 \partial_{x_2}^2 \partial_{x_3}^{r-4} u\|_{\mathcal{X}^{(r-6)e_3}} \right).
\end{aligned}$$

Applying this argument repeatedly leads to

$$I_2 \leq cM^{2(2-r)} \left(\|u\|_{H^2}^2 + \sum_{\substack{i,j=1 \\ i \neq j}}^3 \|\partial_{x_i}^{r-2} \partial_{x_j}^2 u\|_{\mathcal{X}^{(r-4)e_i}}^2 + \sum_{\substack{i,j,k=1 \\ i \neq j \neq k}}^3 \|\partial_{x_i}^{r-4} \partial_{x_j}^2 \partial_{x_k}^2 u\|_{\mathcal{X}^{(r-6)e_i}}^2 \right). \tag{1.56}$$

According to [25, Lemma 8.8], there holds

$$\|\Pi_M^{2,3} u - u\|_{H^2(\Omega)} \leq c \|\Delta(\Pi_M^{2,3} u - u)\|_{L^2(\Omega)},$$

This, together with (1.55) and (1.56) leads to desired result (1.50) with $\mu = 2$. Furthermore, we can follow a similar procedure as above to derive the L^2 -bound for $\Pi_M^{2,3}$. A combination of the above facts and the standard space interpolation leads to (1.50) with $d = 3$. It is straightforward to extend the above derivation to $d > 3$. This completes the proof. \blacksquare

Theorem 1.3.1 *Let $\alpha \in (0, 2)$, $\alpha \neq 1$ and let u, u_M be respectively the solutions of (1.1) and (1.17). If $u \in H_0^{\frac{\alpha}{2}}(\Omega)$ and $u \in H^2(\Omega) \cap \tilde{B}^m(\Omega)$ with $2 \leq m \leq M + 1$, then we have*

$$\|u - u_M\|_{H^{\frac{\alpha}{2}}(\Omega)} \lesssim M^{\frac{\alpha}{2}-m} (\|u\|_{H^2(\Omega)} + |u|_{\tilde{B}^m(\Omega)}) + c_{u, \frac{\alpha}{2}} M^{\frac{\alpha}{2}(2-\frac{\alpha}{2}-m)} (\|u\|_{H^2(\Omega)} + |u|_{\tilde{B}^m(\Omega)})^{\frac{\alpha}{2}}.$$

Proof Then, applying the first Strang Lemma (see, e.g., [26]) to (1.44), we can obtain

$$\begin{aligned}
& \|u - u_M\|_{H^{\frac{\alpha}{2}}(\Omega)} \\
& \lesssim \inf_{w_M \in V_M^d} \left\{ \|u - w_M\|_{H^{\frac{\alpha}{2}}(\Omega)} + \sup_{0 \neq v_M \in V_M^d} \frac{\langle (-\Delta)^{\frac{\alpha}{2}} w_M, v_M \rangle - \langle (-\Delta_M)^{\frac{\alpha}{2}} w_M, v_M \rangle}{\|(-\Delta)^{\frac{\alpha}{4}} v_M\|_{L^2(\Omega)}} \right\} \\
& \lesssim \inf_{w_M \in V_M^d} \left\{ \|u - w_M\|_{H^{\frac{\alpha}{2}}(\Omega)} + \sup_{0 \neq v_M \in V_M^d} \frac{\langle (-\Delta)^{\frac{\alpha}{2}} w_M, v_M \rangle - \langle (-\Delta_M)^{\frac{\alpha}{2}} w_M, v_M \rangle}{\|v_M\|_{H^{\frac{\alpha}{2}}(\Omega)}} \right\} \\
& = \inf_{w_M \in V_M^d} \left\{ \|u - w_M\|_{H^{\frac{\alpha}{2}}(\Omega)} + \|(-\Delta)^{\frac{\alpha}{2}} w_M - (-\Delta_M)^{\frac{\alpha}{2}} w_M\|_{H^{-\frac{\alpha}{2}}(\Omega)} \right\}.
\end{aligned}$$

Take $w_M = \Pi_M^{2,d} u$ in the above, we derive from (1.50) and Lemma 4 that

$$\begin{aligned}
& \|u - u_M\|_{H^{\frac{\alpha}{2}}(\Omega)} \\
& \lesssim M^{\frac{\alpha}{2}-m} (\|u\|_{H^2(\Omega)} + |u|_{\tilde{B}^m(\Omega)}) + \|(-\Delta)^{\frac{\alpha}{2}} (\Pi_M^{2,d} u - u) + (-\Delta)^{\frac{\alpha}{2}} u - (-\Delta_M)^{\frac{\alpha}{2}} \Pi_M^{2,d} u\|_{H^{-\frac{\alpha}{2}}(\Omega)}.
\end{aligned}$$

Thus, it remains to estimate the last term of above equation. By (1.50), the triangle inequality and Lemma 4, we obtain

$$\begin{aligned}
& \|(-\Delta)^{\frac{\alpha}{2}} (\Pi_M^{2,d} u - u) + (-\Delta)^{\frac{\alpha}{2}} u - (-\Delta_M)^{\frac{\alpha}{2}} \Pi_M^{2,d} u\|_{H^{-\frac{\alpha}{2}}(\Omega)} \\
& \lesssim \|(-\Delta)^{\frac{\alpha}{2}} (\Pi_M^{2,d} u - u)\|_{H^{-\frac{\alpha}{2}}(\Omega)} + \|(-\Delta)^{\frac{\alpha}{2}} u - (-\Delta_M)^{\frac{\alpha}{2}} \Pi_M^{2,d} u\|_{H^{-\frac{\alpha}{2}}(\Omega)} \\
& \lesssim \|\Pi_M^{2,d} u - u\|_{H^{\frac{\alpha}{2}}(\Omega)} + c_{u, \frac{\alpha}{2}} \|(-\Delta)u - (-\Delta_M) \Pi_M^{2,d} u\|_{H^{-\frac{\alpha}{2}}(\Omega)}^{\frac{\alpha}{2}} \\
& \lesssim M^{\frac{\alpha}{2}-m} (\|u\|_{H^2(\Omega)} + |u|_{\tilde{B}^m(\Omega)}) + c_{u, \frac{\alpha}{2}} \|(-\Delta)u - (-\Delta) \Pi_M^{2,d} u\|_{H^{-\frac{\alpha}{2}}(\Omega)}^{\frac{\alpha}{2}} \\
& \lesssim M^{\frac{\alpha}{2}-m} (\|u\|_{H^2(\Omega)} + |u|_{\tilde{B}^m(\Omega)}) + c_{u, \frac{\alpha}{2}} \|u - \Pi_M^{2,d} u\|_{H^{2-\frac{\alpha}{2}}(\Omega)}^{\frac{\alpha}{2}} \\
& \lesssim M^{\frac{\alpha}{2}-m} (\|u\|_{H^2(\Omega)} + |u|_{\tilde{B}^m(\Omega)}) + c_{u, \frac{\alpha}{2}} M^{\frac{\alpha}{2}(-\frac{\alpha}{2}-m+2)} (\|u\|_{H^2(\Omega)} + |u|_{\tilde{B}^m(\Omega)})^{\frac{\alpha}{2}}.
\end{aligned}$$

A combination of above facts lead to the desired result. ■

1.3.3 Error bounds for (1.25)

In the error analysis, we compare the numerical solution with a suitable orthogonal projection of the exact solution. The orthogonal projection in time $\pi_N^{0,-1} : L_{\omega^0,-1}^2(I) \rightarrow S_N$, is defined by

$$(\pi_N^{0,-1} v - v, \phi)_{I, \omega^0, -1} = 0, \quad \forall \phi \in S_N. \quad (1.57)$$

Defining

$$\widehat{H}^1(I) := \{u : u \in H^1(I) \cap L^2_{\omega^0, -2}(I)\},$$

one observes that for any $v \in \widehat{H}^1(I)$ and $\psi \in S_N^*$,

$$(\partial_t(\pi_N^{0,-1}v - v), \psi)_I = -(\pi_N^{0,-1}v - v, \omega^{0,1}\partial_t\psi)_{I, \omega^0, -1} = 0, \quad (1.58)$$

which follows from the fact $\omega^{0,1}\partial_t\phi \in S_N$ and the definition (1.57). According to Theorem 1.1 in [27], we have

Lemma 6 *If $v \in L^2_{\omega^0, -1}(I)$ and $\partial_x^k v \in L^2_{\omega^k, k-1}(I)$ for $1 \leq k \leq n$, then*

$$\|\partial_t^l(\pi_N^{0,-1}v - v)\|_{\omega^{l, l-1}} \lesssim N^{l-n} \|\partial_t^n v\|_{\omega^{n, n-1}}, \quad l \leq n, \quad l = 0, 1. \quad (1.59)$$

For notational convenience, we denote by $A^m(D)$ (respectively $B^n(D)$) a function space consisting of measurable functions satisfying $\|u\|_{A^m(D)} < \infty$ (respectively $\|u\|_{B^n(D)} < \infty$), where for integers $m \geq 2$ and $n \geq 0$,

$$\begin{aligned} \|u\|_{A^m(D)} &= \left(\|\partial_t u\|_{H^2(\Omega)} + \|\partial_t u\|_{\widetilde{B}^m(\Omega)}\|_{L^2_{\omega^2, 0}(I)} + \|\|u\|_{H^2(\Omega)} + |u|_{\widetilde{B}^m(\Omega)}\|_{L^2_{\omega^0, -1}(I)} \right)^{\frac{1}{2}}, \\ \|u\|_{B^n(D)} &= \left(\|\partial_t^n u\|_{H^{\frac{\alpha}{2}}(\Omega, L^2_{\omega^{n, n-1}}(I))} + \|\partial_t^n u\|_{L^2(\Omega, L^2_{\omega^{n, n-1}}(I))} \right)^{\frac{1}{2}}. \end{aligned}$$

Theorem 1.3.2 *Let $\alpha \neq 1$, $\epsilon > 0$ and $\beta > 0$, and let u, u_L be respectively the solutions of (1.22) and (1.25). If $u \in L^2_{\omega^1, -1}(I; H^2(\Omega)) \cap \widehat{H}^1(I; L^2(\Omega)) \cap A^m(D) \cap B^n(D)$ and $\partial_t^n u \in H^{2-\frac{\alpha}{2}}(\Omega, L^2_{\omega^{n, n-1}}(I))$ with integers $m \geq 3$ and $n \geq 0$, then we have*

$$\begin{aligned} \|u - u_L\|_{L^2(\Omega, L^2_{\omega^0, -1}(I))} + \|(-\Delta)^{\frac{\alpha}{4}}(u - u_L)\|_{L^2(\Omega, L^2_{\omega^1, -1}(I))} &\lesssim N^{-n} \|u\|_{B^n(D)} + M^{\frac{\alpha}{2}-m} \|u\|_{A^m(D)} \\ &+ d_u^\alpha M^{\frac{\alpha}{2}(-\frac{\alpha}{2}-m+2)} \|\|u\|_{H^2(\Omega)} + |u|_{\widetilde{B}^m(\Omega)}\|_{L^2_{\omega^0, -1}(I)} + d_u^\alpha N^{-\frac{\alpha}{2}n} \|\partial_t^n u\|_{H^{2-\frac{\alpha}{2}}(\Omega, L^2_{\omega^{n, n-1}}(I))}, \end{aligned}$$

where $d_u^\alpha := c(\alpha) (\|\Pi_M^{2,d} u\|_{H^{-\frac{\alpha}{2}}(\Omega, L^2_{\omega^1, -1}(I))} + \|u\|_{H^{-\frac{\alpha}{2}}(\Omega, L^2_{\omega^1, -1}(I))})^{1-\frac{\alpha}{2}}$.

Proof Let us denote $\widetilde{u}_L := \pi_N^{0,-1} \Pi_M^{2,d} u = \Pi_M^{2,d} \pi_N^{0,-1} u$ and $e_L := u_L - \widetilde{u}_L$. By virtue of (1.2) with $\mathcal{N}(u) = \beta u - f$ and (1.25), we have

$$\begin{aligned} a(u, v) &:= (\partial_t u, v)_D + \epsilon \langle (-\Delta)^{\frac{\alpha}{4}} u, (-\Delta)^{\frac{\alpha}{4}} v \rangle_D + \beta (u, v)_D = (f, v)_D, \\ a_M(u_L, v) &:= (\partial_t u_L, v)_D + \epsilon \langle (-\Delta_M)^{\frac{\alpha}{2}} u_L, v \rangle_D + \beta (u_L, v)_D = (f, v)_D, \quad v \in V_M \otimes S_N, \end{aligned} \quad (1.60)$$

which imply

$$a(u, v) = a_M(u_L, v), \quad v \in V_M \otimes S_N.$$

This, along with (1.60), yields

$$\begin{aligned} a_M(e_L, v) &= a(u - \tilde{u}_L, v) + a(\tilde{u}_L, v) - a_M(\tilde{u}_L, v) \\ &= (\partial_t(u - \tilde{u}_L), v)_D + \epsilon((-\Delta)^{\frac{\alpha}{4}}(u - \tilde{u}_L), (-\Delta)^{\frac{\alpha}{4}}v)_D + \beta(u - \tilde{u}_L, v)_D \\ &\quad + \epsilon((-\Delta)^{\frac{\alpha}{2}}\tilde{u}_L - (-\Delta_M)^{\frac{\alpha}{2}}\tilde{u}_L, v)_D, \end{aligned} \quad (1.61)$$

for all $v \in V_M \otimes S_N^*$. Due to (1.58), the above equation can be simplified to

$$\begin{aligned} a_M(e_L, v) &= (\partial_t(u - \Pi_M^{2,d}u), v)_D + \epsilon((-\Delta)^{\frac{\alpha}{4}}(u - \pi_N^{0,-1}\Pi_M^{2,d}u), (-\Delta)^{\frac{\alpha}{4}}v)_D \\ &\quad + \beta(u - \tilde{u}_L, v)_D + \epsilon((-\Delta)^{\frac{\alpha}{2}}\tilde{u}_L - (-\Delta_M)^{\frac{\alpha}{2}}\tilde{u}_L, v)_D. \end{aligned} \quad (1.62)$$

Taking $v = \frac{1-t}{1+t}e_L \in V_M \otimes S_N^*$ in above equation, and using Lemma 2, we arrive at

$$\begin{aligned} &\|e_L\|_{L^2(\Omega, L^2_{\omega^0, -2}(I))} + \sqrt{\epsilon}\|e_L\|_{H^{\frac{\alpha}{2}}(\Omega, L^2_{\omega^1, -1}(I))} + \sqrt{\beta}\|e_L\|_{L^2(\Omega, L^2_{\omega^1, -1}(I))} \\ &\cong \|e_L\|_{L^2(\Omega, L^2_{\omega^0, -2}(I))} + \sqrt{\epsilon}\|(-\Delta)^{\frac{\alpha}{4}}e_L\|_{L^2(\Omega, L^2_{\omega^1, -1}(I))} + \sqrt{\beta}\|e_L\|_{L^2(\Omega, L^2_{\omega^1, -1}(I))} \\ &\lesssim \|\partial_t(u - \Pi_M^{2,d}u)\|_{L^2(\Omega, L^2_{\omega^2, 0}(I))} + \|(-\Delta)^{\frac{\alpha}{4}}(u - \pi_N^{0,-1}\Pi_M^{2,d}u)\|_{L^2(\Omega, L^2_{\omega^1, -1}(I))} \\ &\quad + \|u - \tilde{u}_L\|_{L^2(\Omega, L^2_{\omega^1, -1}(I))} + \|(-\Delta)^{\frac{\alpha}{2}}\tilde{u}_L - (-\Delta_M)^{\frac{\alpha}{2}}\tilde{u}_L\|_{H^{-\frac{\alpha}{2}}(\Omega, L^2_{\omega^1, -1}(I))}. \end{aligned} \quad (1.63)$$

The first two terms at the right-hand side can be bounded by using Lemma 5 - 6, (1.58), (1.59) and (1.50) as follows:

$$\begin{aligned} &\|\partial_t(u - \Pi_M^{2,d}u)\|_{L^2(\Omega, L^2_{\omega^2, 0}(I))} \lesssim M^{-m} \|\|\partial_t u\|_{H^2(\Omega)} + |\partial_t u|_{\tilde{B}^m(\Omega)}\|_{L^2_{\omega^2, 0}(I)}, \\ &\|(-\Delta)^{\frac{\alpha}{4}}(u - \pi_N^{0,-1}\Pi_M^{2,d}u)\|_{L^2(\Omega, L^2_{\omega^1, -1}(I))} \\ &\leq \|(-\Delta)^{\frac{\alpha}{4}}(u - \pi_N^{0,-1}u)\|_{L^2(\Omega, L^2_{\omega^1, -1}(I))} + \|\pi_N^{0,-1}(-\Delta)^{\frac{\alpha}{4}}(u - \Pi_M^{2,d}u)\|_{L^2(\Omega, L^2_{\omega^1, -1}(I))} \\ &\lesssim \|u - \pi_N^{0,-1}u\|_{H^{\frac{\alpha}{2}}(\Omega, L^2_{\omega^1, -1}(I))} + \|u - \Pi_M^{2,d}u\|_{H^{\frac{\alpha}{2}}(\Omega, L^2_{\omega^0, -1}(I))} \\ &\lesssim N^{-n}\|\partial_t^n u\|_{H^{\frac{\alpha}{2}}(\Omega, L^2_{\omega^{n, n-1}}(I))} + M^{\frac{\alpha}{2}-m} \|\|u\|_{H^2(\Omega)} + |u|_{\tilde{B}^m(\Omega)}\|_{L^2_{\omega^0, -1}(I)}, \end{aligned}$$

and

$$\begin{aligned} \|\tilde{u}_L - u\|_{L^2(\Omega, L^2_{\omega^1, -1}(I))} &\lesssim \|\pi_N^{0,-1}(u - \Pi_M^{2,d}u)\|_{L^2(\Omega, L^2_{\omega^0, -1}(I))} + \|u - \pi_N^{0,-1}u\|_{L^2(\Omega, L^2_{\omega^0, -1}(I))} \\ &\lesssim \|u - \Pi_M^{2,d}u\|_{L^2(\Omega, L^2_{\omega^0, -1}(I))} + \|u - \pi_N^{0,-1}u\|_{L^2(\Omega, L^2_{\omega^0, -1}(I))} \\ &\lesssim M^{-m} \|\|u\|_{H^2(\Omega)} + |u|_{\tilde{B}^m(\Omega)}\|_{L^2_{\omega^0, -1}(I)} + N^{-n}\|\partial_t^n u\|_{L^2(\Omega, L^2_{\omega^{n, n-1}}(I))}. \end{aligned}$$

A combination of the above leads to

$$\begin{aligned}
& \|e_L\|_{L^2(\Omega, L^2_{\omega^0, -2}(I))} + \sqrt{\epsilon} \|e_L\|_{H^{\frac{\alpha}{2}}(\Omega, L^2_{\omega^1, -1}(I))} \lesssim M^{-m} \left\| \|\partial_t u\|_{H^2(\Omega)} + |\partial_t u|_{\tilde{B}^m(\Omega)} \right\|_{L^2_{\omega^2, 0}(I)} \\
& + N^{-n} \|\partial_t^n u\|_{H^{\frac{\alpha}{2}}(\Omega, L^2_{\omega^n, n-1}(I))} + M^{\frac{\alpha}{2}-m} \left\| \|u\|_{H^2(\Omega)} + |u|_{\tilde{B}^m(\Omega)} \right\|_{L^2_{\omega^0, -1}(I)} \\
& + N^{-n} \|\partial_t^n u\|_{L^2(\Omega, L^2_{\omega^n, n-1}(I))} + \|(-\Delta)^{\frac{\alpha}{2}} \tilde{u}_L - (-\Delta_M)^{\frac{\alpha}{2}} \tilde{u}_L\|_{H^{-\frac{\alpha}{2}}(\Omega, L^2_{\omega^1, -1}(I))}.
\end{aligned} \tag{1.64}$$

We can estimate the last term by using an argument similar to that for the proof in Theorem 1.3.1,

$$\begin{aligned}
& \|(-\Delta)^{\frac{\alpha}{2}} \tilde{u}_L - (-\Delta_M)^{\frac{\alpha}{2}} \tilde{u}_L\|_{H^{-\frac{\alpha}{2}}(\Omega, L^2_{\omega^1, -1}(I))} \\
& \leq \|(-\Delta)^{\frac{\alpha}{2}} (\tilde{u}_L - u) + (-\Delta)^{\frac{\alpha}{2}} u - (-\Delta_M)^{\frac{\alpha}{2}} \tilde{u}_L\|_{H^{-\frac{\alpha}{2}}(\Omega, L^2_{\omega^1, -1}(I))} \\
& \leq \|(-\Delta)^{\frac{\alpha}{2}} (\tilde{u}_L - u)\|_{H^{-\frac{\alpha}{2}}(\Omega, L^2_{\omega^1, -1}(I))} + \|(-\Delta)^{\frac{\alpha}{2}} u - (-\Delta_M)^{\frac{\alpha}{2}} \tilde{u}_L\|_{H^{-\frac{\alpha}{2}}(\Omega, L^2_{\omega^1, -1}(I))}
\end{aligned} \tag{1.65}$$

By (1.59) and (1.50), the bound of first term in (1.65) is given by

$$\begin{aligned}
& \|(-\Delta)^{\frac{\alpha}{2}} (\tilde{u}_L - u)\|_{H^{-\frac{\alpha}{2}}(\Omega, L^2_{\omega^1, -1}(I))} \lesssim \|\tilde{u}_L - u\|_{H^{\frac{\alpha}{2}}(\Omega, L^2_{\omega^1, -1}(I))} \\
& \lesssim N^{-n} \|\partial_t^n u\|_{H^{\frac{\alpha}{2}}(\Omega, L^2_{\omega^n, n-1}(I))} + M^{\frac{\alpha}{2}-m} \left\| \|u\|_{H^2(\Omega)} + |u|_{\tilde{B}^m(\Omega)} \right\|_{L^2_{\omega^0, -1}(I)}.
\end{aligned} \tag{1.66}$$

Then, by Lemma 4, we estimate the last term of (1.65) by

$$\begin{aligned}
& \|(-\Delta)^{\frac{\alpha}{2}} u - (-\Delta_M)^{\frac{\alpha}{2}} \tilde{u}_L\|_{H^{-\frac{\alpha}{2}}(\Omega, L^2_{\omega^1, -1}(I))} \lesssim d_u^\alpha \|(-\Delta)u - (-\Delta)\tilde{u}_L\|_{H^{-\frac{\alpha}{2}}(\Omega, L^2_{\omega^1, -1}(I))} \\
& \lesssim d_u^\alpha \|\Delta(u - \pi_N^{0, -1}u)\|_{H^{-\frac{\alpha}{2}}(\Omega, L^2_{\omega^1, -1}(I))} + d_u^\alpha \|\pi_N^{0, -1}\Delta(u - \Pi_M^{2, d}u)\|_{H^{-\frac{\alpha}{2}}(\Omega, L^2_{\omega^1, -1}(I))} \\
& \lesssim d_u^\alpha \|u - \pi_N^{0, -1}u\|_{H^{2-\frac{\alpha}{2}}(\Omega, L^2_{\omega^1, -1}(I))} + d_u^\alpha \|u - \Pi_M^{2, d}u\|_{H^{2-\frac{\alpha}{2}}(\Omega, L^2_{\omega^1, -1}(I))} \\
& \lesssim d_u^\alpha N^{-\frac{\alpha}{2}n} \|\partial_t^n u\|_{H^{2-\frac{\alpha}{2}}(\Omega, L^2_{\omega^n, n-1}(I))} + d_u^\alpha M^{\frac{\alpha}{2}(2-\frac{\alpha}{2}-m)} \left\| \|u\|_{H^2(\Omega)} + |u|_{\tilde{B}^m(\Omega)} \right\|_{L^2_{\omega^0, -1}(I)}.
\end{aligned} \tag{1.67}$$

On the other hand, we have $u - u_L = u - \tilde{u}_L + e_L$. Then, using Lemma 6 - 1.50, again yields for $\alpha \neq 1$,

$$\begin{aligned}
& \|(-\Delta)^{\frac{\alpha}{4}} (u - \tilde{u}_L)\|_{L^2(\Omega, L^2_{\omega^1, -1}(I))} \\
& \lesssim N^{-n} \|\partial_t^n u\|_{H^{\frac{\alpha}{2}}(\Omega, L^2_{\omega^n, n-1}(I))} + M^{\frac{\alpha}{2}-m} \left\| \|u\|_{H^2(\Omega)} + |u|_{\tilde{B}^m(\Omega)} \right\|_{L^2_{\omega^0, -1}(I)},
\end{aligned}$$

and

$$\|u - \tilde{u}_L\|_{L^2(\Omega, L^2_{\omega^{0,-1}}(I))} \lesssim M^{-m} \left(\|u\|_{H^2(\Omega)} + \|u|_{\tilde{B}^m(\Omega)}\|_{L^2_{\omega^{0,-1}}(I)} + N^{-n} \|\partial_t^n u\|_{L^2(\Omega, L^2_{\omega^{n,n-1}}(I))} \right).$$

Consequently, the desired result follows from above estimates, the triangle inequality and (1.67). ■

1.4 Numerical results for linear fractional equations

In this section, we present some numerical results obtained by the spectral method (1.17) for (1.1) and the space-time spectral method (1.25) for (1.22).

Example 1 (*with known smooth exact solutions*)

We consider first the following smooth exact solutions for (1.1) with homogeneous Dirichlet boundary conditions:

$$u(x) = \varphi_k(x) \quad \text{and} \quad u(x, y) = \varphi_k(x)\varphi_{k'}(y), \quad k, k' = 0, 1, 2, \dots, \quad (1.68)$$

where $\{\lambda_k, \varphi_k\}_{k \geq 0}$ denote the eigenpairs of spectral Laplacian operator on $(-1, 1)$, and have explicit formulas

$$\varphi_k(x) = \sin(\sqrt{\lambda_k}(x+1)), \quad \lambda_k = \left(\frac{(k+1)\pi}{2}\right)^2. \quad (1.69)$$

The corresponding source term can be calculated by using the definition of spectral fractional Laplacian

$$f(x) = \lambda_k^{\frac{\alpha}{2}} \varphi_k(x), \quad f(x, y) = (\lambda_k + \lambda_{k'})^{\frac{\alpha}{2}} \varphi_k(x)\varphi_{k'}(y).$$

In Fig 1.1, we list the $H^{\frac{\alpha}{2}}$ -errors in semi-log scale with $\alpha = 1.8$. The plots in Fig 1.1 indicate the numerical errors decay exponentially. This is consistent with the theoretical result in Theorem 3.1 which predicts that for this smooth solution, the convergence rate is faster than any algebraic rate.

Example 2 (*with a unknown weakly singular solution*)

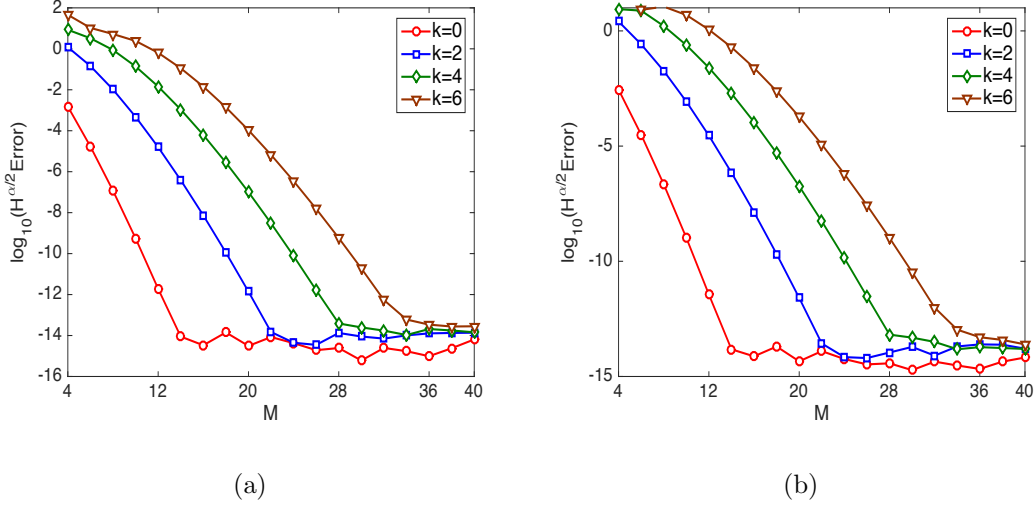


Figure 1.1.: (a). $H^{\frac{\alpha}{2}}$ -error in semi-log scale of (1.1) with $u(x) = \varphi_k(x)$; (b). $H^{\frac{\alpha}{2}}$ -error in semi-log scale of (1.1) with $u(x, y) = \varphi_k(x)\varphi_k(y)$.

We consider now the problem (1.1) with $f(x) = 1$ and homogeneous Dirichlet boundary conditions. Since the exact solution is unknown, we use the truncation of the exact solution

$$u(x) \approx \sum_{j=0}^{10000} \lambda_j^{-\frac{\alpha}{2}} \langle 1, \varphi_j \rangle \varphi_j(x), \quad (1.70)$$

as the reference solution, where $\{\lambda_j, \varphi_j\}_{j \geq 0}$ are given in (1.69). It is known that the exact solution has weak singularities at the boundary [10]. In the left of Fig 1.2, we plot the $H^{\frac{\alpha}{2}}$ -error of our Legendre spectral method in log-log scale. We observe that the convergence rate is clearly $O(M^{-1-\alpha})$. As a comparison, we also plot the $H^{\frac{\alpha}{2}}$ -error of the Fourier spectral method [1] in the right of Fig 1.2. We observe that the Fourier spectral method converge at $O(M^{-0.5-\alpha/2})$, which means the convergence rate of our method is twice that of Fourier spectral method under $H^{\frac{\alpha}{2}}$ -norm.

We plot in Fig 1.3 the L^2 -error of our Legendre spectral method in log-log scale. While one can not use the usual duality argument to improve the error estimate in L^2 -norm, we do observe that the L^2 -error decays as $O(M^{-1-2\alpha})$, an improvement of order α over the $H^{\frac{\alpha}{2}}$ -error.

Example 3 (a fractional diffusion equation)

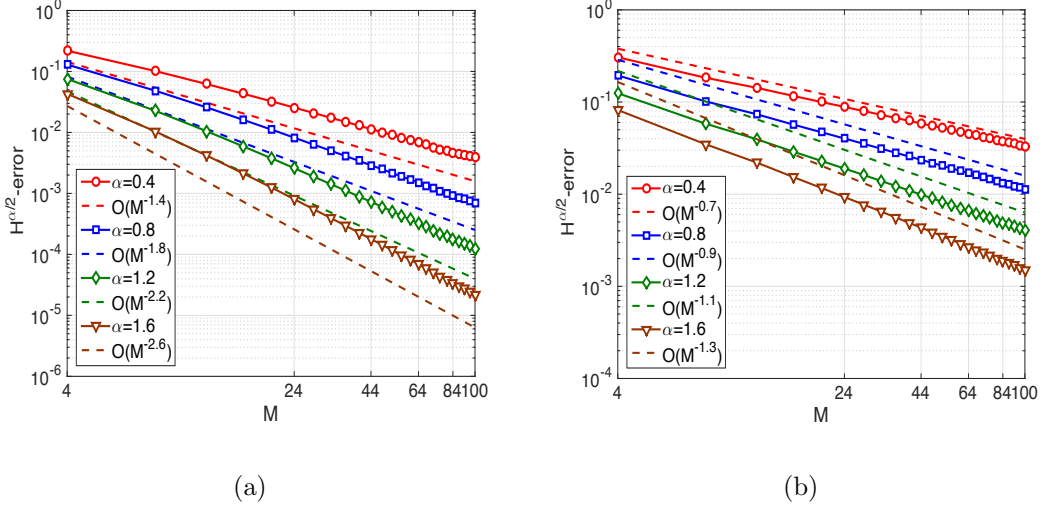


Figure 1.2.: (a). $H^{\frac{\alpha}{2}}$ -error, in log-log scale, of our method for (1.1) with right hand side term $f(x) = 1$; (b). $H^{\frac{\alpha}{2}}$ -error, in log-log scale, of Fourier spectral method in [1] for (1.1) with right hand side term $f(x) = 1$.

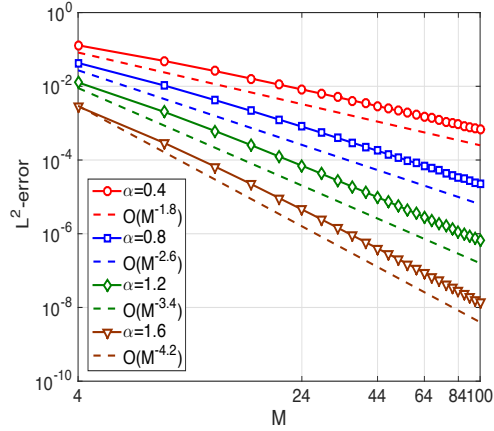


Figure 1.3.: L^2 -error, in log-log scale, of our method for (1.1) with right hand side term $f(x) = 1$.

As the last example, we consider the following fractional diffusion equation

$$\partial_t u + (-\Delta)^{\frac{\alpha}{2}} u = 0, \quad (1.71)$$

with the initial conditions: (a) a Gaussian like function $e^{-25x^2/(1-x^2)}$ (with homogeneous Dirichlet boundary condition); (b) a sigmoid exhibiting sharper gradients $\tanh(25x/\sqrt{1-x^2})$ (with Neumann boundary condition). The numerical solution computed with our space-time spectral method with $M = N = 100$ at $T = 0.1$ are plotted in Figure 1.4, and the black dotted line is the initial conditions. We observe that, as expected, the diffusion rate decreases as the fractional power α decreases.

In Fig 1.5, we list the L^2 -errors of (1.71), compared with an "exact" solution computed with a refined mesh, in semi-log scale against various $M = N$ at $T = 0.1$. We observe an exponential convergence with respect to $M = N$ for our space-time spectral method, but as α decreases, the rate of convergence also decreases. This is due to the fact that, with the given initial conditions, the solution is essentially smooth in the time interval that we considered.

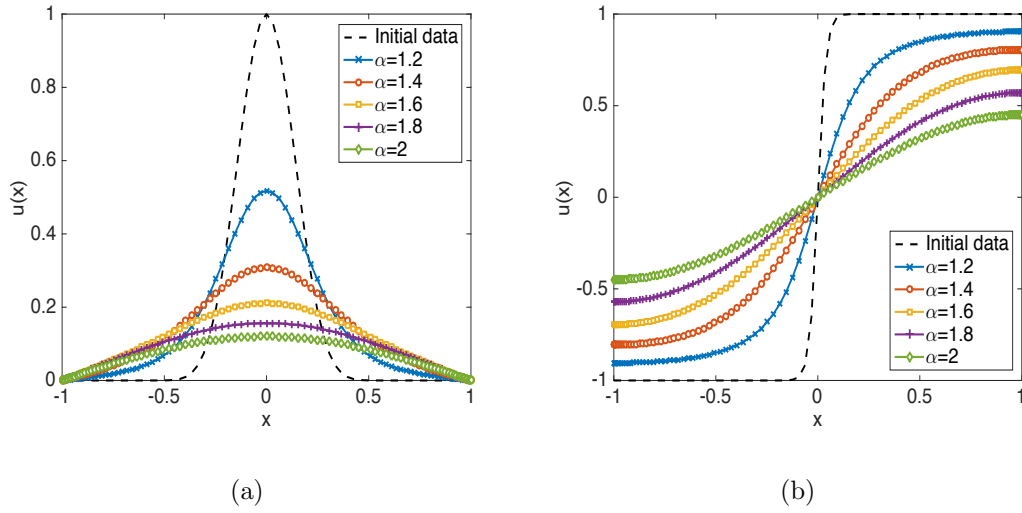


Figure 1.4.: Numerical solution of fractional heat equation (1.71) for different α : (a) initial data: $e^{-25x^2/(1-x^2)}$; (b) initial data: $\tanh(25x/\sqrt{1-x^2})$.

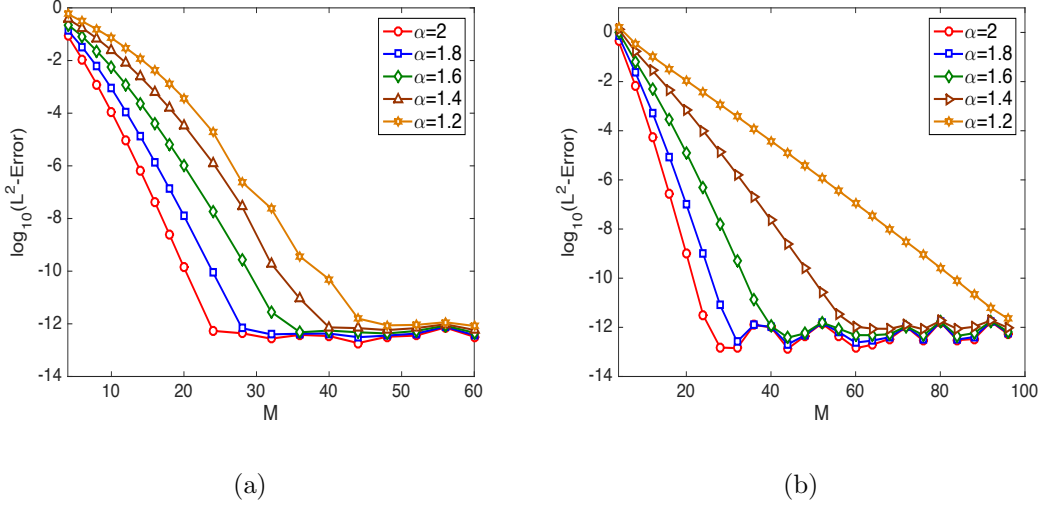


Figure 1.5.: L^2 -error for (1.71) at $T = 0.1$ for different α ; (a) initial data $u_0 = e^{-25x^2/(1-x^2)}$; (b). initial data $u_0 = \tanh(25x/\sqrt{1-x^2})$.

1.5 Application to nonlinear fractional equations

The method presented in Section 2 can be used as an effective preconditioner in the Jacobian-free Newton-Krylov algorithm [28] to solve nonlinear fractional equations (1.2). More precisely, the linearized (about a function w) equation of (1.2) is:

$$\mathcal{L}_w v := \partial_t v + \epsilon^2 (-\Delta)^{\frac{\alpha}{2}} v + \mathcal{N}'(w)v = 0. \quad (1.72)$$

Hence, with a suitable constant β , \mathcal{L}_0 defined by

$$\mathcal{L}_0 v := \partial_t v + \epsilon^2 (-\Delta)^{\frac{\alpha}{2}} v + \beta v$$

will be an effective preconditioner for \mathcal{L}_w . Since $v \rightarrow \mathcal{L}_w v$ and $v \rightarrow \mathcal{L}_0^{-1} v$ can be efficiently performed in the space-time approximation space described in Section 2, we can solve (1.2) efficiently with the the Jacobian-free Newton-Krylov algorithm. In addition, the following strategies are used:

- The convergence rate of the Newton-Krylov iteration depends on the quality of the initial guess. We use the following simple semi-implicit scheme to generate such an initial guess: Find $v_M^{n+1} \in V_M^d$ s.t.

$$\left(\frac{v_M^{n+1} - v_M^n}{t^{n+1} - t^n}, w_M\right) + (\epsilon^2(-\Delta)^{\frac{\alpha}{2}} v_M^{n+1}, w_M) + (N(v_M^n), w_M) = 0 \quad \forall w_M \in V_M^d, \quad (1.73)$$

where t^k are the scaled Legendre-Gauss-Radau points. The above equation can be easily solved by using the Fourier-like basis of V_M^d .

- To integrate the nonlinear problems (1.2) for a large time interval $[0, T]$, we can first divide $[0, T]$ into a number of smaller intervals $[0, T] = \cup_{i=1}^K [T_{i-1} - T_i]$, and apply the space-time spectral method on each interval using the final solution at the interval $[T_{i-1} - T_i]$ as the initial condition for the interval $[T_i - T_{i+1}]$.

1.5.1 Fractional FitzHugh-Nagumo model

The FitzHugh-Nagumo model is a system of reaction-diffusion equations describing wave propagation in an excitable medium. It takes the following form (with $\alpha = 2$):

$$\begin{aligned} \partial_t u &= -K_u(-\Delta)^{\frac{\alpha}{2}} u + u(1-u)(u-a) - v, \\ \partial_t v &= \epsilon(\beta u - \gamma v - \delta), \\ \partial_n u|_{\partial\Omega} &= \partial_n v|_{\partial\Omega} = 0, \end{aligned} \quad (1.74)$$

where u is a "fast" variable which describes membrane potential of a cell and v is a "slow" variable which connects with the medium conductivity by inverse ratio. Here, we also consider the fractional FitzHugh-Nagumo model, represented by the above system with $\alpha \in (1, 2)$, which takes into accounts non-local interactions [1].

Let $\Omega = (-1, 1)^2$, and set the parameters in (1.74) to be $a = 0.1, \epsilon = 0.01, \beta = 0.5, \gamma = 1, \delta = 0$. These parameters are considered in [1], and they lead to stable patterns in the system in the form of re-entrant spiral waves. In our simulations, the trivial state $(u, v) = (0, 0)$ was perturbed by setting the lower-left quarter of

the domain to $u = 1$ and the upper half part to $v = 0.1$, which allows the initial condition to rotate clockwise to generate spiral patterns. We discretize the spatial domain using 256×256 points, and compute the solution up to $T = 2000$ so that the solution reaches the steady state.

The steady state rotating solutions at $t = 2000$, with different diffusion coefficient K and fractional order α , are presented in Fig. 1.6. we observe similar behaviors as reported in [1]. Namely, as α decreases, the width of the excitation wavefront decreases (cf. the top row of Fig. 1.6), which also happens as we decrease the diffusion coefficient (cf. the bottom row of Fig. 1.6). However, there is also a significant difference between our simulation with homogeneous Neumann boundary conditions and the simulation in [1] with a periodic boundary condition: in our simulations, the rotation angles are more aligned with the boundary which reflects the effect of the homogeneous Neumann boundary conditions, while in their simulations the curvatures are essentially uniform.

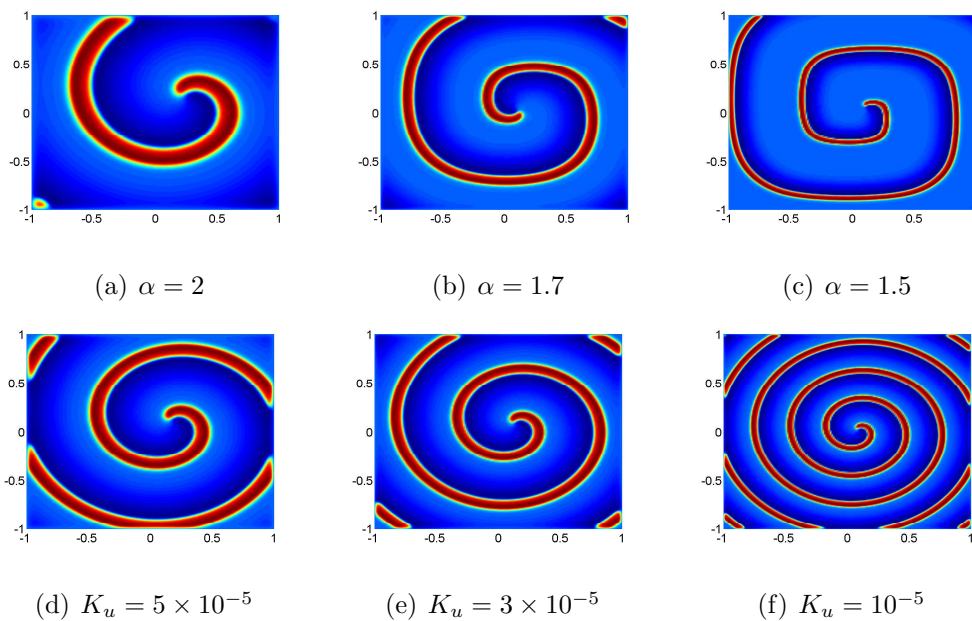


Figure 1.6.: Spiral wave in FitzHugh-Nagumo model for various α and K_u ; top: $K_u = 10^{-4}$; bottom: $\alpha = 1.7$.

1.5.2 Fractional Allen-Cahn equation

The Allen-Cahn equation is a reaction-diffusion equation describing the process of phase separation in crystalline solids. It takes the following form (with $\alpha = 2$):

$$\partial_t u + \epsilon^2 (-\Delta)^{\frac{\alpha}{2}} u + (u^2 - 1)u = 0. \quad (1.75)$$

The fractional Allen-Cahn equation (with $\alpha \in (1, 2)$) has received some attention recently [3, 29, 30]. In the following, we shall present some numerical results for both the regular and fractional Allen-Cahn equation. In all computations below, we set $\epsilon = 0.1$.

Solution transition presentation

We then give an example to show the transition process of the solution, see, e.g., Fig 1.7. In our example, $x \in [-1, 1]$, $t \in [0, 3000]$ and 128×128 points used to discretize the region. Here initial solution is selected as $u(x, 0) = \frac{1}{2} \sin(\frac{3\pi}{2}x)(\cos(\pi x) - 1)$. As mentioned in [1], in $\alpha = 2$ and 1.7 cases, the initial solution evolves to an unstable intermediate equilibrium and then quickly transform to a settlement with one interface. However in $\alpha = 1.4$ case, the unstable state lasts longer and when α continues decreasing, the final equilibrium will become two waves. In Figure 1.8 we also plot the initial transition of the solution for $\alpha = 1.4$, where $t \in [0, 10]$. This figure shows the sudden transform of the initial state which may not be observed in Fig. 1.7 because of the large time scale.

width of 1-D interfacial layer

It is well-known that the parameter ϵ represents the interfacial width of the regular Allen-Cahn equation, and that the interfacial width decreases as α decreases in the fractional Allen-Cahn equation [3, 29, 30]. More precisely, it has been observed com-

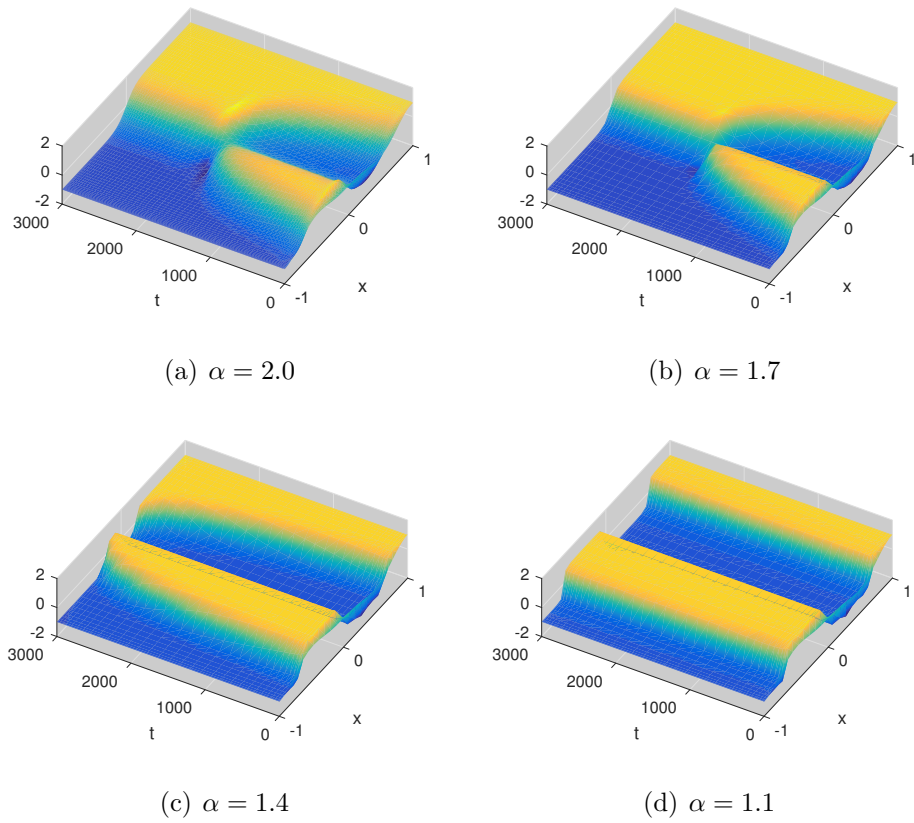


Figure 1.7.: Solution transitions in Allen-Cahn equation with $t \in [0, 3000]$ for various α .

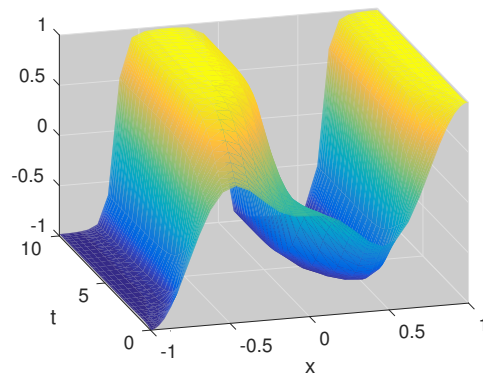


Figure 1.8.: Initial transition of the Allen-Cahn equation with $t \in [0, 10]$.

putationally [30] in and proved in [3] that the interfacial width behaves like $O(\epsilon^{1/\alpha})$. In this example, We take the initial solution to be

$$u_0(x) = \begin{cases} 1, & 0 \leq x \leq 1, \\ -1, & -1 \leq x < 0, \end{cases} \quad (1.76)$$

and compute the solution up to time=1 using $N = 64$, $M = 1024$ in our space-time spectral method. In the left of Fig. 1.9, we plot the interfacial layer for different α at time $T = 1$. And the thickness L is defined to be $\{x | -1 < x < 1 \text{ and } |u(x)| < 0.99\}$ (as is shown in Fig 1.9 (a)). In the right of Fig. 1.9, we plot the interfacial width L with different α and ϵ , and we observe indeed that as the interfacial width decreases as α decreases, and behaves like $L = O(\epsilon^{1/\alpha})$ [3, 30].

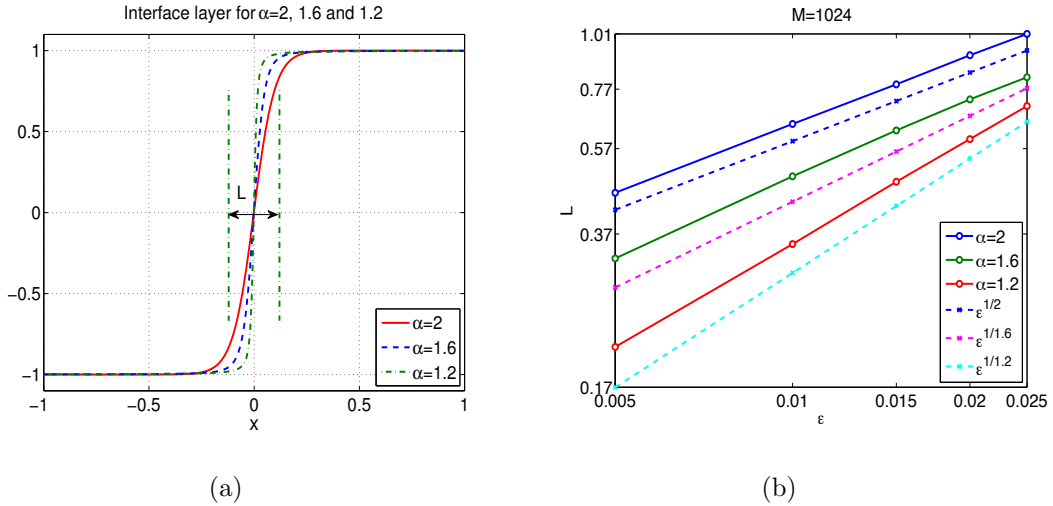


Figure 1.9.: (a) Interfacial layers with different α ; (b) Layer width L against ϵ for different values of α .

2D kissing balls

We simulate the coalescence of two kissing bubbles, i.e. with the following initial condition

$$u_0(x, y) = \begin{cases} 1, & (x + \frac{1}{4})^2 + y^2 \leq \frac{1}{4} \text{ or } (x - \frac{1}{4})^2 + y^2 \leq \frac{1}{4}, \\ -1, & \text{otherwise.} \end{cases} \quad (1.77)$$

Here we take $\epsilon = 0.1$, $M = 128$. In order to illustrate the effect of changing the value of fractional derivative α on the character of the solution of fractional Allen-Cahn equation, we present plots of the solution for different values of fractional order α at various times in Fig. 1.10 . We observe that in all cases, as time evolves, the two bubbles coalesce into a single bubble but then shrink and disappear. This is because Allen-Cahn equation doesn't conserve mass. On the other hand, when α decreases to fractional case, the shrinking speed becomes slower.

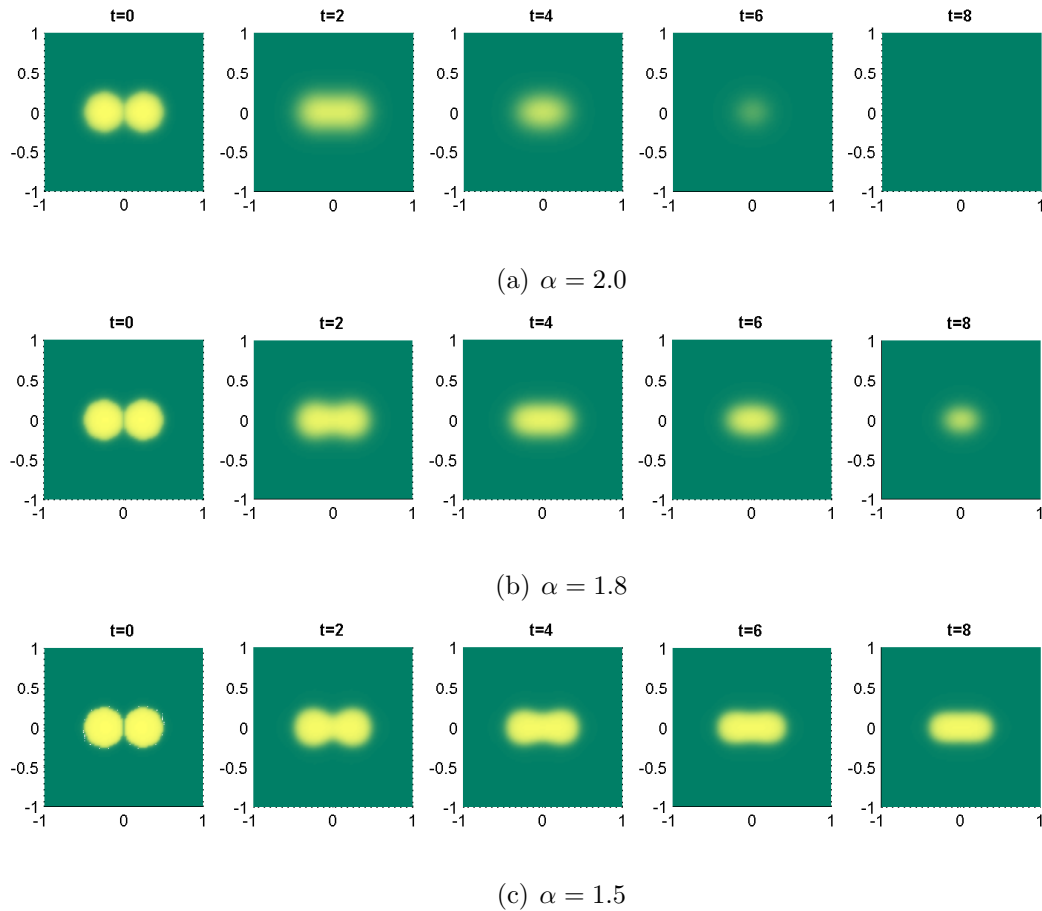


Figure 1.10.: Evolution of solution of fractional Allen-Cahn equation with initial condition (1.77) for various fractional order α .

Velocity of 2-D moving interface

As suggested in [31], in order to predict quantitatively the kinetics of microstructural evolution, we have to calculate not only the accurate equilibrium profiles but also the accurate velocity of a moving interface. To compare the influence of fractional order α on the velocity of a moving interface, we consider the two dimensions Allen-Cahn equation with system size 128×128 in domain $[-1, 1]^2$. In Fig. 1.11 we plotted the contour near $u = 0$ which captures the movement of the interface. At time $t = 0$, there is a circular interface boundary with a radius of 74. The order parameter values inside the circle are assigned to be +1 and -1 outside. Such a circular interface is unstable and will shrink under the mean curvature. In Fig. 1.12 we compute the radius of the inner circle with respect to time t for different α . It is numerically observed that the radius of the circle shrinks as $R_0^2 - R^2 = O(t^{\alpha/2})$ where R_0 is the initial radius.

1.6 Stochastic pde with fractional laplacian

1.6.1 Formulation

In this section we present one application of our algorithm in stochastic PDE with polynomial chaos. In this problem setting the fractional order α is a random variable satisfying certain distribution. The problem we are going to deal with is:

$$\Delta_x^{(y+1)/2} u(x, y) = f(x, y) \quad (1.78)$$

Here $y \in [-1, 1]$ and satisfy uniform distribution for simple calculation. Following our previous definition of fractional Laplacian, we have

$$\Delta^{\alpha/2} \Phi_i = \lambda^{\alpha/2} \Phi_i$$

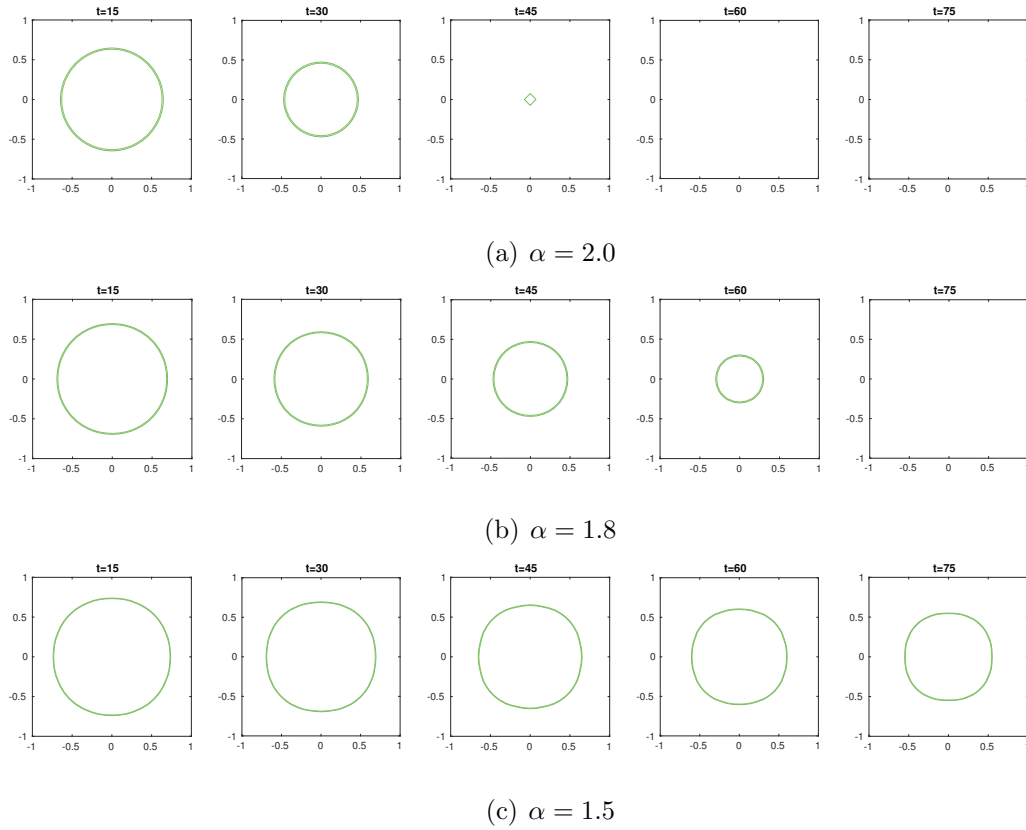


Figure 1.11.: Temporal evolution of circular domain for various α .

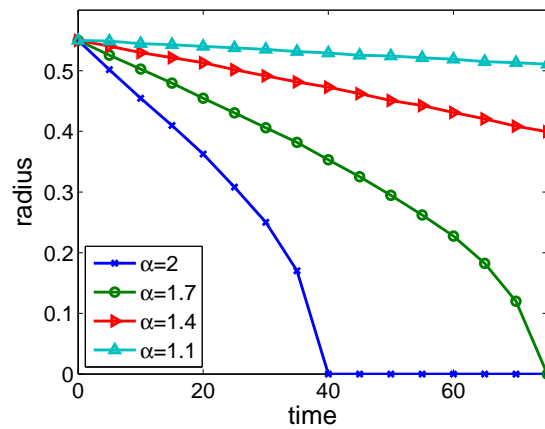


Figure 1.12.: Radius of the circular domain as a function of time obtained with different fractional order α using time step $\Delta t = 0.5$.

where $\Phi_i(x)$ are the eigenfunction of Laplacian operator. As mentioned in [32], with uniform distribution, one should use Legendre polynomials as the basis for stochastic variable. Thus we have:

$$\Delta_x^{(y+1)/2} u_N(x, y) = \sum_{i=1}^M \sum_{j=1}^N u_{ij} \lambda_i^{(y+1)/2} \Phi_i(x) L_j(y) = f(x, y)$$

Then we take expectation of the equation and get the following inner product:

$$(f(x, y), \Phi_p(x) L_q(y)) = \sum_{i=1}^M \sum_{j=1}^N u_{ij} (\Phi_i(x), \Phi_p(x)) (\lambda_i^{(y+1)/2} L_j(y), L_q(y)) \quad (1.79)$$

$$= \sum_{j=1}^N u_{pj} (\lambda_p^{1-(y+2)/2} L_j(y), L_q(y)) \quad (1.80)$$

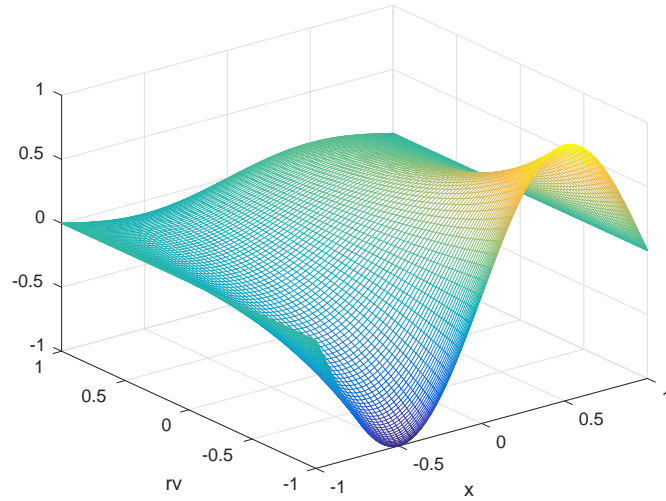
1.6.2 Numerical Examples

We test the solution with: $f(x, y) = \sin(\pi x)$. In Fig. (1.13) a, the stochastic solution is given, the y axis is the random variable and one could reach different solution when y varies. Fig. (1.13) b is the expectation of the function $u(\cdot, Y = y)$ which would be the exact solution of the FPDE.

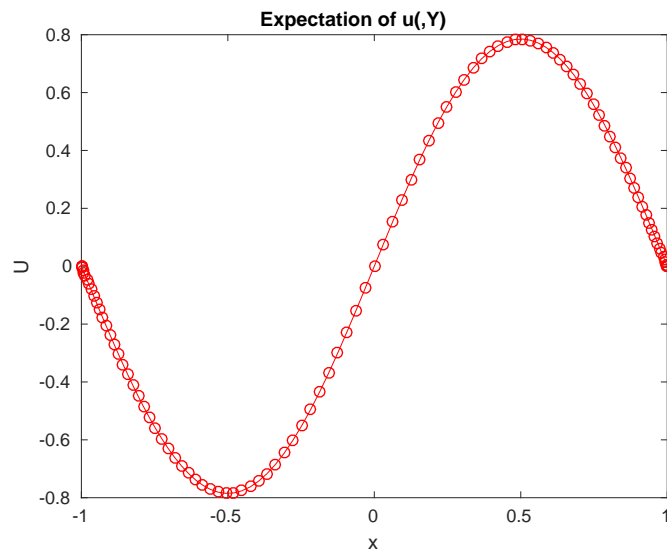
1.7 Conclusion

In this paper, we developed efficient spectral methods for solving PDEs with fractional Laplacians, and carried out rigorous error analysis for them. The methods are based on the Fourier-like basis functions which are the eigenfunctions of the discrete fractional Laplacian with non periodic boundary conditions. Therefore, the nonlocal fractional Laplacian operator can be naturally handled, leading to simple, efficient and accurate numerical algorithms. Our numerical experiments demonstrated that our algorithms are robust, efficient and accurate for a variety of linear and nonlinear PDEs with fractional Laplacian.

The analytical framework we introduced to estimate the errors between fractional Laplacian and discrete fractional Laplacian is not restricted to spectral methods and



(a) Stochastic solution



(b) Exact solution

Figure 1.13.: Stochastic solution of fractional PDE

can be used to analyze numerical approximations of fractional Laplacian by using other Galerkin type approximations such as finite-element methods.

We only considered rectangular domains in this paper. However, by using a recently developed spectral method for general domains [17], we expect to be able to extend the approach proposed here to problems in more general domains.

2. EFFICIENT NUMERICAL SCHEME FOR COMPUTING STABILITY OF QUASI-CRYSTALLINE INTERFACE

2.1 Introduction

When we mention a modulated structure in space, for a long time in the history we think of a parallelepiped, typically cubic, unit cell occurring repeatedly in the space. A few structures easy to imagine include lamellae, cylinder, and sphere structures. Some complex structures are also observed, such as gyroid structure. Despite they might seem fancy, we can always cut a unit cell from the structure. These structures have been found in various systems, including metals, colloids, block copolymer, liquid crystals, etc. [33–35]. Mathematically, they can be described by periodic functions in \mathbb{R}^3 . It was not until the 1980s that the first discovery of a 5-fold symmetry structure in a rapidly cooled Al-Mn alloy is reported [36], which is recognized as quasicrystals years later. Since then, quasicrystals are observed in several other physical systems [37–39]. In quasicrystals, local morphology can be found repeatedly, but one is not able to find a unit cell. To describe quasicrystals, periodic functions are no longer appropriate and have been extended to quasiperiodic functions, which can be generated by the limitation of a periodic function in \mathbb{R}^n onto an \mathbb{R}^3 subspace. In this sense, a periodic structure can be regarded as special cases of quasicrystals. The most interesting fact about quasicrystals is that they can form symmetries not allowed by crystallographic space groups, such as five-, eight-, ten- and twelve-fold rotations and icosahedral symmetries [40–45].

Studies of quasicrystals have been focusing on the structures themselves. For the phase transitions involving quasicrystals, we currently know very little. Phase transitions can typically occur in two different ways. One is that one phase loses

stability and transforms into another as a whole. The other is that two phases coexist for some time and the change mainly happens in the transition zone. In the latter, the transition zone is understood as an interface between two structures. The driving force of the phase transitions comes from the interface where excess energy is stored. When modulated phases are involved, the morphology of interfacial more complex, since the modulated phase possesses different intrinsic structures with different symmetries. For many materials consisting of modulated phases, the morphology of interface has a great effect on physical properties, such as elasticity and conductivity.

There are different viewpoints held on the interface. In many works, the interface is regarded as a transient state [46–48]. One could choose a finite domain, let two phases occupy part of the domain, and focus on the dynamics showing the movement of the interface. Studies of this kind are common for the interface between disordered phases such as water-vapor interface. The interface between modulated phases, however, usually has a long lifetime and is dependent on relative position and orientation. It is desirable to view the interface as a steady state under some constraints, so as to figure out the mechanism of connecting two modulated structures with different symmetries. From the above setting, it is difficult to control the relative position and orientation, and typically multiple structures are obtained that could interplay each other, making it difficult for us to identify the mechanism. Therefore, we choose the framework proposed in [49]. In that framework, the whole space is divided into three regions by two parallel planes, the two phases, with each phase being displaced or rotated, occupy the two on the sides, and a transition zone occurs in between. After posing the two phases as above, one then chooses the appropriate function space and boundary conditions that are able to describe both phases and constrain the relative position and orientation. In this function space, one could then let the system evolve to a local minimizer, typically under a gradient flow, to obtain the process for the interface to reach the optimal structure. Under this framework, we would understand the mechanism more clearly.

Although the framework in [49] is clear, the numerical methods are not carefully designed previously. Only the special cases are examined where two phases are matched with common periodicity, and the numerical schemes adopted are naive. When quasicrystals are put into consideration, further difficulties arise. The first one is that high-order spatial derivatives will likely be involved, which is common in the models of quasicrystals. We use the Lifschitz–Petrich free energy [50], a model system that contains up eighth-order spatial derivatives. The free energy requires conservation of mass, so the H^{-1} gradient flow will be studied. As a result, we need to solve a PDE with tenth-order spatial derivatives. To reach the accuracy that will not destruct the quasicrystalline structures, it is crucial to choose an appropriate spatial discretization. Problems of this kind have been studied for capturing the bulk profile [51], where one either needs to use Fourier series of higher dimensional space, or approximate by the Fourier series in three-dimensional space with a carefully chosen length of period. In the system for computing the interfacial structure, however, the Fourier series cannot be adopted directly. This will bring a second difficulty, that is, to specify the boundary conditions numerically. We need to displace and rotate its profile into a given position and orientation, then find the boundary conditions and set them for the interface system. These two steps are trivial for PDE, but become a problem for the discretized system. For the special cases where common periodicity exists, this problem could be evaded by using the same spatial discretization for both the bulk profile and the interface system. However, this is no longer applicable for quasiperiodic interface. Since the spatial discretization will be different, when implementing the rotation and transformation between different discretization, we also need to guarantee reasonable accuracy that is able to keep the two phases on both sides. A third difficulty brought by the high-order spatial derivatives is for the time discretization of the gradient flow that requires energy stability. An ideal time discretization would combine energy stability, efficiency and easy implementation.

Taking these difficulties into consideration, the finite difference and finite element methods that are commonly used in previous works [52–55] are not very convenient,

because for solving high order PDEs the long grid stencils for high order derivative discretization will have a problem on accuracy. Spectral-collocation method is also not appropriate as the quadratures involving derivatives at the boundary points are difficult to derive [56]. We propose to use the spectral methods for spatial discretization, which are accurate enough to describe the quasiperiodic structures and are convenient to implement rotation and specify boundary conditions. Spectral methods have proved to be efficient and accurate for solving PDEs involving high order derivatives in simple geometries, which have been applied to the third-order KdV equation [57] and some fourth-order equations [58, 59]. Spectral methods embrace the advantage that the resulting linear system is sparse and well-conditioned, and in some cases fast direct solvers are available. Theoretical analysis and numerical results have shown the accuracy and efficiency [57]. For the interface system, we propose to use mixing of Fourier series and generalized Jacobi polynomials as spatial discretization. It is worth pointing out that when dealing with quasiperiodicity, to describe a system with certain physical dimension, usually the dimension of computation is necessarily higher (cf. [51], where four-dimensional Fourier series are needed for two-dimensional dodecagonal structures). The system to be solved numerically could become very large if we do not carefully control the size of spatial discretization. The spectral methods are able to reach adequate accuracy with a relatively small the number of variables in each dimension. Thus, spectral methods can greatly reduce the size of the discretized system, thereby improve the efficiency.

For the time discretization, we use the SAV approach proposed recently for gradient flows [60, 61]. The SAV approach leads to numerical schemes linearly implicit with unconditional energy stability. Furthermore, the resulting linear system has constant coefficients that is easy to solve efficiently. This approach is extremely suitable when the free energy of the gradient flow has a dominant quadratic part, which is exactly the case for the Lifshitz–Petrich energy. Together with the spectral methods for spatial discretization, the linear system is block diagonalized so that we can solve

without much effort. For the Lifshitz–Petrich energy, the convergence of the time discretization has actually been covered by the analysis in [62].

On applying the above numerical scheme for the quasicrystal interface, we examine some cases that are not dealt with previously. In particular, apart from the interface with a periodic structure, we focus on the quasiperiodic cases. These cases include the interface between periodic phases without common periodicity, or the interface involving quasicrystals. Some novel structures are presented. From these examples, we can see the potential of applying our scheme to deal with a larger class of free energy functionals, such as free energy characterizing long-range pairwise interactions proposed for 3D icosahedral quasicrystals [43].

The rest of the paper is organized as follows. In Section 2, we describe the basic setting and discretization. We introduce the Lifshitz–Petrich free energy and the function space for quasicrystal solutions, followed by explaining the function space and boundary conditions for the interface system. Then, we discretize using the SAV scheme, followed by spatial discretization. In two of the three directions we use the Fourier series. For the other direction, we explain how to construct an approximation space by Jacobi polynomials. Significant details in the implementation are explained. Numerical results of interfacial structures will be presented in Section 3. Concluding remarks are given in Section 4.

2.2 Model and numerical algorithms

2.2.1 Lifshitz–Petrich model and quasicrystal solutions

The free energy for modulated phases might originate from Brazovskii [63], known as the Landau–Brazovskii model, and is later studied in different context [64–66]. By modifying the Landau–Brazovskii model, some free energy functionals are proposed for quasicrystals [50, 67, 68]. We will consider the Lifshitz–Petrich (LP) free energy

proposed in [50] and has received much attention. The free energy density in a domain $\Omega \subseteq \mathbb{R}^3$ is given by

$$E[\phi(\mathbf{r}); \Omega] = \frac{1}{V(\Omega)} \int_{\Omega} \left\{ \frac{c}{2} [(\Delta + 1)(\Delta + q^2)\phi]^2 - \frac{\epsilon}{2}\phi^2 - \frac{\alpha}{3}\phi^3 + \frac{1}{4}\phi^4 \right\} d\mathbf{r}, \quad (2.1)$$

where $\mathbf{r} = (x, y, z)^t$, $V(\Omega)$ is the volume of Ω , and $q > 0$, $c > 0$, ϵ , α are phenomenological parameters. This free energy is simple while is able to describe many modulated phases including quasicrystals.

The bulk profile of a phase is obtained by minimizing the functional (2.1) when letting $\Omega \rightarrow \mathbb{R}^3$. If the phase is periodic with the unit cell Ω_0 , we can verify that

$$\lim_{\Omega \rightarrow \mathbb{R}^3} E[\phi(\mathbf{r}); \Omega] = E[\phi(\mathbf{r}); \Omega_0], \quad (2.2)$$

which is the energy density in the unit cell. However, the limit on the left-hand side is also suitable for quasicrystals. The free energy is characterized by the first term involving derivatives. We could see it by taking a simple wave $\cos(\mathbf{p} \cdot \mathbf{r})$ into the energy where \mathbf{p} is a constant vector. The first term yields

$$\frac{c}{4}(1 - |\mathbf{p}|^2)^2(q^2 - |\mathbf{p}|^2)^2,$$

indicating that this term favors $|\mathbf{p}| = 1$ or $|\mathbf{p}| = q$. This term acts as a role of wavelength selection that damps out all modes except those near the above two spherical surface.

No matter for periodic or quasiperiodic phases, the profile could be written in the following form,

$$\phi(\mathbf{r}) = \sum_{k_1, \dots, k_n \in \mathbb{Z}} \hat{\phi}_{k_1, \dots, k_n} \exp(i \sum_{j=1}^n k_j \mathbf{b}_j \cdot \mathbf{r}). \quad (2.3)$$

In the above, \mathbf{b}_j ($j = 1, \dots, n$) are n vectors in \mathbb{R}^3 that are linearly independent about the field of rational numbers \mathbb{Q} . It implies that $\sum_{j=1}^n k_j \mathbf{b}_j = 0$ for some integers k_j is equivalent to $k_j = 0$. We define the n -dimensional integer vector \mathbf{k} and the $3 \times n$ matrix B as

$$\mathbf{k} = (k_1, \dots, k_n)^t, \quad B = (\mathbf{b}_1, \dots, \mathbf{b}_n). \quad (2.4)$$

The profile $\phi(\mathbf{r})$ can then be written as

$$\phi(\mathbf{r}) = \sum_{\mathbf{k} \in \mathbb{Z}^n} \hat{\phi}_{\mathbf{k}} \exp(i\mathbf{k}^t B^t \mathbf{r}). \quad (2.5)$$

Taking the profile into the free energy, noticing the linear independence of \mathbf{b}_j and the equality

$$\lim_{\Omega \rightarrow \mathbb{R}^3} \frac{1}{V(\Omega)} \int_{\Omega} \exp(i\mathbf{p} \cdot \mathbf{r}) d\mathbf{r} = 0, \quad \mathbf{p} \neq \mathbf{0}, \quad (2.6)$$

we obtain

$$\begin{aligned} \lim_{\Omega \rightarrow \mathbb{R}^3} E[\phi(\mathbf{r}); \Omega] &= \frac{1}{2} \sum_{\mathbf{k} \in \mathbb{Z}^n} \left(c(1 - |B\mathbf{k}|^2)^2 (q^2 - |B\mathbf{k}|^2)^2 - \epsilon \right) \hat{\phi}_{\mathbf{k}} \hat{\phi}_{-\mathbf{k}} \\ &\quad - \frac{\alpha}{3} \sum_{\mathbf{k}_1 + \mathbf{k}_2 + \mathbf{k}_3 = 0} \hat{\phi}_{\mathbf{k}_1} \hat{\phi}_{\mathbf{k}_2} \hat{\phi}_{\mathbf{k}_3} + \frac{1}{4} \sum_{\mathbf{k}_1 + \mathbf{k}_2 + \mathbf{k}_3 + \mathbf{k}_4 = 0} \hat{\phi}_{\mathbf{k}_1} \hat{\phi}_{\mathbf{k}_2} \hat{\phi}_{\mathbf{k}_3} \hat{\phi}_{\mathbf{k}_4}. \end{aligned} \quad (2.7)$$

From the above expressions, we can see that the structure of a phase weighs heavily on the $3 \times n$ matrix B that is full column-rank on \mathbb{Q} . The matrix B determines whether the phase is periodic: if $n \leq 3$, and the column rank of B on \mathbb{R} is also n , then ϕ is periodic in \mathbb{R}^3 ; if $n \geq 4$, or $n \leq 3$ but the column rank of B on \mathbb{R} is less than n , then ϕ is no longer periodic, and is called quasiperiodic. In what follows, we write down the matrix B , under specific orientation, for three phases we will discuss in this paper: striped, hexagonal, and dodecagonal, which are drawn in Fig. 2.1. They all show modulation in at most two directions and are homogeneous in the third, which we can see from the matrix B . The former two phases are periodic, while the third is quasiperiodic. Rigorously speaking, the matrix B shall be optimized by minimizing (2.7). However, we choose to write down directly with $|\mathbf{b}_j| = 1$ or $|\mathbf{b}_j| = q$, which is an approximation good enough.

- Stiped phase. Because we have two favored wavelength, there are two cases.

$$B = \begin{pmatrix} 0 \\ 1 \\ 0 \end{pmatrix}, \quad B = \begin{pmatrix} 0 \\ q \\ 0 \end{pmatrix}. \quad (2.8)$$

The striped pattern is shown in Fig. 2.1 (a), where two matrices will give different widths of the stripe. Since the second and the third rows of B are zero, the phase profile ϕ does not depend on y and z and only shows modulation in the x -direction.

- Hexagonal phase. Similar to the striped phase, we have two cases.

$$B = \begin{pmatrix} 0 & \frac{\sqrt{3}}{2} \\ 1 & \frac{1}{2} \\ 0 & 0 \end{pmatrix}, \quad B = \begin{pmatrix} 0 & \frac{\sqrt{3}q}{2} \\ q & \frac{q}{2} \\ 0 & 0 \end{pmatrix}. \quad (2.9)$$

The third row of B is zero, indicating that profile ϕ is independent of z . The hexagonal pattern is drawn in Fig. 2.1 (b), where the two matrices will give different distances between circles.

- Dodecagonal phase. We require $q = 2 \cos(\pi/12)$, and let

$$B = (\mathbf{b}_1, \mathbf{b}_2, \mathbf{b}_3, \mathbf{b}_4) = \begin{pmatrix} 1 & \frac{1}{2} & \frac{\sqrt{3}}{2} & 0 \\ 0 & \frac{\sqrt{3}}{2} & \frac{1}{2} & 1 \\ 0 & 0 & 0 & 0 \end{pmatrix}. \quad (2.10)$$

Since the third row of B is zero, the dodecagonal phase only has modulation in two directions. The value of q is chosen such that it equals to the length of the vector $\mathbf{b}_1 + \mathbf{b}_2$. Note that B has four columns. We could verify that the vectors \mathbf{m}_j are linearly independent on \mathbb{Q} , by noting that 1 and $\sqrt{3}$ are linearly independent on \mathbb{Q} . Thus, from B we can see that the phase is quasiperiodic. The pattern is drawn in Fig. 2.1 (c), showing 12-fold symmetries that cannot be allowed in periodic phases.

2.2.2 General setting for the interface system

As we have mentioned, we divide the whole space into three regions by two parallel planes $x = -L$ and $x = L$ for some L . We assume that the phase 1 occupies the

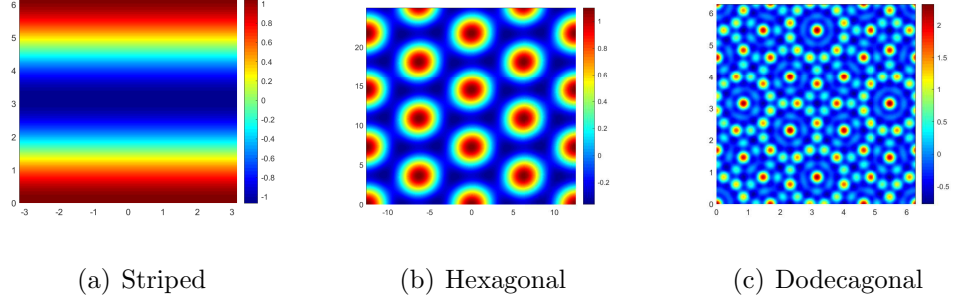


Figure 2.1.: Three patterns formed under LP model.

region $x \leq -L$, and the phase 2 occupies the region $x \geq L$. The interface will emerge in the region $-L < x < L$. In this region, we solve the gradient flow below to let the interface evolve to the equilibrium state,

$$\frac{\partial \phi}{\partial t} = \Delta \mu, \quad (2.11)$$

$$\mu = \frac{\delta E}{\delta \phi} = (\Delta + 1)^2 (\Delta + q^2)^2 \phi - \epsilon \phi - \alpha \phi^2 + \phi^3. \quad (2.12)$$

To make the gradient flow indeed describe the interface for certain relative position and orientation, we need to specify some conditions as we explain below.

First, we need to pose the two phases in certain position and orientation. Let us express the two phase profiles after some rotation and displacement, which we denote by ϕ_1^R and ϕ_2^R . For $T_s \in SO(3)$ and $\mathbf{d}_s \in \mathbb{R}^3$, the profile of the phase s ($s = 1, 2$) becomes

$$\begin{aligned} \phi_s^R(\mathbf{r}) &= \phi(T_s \mathbf{r} + \mathbf{d}_s) = \sum_{\mathbf{k}_s \in \mathbb{Z}^{n_s}} \hat{\phi}_{s\mathbf{k}_s} \exp\left(i\mathbf{k}_s^t B_s^t (T_s \mathbf{r} + \mathbf{d}_s)\right) \\ &= \sum_{\mathbf{k}_s \in \mathbb{Z}^{n_s}} \left(\hat{\phi}_{s\mathbf{k}_s} \exp(i\mathbf{k}_s^t B_s^t \mathbf{d}_s) \right) \exp\left(i\mathbf{k}_s^t (T_s^t B_s)^t \mathbf{r}\right) \\ &= \sum_{\mathbf{k}_s \in \mathbb{Z}^{n_s}} \hat{\phi}_{s\mathbf{k}_s}^R \exp\left(i\mathbf{k}_s^t (T_s^t B_s)^t \mathbf{r}_s\right), \end{aligned} \quad (2.13)$$

where we denote $\hat{\phi}_{s\mathbf{k}_s}^R = \hat{\phi}_{s\mathbf{k}_s} \exp(i\mathbf{k}_s^t B_s^t \mathbf{d}_s)$.

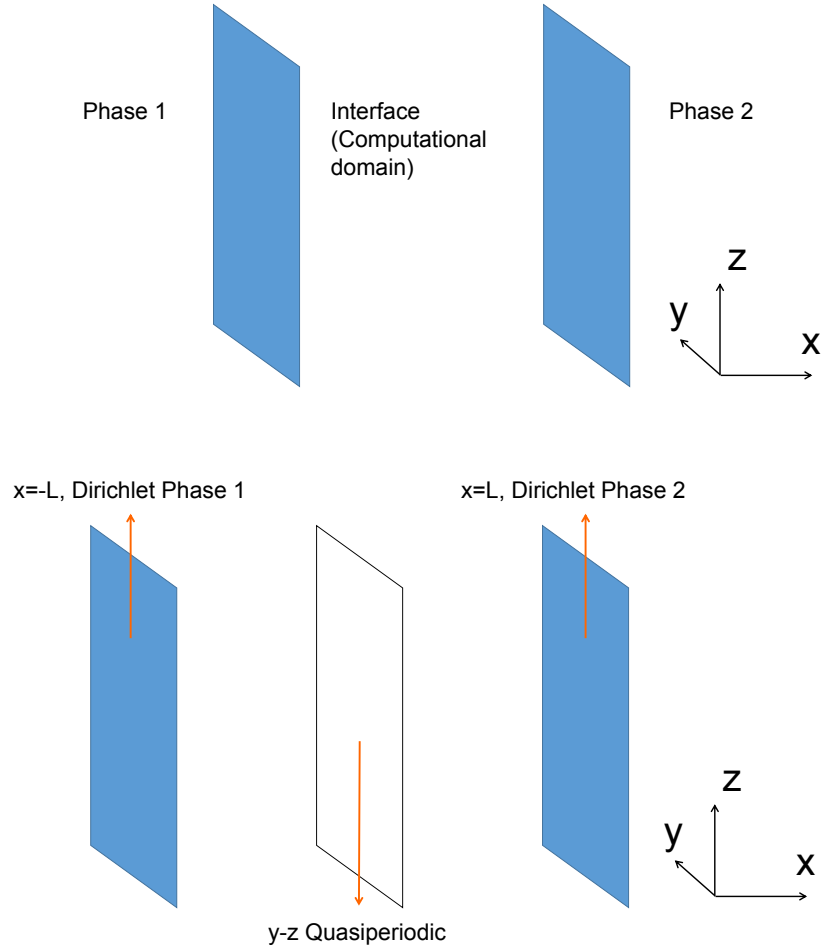


Figure 2.2.: Setting of the interface problem

The information for $x \leq -L$ and $x \geq L$ is translated into the Dirichlet boundary condition. The function value and the normal derivatives of ϕ on the boundary shall be identical to the bulk values. Denote $\tilde{\mathbf{r}} = (y, z)^t$. Then we have

$$\frac{\partial^k}{\partial x^k} \phi(-L, \tilde{\mathbf{r}}) = \frac{\partial^k}{\partial x^k} \phi_1^R(-L, \tilde{\mathbf{r}}), \quad \frac{\partial^k}{\partial x^k} \phi(L, \tilde{\mathbf{r}}) = \frac{\partial^k}{\partial x^k} \phi_2^R(L, \tilde{\mathbf{r}}), \quad k = 0, 1, 2, 3 \quad (2.14)$$

Besides, we require the mass equation $-L < x < L$, so that we impose the Neumann condition on μ ,

$$\frac{\partial \mu}{\partial \mathbf{n}} = 0. \quad (2.15)$$

Furthermore, since we are studying a PDE on the whole y - z plane, we need to specify the function space in the y - z plane in which we solve the PDE. To this end, let us look back into the phase profile ϕ_s^R . For $s = 1, 2$, let us decompose the rotation matrix T_s as (T_{sx}, \tilde{T}_s) , where T_{sx} is the first column, and \tilde{T}_s is the second and third columns of T_s . Then, we write

$$\phi_s^R(x, \tilde{\mathbf{r}}) = \sum_{\mathbf{k}_s \in \mathbb{Z}^{n_s}} \hat{\phi}_{s\mathbf{k}_s}^R \exp\left(i\mathbf{k}_s^t (T_{sx}^t B_s)^t x\right) \exp\left(i\mathbf{k}_s^t (\tilde{T}_s^t B_s)^t \tilde{\mathbf{r}}\right), \quad (2.16)$$

Define $\tilde{B}_s = \tilde{T}_s^t B_s$ that is a $2 \times n_s$ matrix. For fixed x , $\phi_s^R(x, \tilde{\mathbf{r}})$ is in the function space

$$A_s = \left\{ \sum_{\mathbf{k}_s \in \mathbb{Z}^{n_s}} a_{\mathbf{k}_s}(x) \exp\left(i\mathbf{k}_s^t \tilde{B}_s^t \tilde{\mathbf{r}}\right) \right\}. \quad (2.17)$$

Now, let us consider the $2 \times (n_1 + n_2)$ matrix $(\tilde{B}_1, \tilde{B}_2)$. The column rank of this matrix on \mathbb{Q} is $n \leq n_1 + n_2$. Therefore, we could find a $2 \times n$ matrix B such that there exists an $n \times (n_1 + n_2)$ integer matrix Z satisfying

$$\tilde{B}Z = (\tilde{B}_1, \tilde{B}_2). \quad (2.18)$$

We define the function space

$$A = \left\{ a(\mathbf{r}) = \sum_{\mathbf{k} \in \mathbb{Z}^n} a_{\mathbf{k}}(x) \exp\left(i\mathbf{k}^t \tilde{B}^t \tilde{\mathbf{r}}\right) \right\}. \quad (2.19)$$

It can be verified that $A_1, A_2 \subseteq A$, since we have

$$\tilde{B}_1 \mathbf{k}_1 = (\tilde{B}_1, \tilde{B}_2) \begin{pmatrix} \mathbf{k}_1 \\ \mathbf{0} \end{pmatrix} = \tilde{B}Z \begin{pmatrix} \mathbf{k}_1 \\ \mathbf{0} \end{pmatrix}. \quad (2.20)$$

In this sense, the function space A is suitable for both phases. It is easy to verify that A is closed for linear combination, function multiplication and derivatives. So, if the initial condition of the gradient flow (2.11)–(2.12) is in A , the solution will remain in A .

It should be noted that the the definition of the space A depends on \tilde{B}_1 and \tilde{B}_2 , which are determined by the bulk profile and the rotations T_1 and T_2 . In particular,

even if the bulk phases are the same, for different rotations, the resulting function space is also different.

We are now ready to define the inner product,

$$(u, v) = \lim_{\mathfrak{D} \rightarrow \mathbb{R}^2} \frac{1}{2LS(\mathfrak{D})} \int_{[-L, L] \times \mathfrak{D}} u(\mathbf{r})v(\mathbf{r}) d\mathbf{r} = \frac{1}{2L} \sum_{\mathbf{k} \in \mathbb{Z}^n} \int_{[-L, L]} u_{\mathbf{k}}(x)v_{-\mathbf{k}}(x) dx. \quad (2.21)$$

For the second equality, we need to use the fact that \tilde{B} is column full-rank on \mathbb{Q} .

The interfacial energy density is defined as

$$E_i = \lim_{\mathfrak{D} \rightarrow \mathbb{R}^2} E[\phi(\mathbf{r}); -[L, L] \times \mathfrak{D}], \quad (2.22)$$

for which we have the energy dissipation,

$$\frac{dE_i(\phi)}{dt} = \left(\frac{\delta E}{\delta \phi}, \frac{\partial \phi}{\partial t} \right) = -(\nabla \mu, \nabla \mu). \quad (2.23)$$

We could write ϕ_1^R in the form given in (2.19) as follows,

$$\phi_{1\mathbf{k}}^R(x) = \sum_{\mathbf{k}_1} \hat{\phi}_{1\mathbf{k}_1}^R \exp(i\mathbf{k}_1^t B_1 T_{1x} x), \quad \text{the sum is taken over } \mathbf{k} = Z \begin{pmatrix} \mathbf{k}_1^t \\ \mathbf{0} \end{pmatrix}. \quad (2.24)$$

Then, the boundary conditions are actually given on the coefficients $\phi_{\mathbf{k}}(x)$ by

$$\frac{\partial^k}{\partial x^k} \phi_{\mathbf{k}}(-L) = \frac{\partial^k}{\partial x^k} \phi_{1\mathbf{k}}^R(-L), \quad \frac{\partial^k}{\partial x^k} \phi_{\mathbf{k}}(L) = \frac{\partial^k}{\partial x^k} \phi_{2\mathbf{k}}^R(L), \quad k = 0, 1, 2, 3; \quad (2.25)$$

and on $\mu_{\mathbf{k}}(x)$ by

$$\frac{\partial \mu_{\mathbf{k}}}{\partial \mathbf{n}} = 0. \quad (2.26)$$

For the initial condition, we could construct by a simple mixing ansatz,

$$\phi_{\mathbf{k}}(x) = (1 - \alpha(x))\phi_{1\mathbf{k}}^R(x) + \alpha(x)\phi_{2\mathbf{k}}^R(x). \quad (2.27)$$

where $\alpha(x)$ is a smooth monotone function satisfying $\alpha(-L) = 0$ and $\alpha(L) = 1$, which we could approximate by

$$\alpha(x) = \frac{1 - \tanh(\sigma x)}{2}, \quad (2.28)$$

with σ large.

To discretize the gradient flow (2.11)–(2.12), we first present the semi-discretized scheme in time using the SAV approach that is unconditionally stable, followed by spatial discretization by generalized Jacobi polynomials. Several details of computation will be presented, from which the efficiency can be recognized.

2.2.3 SAV approach

For the interface system, we are more interested in the steady state, so we use the first-order scheme. Let

$$E_1[\phi] = (F(\phi), 1), \quad F(\phi) = C_0 - \frac{\epsilon + \beta}{2}\phi^2 - \frac{\alpha}{3}\phi^3 + \frac{1}{4}\phi^4. \quad (2.29)$$

where $\beta > 0$ is a constant, C_0 is chosen such that $F(\phi) > 0$ for any ϕ . An auxiliary variable $r(t) = \sqrt{E_1[\phi]}$ is introduced, so that the gradient flow is rewritten as

$$\begin{aligned} \frac{\partial \phi}{\partial t} &= \Delta \mu \\ \mu &= (c(\Delta + 1)^2(\Delta + q^2)^2 + \beta)\phi + \frac{r(t)}{\sqrt{E_1[\phi]}}F'(\phi) \\ r_t &= \lim_{\mathfrak{D} \rightarrow \mathbb{R}^2} \frac{1}{2LS(\mathfrak{D})} \int_{[-L,L] \times \mathfrak{D}} \frac{F'(\phi)}{2\sqrt{E_1[\phi]}} \phi_t \, d\mathbf{r}. \end{aligned} \quad (2.30)$$

Multiplying above equations with μ , $\frac{\partial \phi}{\partial t}$ and $2r$ respectively, integrating the first two equations and add them together, we achieve the following energy dissipation law:

$$\frac{dE_i[\phi(t)]}{dt} = \frac{d}{dt} \left[\frac{c}{2} ((\Delta + 1)(\Delta + q^2)\phi, (\Delta + 1)(\Delta + q^2)) + \frac{\beta}{2} (\phi, \phi) + r^2 \right] = -(\nabla \mu, \nabla \mu). \quad (2.31)$$

Let Δt be a time step, and ϕ^n denote the numerical approximation to $\phi(\mathbf{r})$ at $t = t_n$. Then a first-order scheme in time for the above system can be constructed as follows:

$$\begin{aligned} \frac{\phi^{n+1} - \phi^n}{\Delta t} &= \Delta \mu^{n+1} \\ \mu^{n+1} &= (c(\Delta + 1)^2(\Delta + q^2)^2 + \beta)\phi^{n+1} + \frac{r^{n+1}}{\sqrt{E_1[\phi^n]}}F'(\phi^n) \\ \frac{r^{n+1} - r^n}{\Delta t} &= \lim_{\mathfrak{D} \rightarrow \mathbb{R}^2} \frac{1}{2LS(\mathfrak{D})} \int_{[-L,L] \times \mathfrak{D}} \frac{F'(\phi^n)}{2\sqrt{E_1[\phi^n]}} \frac{\phi^{n+1} - \phi^n}{\Delta t} d\mathbf{r} \end{aligned} \quad (2.32)$$

By taking the inner product of the three equations with μ^{n+1} , $\phi^{n+1} - \phi^n$ and $2r^{n+1}$ respectively and use the equality $(b - a, 2b) = b^2 - a^2 + (b - a)^2$ we will reach

Theorem 1 *The scheme (2.32) admits a unique solution and is unconditionally energy stable in the sense that*

$$\begin{aligned} &\frac{1}{\Delta t} \left(\tilde{E}_i[\phi^{n+1}, r^{n+1}] - \tilde{E}_i[\phi^n, r^n] \right) \\ &+ \frac{1}{\Delta t} \left(\frac{c}{2} ((\Delta + 1)(\Delta + q^2)(\phi^{n+1} - \phi^n), (\Delta + 1)(\Delta + q^2)(\phi^{n+1} - \phi^n)) \right. \\ &\left. + \frac{\beta}{2} (\phi^{n+1} - \phi^n, \phi^{n+1} - \phi^n) + (r^{n+1} - r^n)^2 \right) = -(\nabla \mu^{n+1}, \nabla \mu^{n+1}) \end{aligned} \quad (2.33)$$

where the modified energy is defined as

$$\tilde{E}_i[\phi^n, r^n] = \frac{c}{2} ((\Delta + 1)(\Delta + q^2)\phi^n, (\Delta + 1)(\Delta + q^2)\phi^n) + \frac{\beta}{2} (\phi^n, \phi^n) + (r^n)^2 \quad (2.34)$$

Adaptive time stepping

In our interface system, the energy curve about the time descends drastically at the early stage but becomes flat afterwards as it approaches the steady state. Therefore, we adopt an adaptive time stepping method, using small time steps initially and large time steps when the energy is decreasing slowly. We choose the time step updating strategy suggested in [69],

$$\Delta t_n = \max \left(\Delta t_{min}, \frac{\Delta t_{max}}{\sqrt{1 + \eta |E^{n+1}(t) - E^n(t)|^2 / \Delta t^2}} \right), \quad (2.35)$$

where t_{min} , t_{max} are predetermined minimum and maximum time steps and η is a suitable parameter, taken as $\eta = 1000$ in our simulation. Interested readers could refer to [69, 70] for more details.

2.2.4 Spatial discretization

We are actually approximating the function space A given in (2.19). In the y - z direction, the function has already been expressed in Fourier series, so we just truncate according to the indices \mathbf{k} . Let us define $|\mathbf{k}| = \max\{k_j\}$. The truncation is made by $|\mathbf{k}| \leq N_1$. Thus, we only need to consider the approximation in the x -direction for $\phi_{\mathbf{k}}^n(x)$ and $\mu_{\mathbf{k}}^n(x)$. We need to choose a finite dimensional function space, which is dependent on the boundary conditions. Because we impose Dirichlet boundary conditions on $\phi_{\mathbf{k}}^n$ and Neumann boundary conditions on $\mu_{\mathbf{k}}^n(x)$, we need two different function spaces. In particular, we use polynomials to form the approximation function spaces.

Let W_N and V_N be two finite dimensional polynomial spaces. For any polynomial $\varphi(x) \in W_N$, it satisfies

$$\frac{\partial^k}{\partial x^k} \varphi(-L) = \frac{\partial^k}{\partial x^k} \varphi(L) = 0, \quad k = 0, 1, 2, 3. \quad (2.36)$$

For $h(x) \in V_N$, it satisfies

$$\frac{\partial}{\partial x} h(-L) = \frac{\partial}{\partial x} h(L) = 0. \quad (2.37)$$

We will discuss the construction of the two spaces later. Whatever the function spaces we choose, denote by $\phi_{N\mathbf{k}}^n(x)$ the approximation of $\phi_{\mathbf{k}}^n(x)$ that belongs to $W_N + \phi_{0\mathbf{k}}(x)$, where $\phi_{0\mathbf{k}}(x)$ is a function satisfying the boundary conditions (2.25). Similarly, we denote by $\mu_{N\mathbf{k}}^n(x)$ the approximation of $\mu_{\mathbf{k}}^n(x)$ that belongs to V_N .

Denote by $\phi_N^n(x, \tilde{\mathbf{r}})$ and $\mu_N^n(x, \tilde{\mathbf{r}})$ the approximation at t_n of ϕ and μ , respectively. Then,

$$\phi_N^n(x, \tilde{\mathbf{r}}) = \sum_{|\mathbf{k}| \leq N_1} \phi_{N\mathbf{k}}^n(x) \exp\left(i\mathbf{k}^t \tilde{B}^t \tilde{\mathbf{r}}\right). \quad (2.38)$$

Similarly,

$$\mu_N^n(x, \tilde{\mathbf{r}}) = \sum_{|\mathbf{k}| \leq N_1} \mu_{N\mathbf{k}}^n(x) \exp\left(i\mathbf{k}^t \tilde{B}^t \tilde{\mathbf{r}}\right). \quad (2.39)$$

The fully discretized scheme of (2.32), in weak formulation, is then given by: find ϕ_N^n in the form (2.38) and μ_N^n in the form (2.39), such that for any $v_N(x) \in V_N$, $w_N(x) \in W_N$, and $|\mathbf{k}| \leq N_1$, they satisfy

$$\begin{aligned} & \left(\frac{\phi_N^{n+1} - \phi_N^n}{\Delta t}, v_N(x) \exp\left(-i\mathbf{k}^t \tilde{B}^t \tilde{\mathbf{r}}\right) \right) = - \left(\nabla \mu_N^{n+1}, \nabla v_N(x) \exp\left(-i\mathbf{k}^t \tilde{B}^t \tilde{\mathbf{r}}\right) \right), \\ & \left(\mu_N^{n+1}, w_N(x) \exp\left(i\mathbf{k}^t \tilde{B}^t \tilde{\mathbf{r}}\right) \right) = \\ & \quad c \left((\Delta + 1)(\Delta + q^2)\phi_N^{n+1}, (\Delta + 1)(\Delta + q^2)w_N(x) \exp\left(-i\mathbf{k}^t \tilde{B}^t \tilde{\mathbf{r}}\right) \right) \\ & \quad + \beta \left(\phi_N^{n+1}, w_N(x) \exp\left(-i\mathbf{k}^t \tilde{B}^t \tilde{\mathbf{r}}\right) \right) \\ & \quad + \frac{r^{n+1}}{\sqrt{E_1[\phi_N^n]}} \left\langle F'(\phi_N^n), w_N(x) \exp\left(-i\mathbf{k}^t \tilde{B}^t \tilde{\mathbf{r}}\right) \right\rangle \\ & \frac{r^{n+1} - r^n}{\Delta t} = \left\langle \frac{F'(\phi_N^n)}{2\sqrt{E_1[\phi_N^n]}}, \frac{\phi_N^{n+1} - \phi_N^n}{\Delta t} \right\rangle. \end{aligned} \quad (2.40)$$

In the above, the notation $\langle \cdot, \cdot \rangle$ is a numerical integration to approximate the inner product (\cdot, \cdot) and is bilinear, i.e.

$$\begin{aligned} \langle \lambda_1 a_1(\mathbf{r}) + \lambda_2 a_2(\mathbf{r}), b(\mathbf{r}) \rangle &= \lambda_1 \langle a_1(\mathbf{r}), b(\mathbf{r}) \rangle + \lambda_2 \langle a_2(\mathbf{r}), b(\mathbf{r}) \rangle, \\ \langle a(\mathbf{r}), \lambda_1 b_1(\mathbf{r}) + \lambda_2 b_2(\mathbf{r}) \rangle &= \lambda_1 \langle a(\mathbf{r}), b_1(\mathbf{r}) \rangle + \lambda_2 \langle a(\mathbf{r}), b_2(\mathbf{r}) \rangle. \end{aligned} \quad (2.41)$$

We will specify it later.

By choosing $v_N = \mu_{N,-\mathbf{k}}^{n+1}$, $w_N = \phi_{N,-\mathbf{k}}^{n+1} - \phi_{N,-\mathbf{k}}^n$ in (2.40) and summing up over \mathbf{k} , followed by multiplying the last equation of by $2r^{n+1}$, one could reach the discretized version of energy dissipation about

$$\tilde{E}[\phi_N^n, r^n] = \frac{c}{2} \left((\Delta + 1)(\Delta + q^2)\phi_N^n, (\Delta + 1)(\Delta + q^2)\phi_N^n \right) + \frac{\beta}{2} (\phi_N^n, \phi_N^n) + |r^n|^2 \quad (2.42)$$

Next, we discuss some details in the scheme (2.40).

Solving the linear system

Define an operator

$$\sigma(\tilde{B}\mathbf{k}) = (\partial_x^2 - |\tilde{B}\mathbf{k}|^2 + 1)(\partial_x^2 - |\tilde{B}\mathbf{k}|^2 + q^2). \quad (2.43)$$

After some calculations, the scheme (2.40) can be simplified into

$$\begin{aligned} \left(\frac{\phi_{N\mathbf{k}}^{n+1} - \phi_{N\mathbf{k}}^n}{\Delta t}, v_N \right) &= -(\partial_x \mu_{N\mathbf{k}}^{n+1}, \partial_x v_N) - |\tilde{B}\mathbf{k}|^2 (\mu_{N\mathbf{k}}^{n+1}, v_N), \\ (\mu_{N\mathbf{k}}^{n+1}, w_N) &= c \left(\sigma(\tilde{B}\mathbf{k}) \phi_{N\mathbf{k}}^{n+1}, \sigma(\tilde{B}\mathbf{k}) w_N \right) + \beta (\phi_{N\mathbf{k}}^{n+1}, w_N) \\ &\quad + \frac{r^{n+1}}{\sqrt{E_1[\phi_{N\mathbf{k}}^n]}} \left\langle F'(\phi_{N\mathbf{k}}^n), w_N(x) \exp(-i\mathbf{k}^t \tilde{B}^t \tilde{\mathbf{r}}) \right\rangle, \\ \frac{r^{n+1} - r^n}{\Delta t} &= \left\langle \frac{F'(\phi_{N\mathbf{k}}^n)}{2\sqrt{E_1[\phi_{N\mathbf{k}}^n]}}, \frac{\phi_{N\mathbf{k}}^{n+1} - \phi_{N\mathbf{k}}^n}{\Delta t} \right\rangle, \end{aligned} \quad (2.44)$$

where $\phi_{N\mathbf{k}}^n \in W_N + \phi_{0\mathbf{k}}$, $\mu_{N\mathbf{k}}^n \in V_N$.

Looking at (2.44), we notice that for different \mathbf{k} , the equation is only coupled by the scalar r^{n+1} . We could decouple the equations for different \mathbf{k} as described below. Let $\varphi_j(x)$ and $h_j(x)$ be a basis of W_N and V_N , respectively. We expand $\phi_{N\mathbf{k}}^n(x)$ and $\mu_{N\mathbf{k}}^n(x)$ by the basis,

$$\phi_{N\mathbf{k}}^n(x) = \sum_j \bar{\phi}_{j\mathbf{k}}^n \varphi_j(x), \quad (2.45)$$

$$\mu_{N\mathbf{k}}^n(x) = \sum_j \bar{\mu}_{j\mathbf{k}}^n h_j(x). \quad (2.46)$$

Define the vector $y_{\mathbf{k}}^n = (\bar{\phi}_{j\mathbf{k}}^n, \bar{\mu}_{j\mathbf{k}}^n)$, $y^n = (y_{\mathbf{k}}^n)$, and the matrices

$$(S_{1\mathbf{k}})_{j_1 j_2} = c \left(\sigma(\tilde{B}\mathbf{k}) \varphi_{j_1}, \sigma(\tilde{B}\mathbf{k}) \varphi_{j_2} \right) + \beta (\varphi_{j_1}, \varphi_{j_2}), \quad (2.47)$$

$$(S_{2\mathbf{k}})_{j_1 j_2} = c (\partial_x h_{j_1}, \partial_x h_{j_2}) + |\tilde{B}\mathbf{k}|^2 (h_{j_1}, h_{j_2}), \quad (2.48)$$

$$(S_{3\mathbf{k}})_{j_1 j_2} = (h_{j_1}, \varphi_{j_2}). \quad (2.49)$$

Then, (2.44) can be written in the form

$$\begin{pmatrix} S & * \\ * & * \end{pmatrix} \begin{pmatrix} y^{n+1} \\ r^{n+1} \end{pmatrix} = b^n. \quad (2.50)$$

where the matrix S is block diagonal,

$$S = \text{diag}(S_{\mathbf{k}}), \quad S_{\mathbf{k}} = \begin{pmatrix} S_{1\mathbf{k}} & -S_{3\mathbf{k}}^t \\ \frac{1}{\Delta t} S_{3\mathbf{k}} & S_{2\mathbf{k}} \end{pmatrix}. \quad (2.51)$$

Therefore, to solve (2.50), we could apply the block Gauss elimination by solving the equation of the form $Sy = b$ twice.

Numerical integration

We notice that in the scheme (2.44), we need to compute a numerical integration of the form $\langle F'(u), v \rangle$. Here, the two functions $u(\mathbf{r})$ and $v(\mathbf{r})$ are given in the form

$$u(\mathbf{r}) = \sum_{|\mathbf{k}| \leq N_1} u_{\mathbf{k}}(x) \exp(i\mathbf{k}^t \tilde{B}^t \tilde{\mathbf{r}}).$$

Furthermore, we notice that F' is a third-order polynomial. So, we focus on computing the highest-order term $\langle u^3, v \rangle$. Since $\langle u^3, v \rangle$ is an approximation of (u^3, v) , we first write down the latter according to the definition (2.21),

$$(u^3, v) = \frac{1}{2L} \sum_{\mathbf{k}_1 + \mathbf{k}_2 + \mathbf{k}_3 + \mathbf{k}_4} \int_{[-L, L]} u_{\mathbf{k}_1}(x) u_{\mathbf{k}_2}(x) u_{\mathbf{k}_3}(x) v_{\mathbf{k}_4}(x) dx. \quad (2.52)$$

In the x -direction, we choose the Gauss–Lobatto points x_j in $[-L, L]$ with the corresponding weights λ_j , and approximate an integral as

$$\frac{1}{2L} \int_{-L}^L f(x) dx \approx \sum_j \lambda_j f(x_j). \quad (2.53)$$

It remains to calculate

$$\sum_{\mathbf{k}_1 + \mathbf{k}_2 + \mathbf{k}_3 + \mathbf{k}_4} u_{\mathbf{k}_1}(x_j) u_{\mathbf{k}_2}(x_j) u_{\mathbf{k}_3}(x_j) v_{\mathbf{k}_4}(x_j). \quad (2.54)$$

This can be done by constructing new Fourier series in \mathbb{R}^n , where we recall that the n here is the dimension of \mathbf{k} : let $\mathbf{z} = (z_1, \dots, z_n)$ and consider

$$U(\mathbf{z}) = \sum_{|\mathbf{k}| \leq N_1} u_{\mathbf{k}} \exp(2\pi i \mathbf{k} \cdot \mathbf{z}). \quad (2.55)$$

With the help of the above function, (2.54) can be calculated by n -dimensional FFT.

2.2.5 Discretization in the x -direction

We describe how to construct the functions spaces V_N and W_N , for which we make use of the Jacobi Polynomials.

In these two spaces, the boundary conditions are given on $x = \pm L$. We could introduce a scaling $x' = x/L$, so that it is equivalent to consider the functions on the interval $[-1, 1]$. For the discussion below, we shall assume $L = 1$.

Jacobi polynomials

We first recall the classical Jacobi polynomials and their properties. For $\alpha, \beta > -1$, let $J_n^{\alpha, \beta}$ be the classical Jacobi polynomials which are orthogonal with respect to the weight function $\omega^{\alpha, \beta}(x) = (1-x)^\alpha(1+x)^\beta$ over $(-1, 1)$, i.e.

$$\int_{-1}^1 J_n^{\alpha, \beta}(x) J_m^{\alpha, \beta}(x) \omega^{\alpha, \beta}(x) dx = \gamma_n^{\alpha, \beta} \delta_{mn} \quad (2.56)$$

where

$$\gamma_n^{\alpha, \beta} = \|J_n^{\alpha, \beta}\|_{\omega^{\alpha, \beta}(x)}^2 = \frac{2^{\alpha+\beta+1} \Gamma(n+\alpha+1) \Gamma(n+\beta+1)}{(2n+\alpha+\beta+1)n! \Gamma(n+\alpha+\beta+1)} \quad (2.57)$$

and δ_{mn} is the Dirac Delta symbol. And Jacobi polynomials have the following properties:

Property 1 *Three-term recurrence relationship:*

$$\begin{aligned} J_{n+1}^{\alpha, \beta}(x) &= (a_n^{\alpha, \beta} x - b_n^{\alpha, \beta}) J_n^{\alpha, \beta}(x) - c_n^{\alpha, \beta} J_{n-1}^{\alpha, \beta}(x), \quad n \geq 1 \\ J_0^{\alpha, \beta}(x) &= 1, \quad J_1^{\alpha, \beta}(x) = \frac{1}{2}(\alpha + \beta + 2)x + \frac{1}{2}(\alpha - \beta) \end{aligned} \quad (2.58)$$

Property 2 *Derivative relationship:*

$$\partial_x^k J_n^{\alpha, \beta}(x) = d_{n,k}^{\alpha, \beta} J_{n-k}^{\alpha+k, \beta+k}(x), \quad n \geq k, \quad (2.59)$$

where

$$d_{n,k}^{\alpha, \beta} = \frac{\Gamma(n+k+\alpha+\beta+1)}{2^k \Gamma(n+\alpha+\beta+1)}. \quad (2.60)$$

We then recall the generalized Jacobi polynomials (GJP) introduced in [71]:

$$J_n^{k,l}(x) = \begin{cases} (1-x)^{-k}(1+x)^{-l}J_{n-n_0}^{-k,-l}(x) & \text{if } k, l \leq -1 \\ (1-x)^{-k}J_{n-n_0}^{-k,l}(x) & \text{if } k \leq -1, l > -1 \\ (1+x)^{-l}J_{n-n_0}^{k,-l}(x) & \text{if } k > -1, l \leq -1 \end{cases} \quad (2.61)$$

where $n \geq n_0$, $n_0 = -(k+l)$, $-k$, $-l$ for the above 3 cases respectively and $J_n^{k,l}$ is classical Jacobi polynomial with $k, l \geq -1$. We now present some basic properties of GJP:

Property 3 *The GJPs are mutually $L_{\omega^{\alpha,\beta}(x)}^2$ -orthogonal, i.e.,*

$$\int_{-1}^1 J_n^{k,l}(x)J_m^{k,l}(x)\omega^{\alpha,\beta}(x)dx = \gamma_{n-n_0}^{\bar{k},\bar{l}}\delta_{mn}, \quad (2.62)$$

where $\gamma_{n-n_0}^{\bar{k},\bar{l}}$ is defined in (2.57) and

$$\bar{n} = \begin{cases} -n, & n \leq -1 \\ n, & n > -1 \end{cases} \quad (2.63)$$

Property 4 $\forall k, l \in \mathbb{Z}$ and $k, l \geq 1$

$$\partial_x^i J_n^{-k,-l}(1) = 0, \text{ for } i = 0, 1, \dots, k-1 \quad (2.64)$$

$$\partial_x^j J_n^{-k,-l}(-1) = 0, \text{ for } j = 0, 1, \dots, l-1. \quad (2.65)$$

thus $\{J_n^{-k,-l}\}$ are natural candidates as basis function for PDEs with the boundary conditions:

$$\partial_x^i u(1) = a_i, \text{ for } i = 0, 1, \dots, k-1 \quad (2.66)$$

$$\partial_x^j u(-1) = b_j, \text{ for } j = 0, 1, \dots, l-1. \quad (2.67)$$

And we have the similar derivative recurrence relation:

Property 5 Let $k, l, m \in \mathbb{N}$, and if $m \leq k, l$ then

$$\partial_x^m J_n^{-k, -l}(x) = (-2)^m \frac{(n - k - l + m)!}{(n - k - l)!} J_{n-m}^{-k+m, -l+m}(x), \quad n \geq \max(k + l, m). \quad (2.68)$$

Using above properties, GJP and their derivatives can be computed recursively.

Construction of V_N

The polynomials in V_N satisfy the boundary conditions (2.37). We could construct the basis of V_N , $h_k(x)$, is the linear combination of Legendre polynomials $L_k(x)$,

$$h_k(x) = L_k(x) + a_k L_{k+1}(x) + b_k L_{k+2}(x), \quad (2.69)$$

for $k = 1, \dots, N$. Legendre polynomials are a special case of GJP with $\omega^{\alpha, \beta}(x) = 1$. More properties about Legendre polynomials can be found in books like [25, 72]. It is shown in [19] that there exists a unique set $\{a_k, b_k\}$.

Construction of W_N

By Property (4), we choose the basis of W_N as follows that satisfy boundary conditions (2.36), Define the basis functions using GJPs

$$\varphi_l(x) := c_l J_{l+7}^{-4, -4}(x), \quad l = 1, \dots, \leq N, \quad (2.70)$$

where c_l is the scaling factor such that $(\partial_x^4 \varphi_k, \partial_x^4 \varphi_l) = \delta_{kl}$.

Construction of $\phi_{0\mathbf{k}}(x)$

The boundary conditions on $\phi_{\mathbf{k}}$ are not homogeneous, so that we need to find a $\phi_{0\mathbf{k}}(x)$ satisfying the non-homogeneous boundary conditions. There are eight conditions in total, so it can be done by using a seventh-order polynomial.

Computation of matrix elements

We have specified the basis $\varphi_j(x)$ and $h_j(x)$ above. It remains to calculate the matrix elements of $S_{\mathbf{k}}$ in (2.51), defined in (2.47)–(2.49). They can be pre-computed using Property (3) and (5). Notice that because of orthogonality of polynomials, $S_{1\mathbf{k}}$, $S_{2\mathbf{k}}$ and $S_{3\mathbf{k}}$ are sparse matrices and elements are non-zero on at most 9 sub-diagonals. When solving the linear equation with the coefficient matrix $S_{\mathbf{k}}$, we use the LU factorization, because the size is $2N \times 2N$ that is moderate. In particular, since the matrix $S_{\mathbf{t}}$, the LU factorization can be done as a preprocessing.

2.2.6 Outline of the numerical method

For the computing of quasiperiodic interfacial structure, we list the outline of implementation:

- Find the bulk phase profile in the form (2.3) by minimizing the free energy density (2.2). Impose the desired rotation and displacement by (2.13), from which the boundary conditions and the initial state come from.
- Find the matrix \tilde{B} , column full-rank on \mathbb{Q} , for the space (2.19). Set the boundary conditions (up to third-order derivatives) and initial state using (2.24)–(2.28).
- Discretize the gradient flow (2.11)–(2.12) in time using SAV approach. We apply an unconditional energy stable first order scheme in order to reach the steady state quickly.
- Discretize in space using spectral method. In the y - z plane, we truncate the Fourier series. In the x -direction, we use generalized Jacobi polynomials in accordance with the boundary conditions. With non-periodic boundary conditions, this task is not easy using finite difference or finite element method as instability would arise. Spectral method with generalized Jacobi polynomials

will generate sparse matrix when dealing with high order derivatives and are free from this problem.

- Different Fourier modes in y - z can be decoupled under SAV. The nonlinear terms in the scheme are polynomials. For quasiperiodic functions, it can be calculated efficiently by higher dimensional FFT.

We must emphasize here that all our derivation depends on that \tilde{B} is column full-rank on \mathbb{Q} . Moreover, the number of columns of \tilde{B} , n , gives the the computational cost, which is $O(N_1^n N)$. Since \tilde{B} depends on the rotations of the two phases, it implies that under different phases or relative orientations, the computational cost will be different. We will illustrate it in the numerical examples.

2.3 Numerical simulations

2.3.1 Dirichlet boundary condition

All simulations are conducted on Intel i7-4790 CPU with 3.6GHz. In x -direction, polynomials order N is chosen to be 256 and 512 Gauss-Lobatto points are used to compute the integrals. The interpolation smoothing parameter σ in (2.28) is chosen to be 250.

We will consider the three phases introduced above, for which the B matrices are given in (2.8)–(2.10). Note that the third row of B are zero for all the three phases. So, the three phases can all be place in the x - y plane and homogeneous in z -direction. When doing the rotation, we also constrain in the x - y plane, i.e. the rotation matrix T is given by

$$T(\theta) = \begin{pmatrix} \cos \theta & -\sin \theta & 0 \\ \sin \theta & \cos \theta & 0 \\ 0 & 0 & 1 \end{pmatrix}. \quad (2.71)$$

As a result, in the interface system, only the first row of the two-row \tilde{B} matrix is nonzero. When determining the column rank of \tilde{B} on \mathbb{Q} , we are actually determining the number of linearly independent real numbers on \mathbb{Q} .

Grain boundaries of striped phase

The phrase 'grain boundary' means the interface with two identical phases with different orientations. The grain boundary of striped phases have been studied extensively. Thus, we start from some grain boundaries as a verification of our numerical method.

We examine the kink grain boundaries of the striped phases. That is, the phase 1 and phase 2 are both the striped phases of the same type with the first B in (2.8). The phase 1 is rotated by $T_1 = T(\theta)$, while the phase 2 is rotated by $T_2 = T(-\theta)$. Recall that we define $\tilde{B}_1 = \tilde{T}_1^t B$ where \tilde{T}_1 is the second and third columns of T_1 . In this case, we calculate that

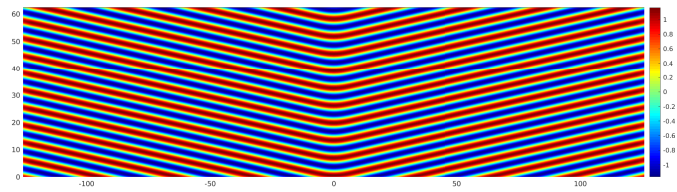
$$\tilde{B}_1 = \tilde{T}_1^t B = \begin{pmatrix} \cos \theta \\ 0 \end{pmatrix}, \quad \tilde{B}_2 = \tilde{T}_2^t B = \begin{pmatrix} \cos \theta \\ 0 \end{pmatrix}.$$

Therefore, the \tilde{B} matrix can just be chosen as

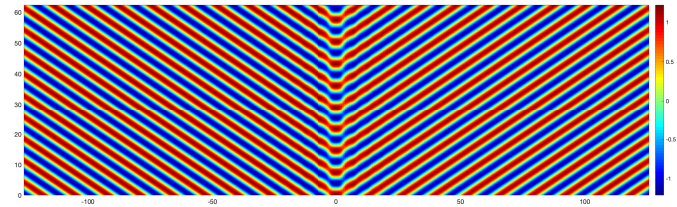
$$\tilde{B} = \begin{pmatrix} \cos \theta \\ 0 \end{pmatrix}.$$

It implies that we are actually considering a periodic boundary condition on the y -direction, which is the special case discussed in [49].

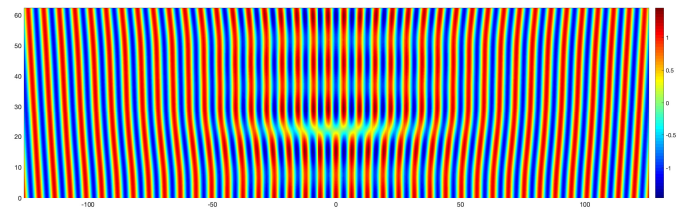
We choose $c = 1$, $\alpha = 0$, $\epsilon = 1$ and $q = 2\cos(\pi/12)$. We consider three different θ , for which the steady state is reached at $t = 5000$ shown in Fig. 2.3(a), (b) and (c). When θ is small, a smooth transition layer will form; for a larger θ we observe the Omega-shaped patterns in the interface; when θ is near $\pi/2$, a dislocation emerges. These patterns are identical to the previous studies using different free energy [73–75].



(a) $\theta = 0.2$ equilibrium state



(b) $\theta = 0.5$ equilibrium state



(c) $\theta = 1.5$ equilibrium state

Figure 2.3.: Laminar flow interface steady state with small and big rotation angle θ .

Grain boundaries of the hexagonal phase

We turn to the grain boundaries of the hexagonal phase. We still consider the kink grain boundaries, letting $T_1 = T(\theta)$ and $T_2 = T(-\theta)$. The case is different from the striped phase, because we may have \tilde{B} of different columns. Let us explain it below.

These results are calculated under $c = 1, \alpha = 1, \epsilon = 0.15$. The B matrix is given as the first one in (2.9).

We first examine the case when all the four coefficients $\pm \sin\theta$ and $\pm(\frac{1}{2}\sin\theta + \frac{\sqrt{3}}{2}\cos\theta)$ are rational to each other and the 8 reciprocal basis decays to one. One could verify that $\tan\theta/\sqrt{3}$ is a rational number in this case. So we could set $\theta = \arctan\frac{\sqrt{3}}{4}$ and it can be shown that the basis is written as

The evolution of interface and energy dissipation are shown in Fig. 2.4.

We then consider examples where only two pairs of coefficients are rational to each other or $\tan\theta/\sqrt{3}$ is not a rational number. In these cases, our phase profile is written as:

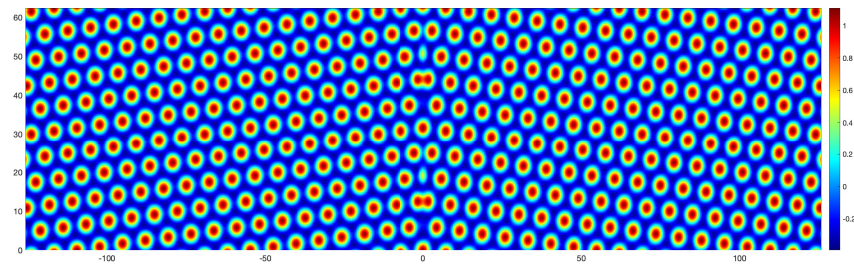
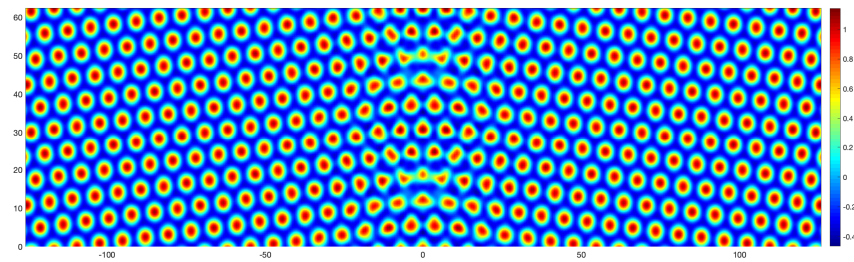
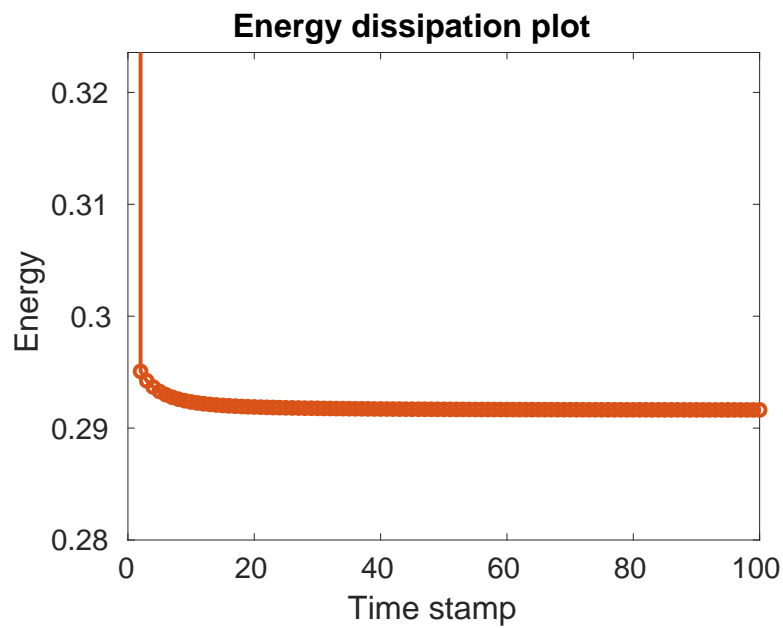
$$\phi(x, y) = \sum_{k_1, k_2} \hat{\phi}_{k_1, k_2}(x) e^{iy(\frac{1}{2}k_1 \sin\theta + \frac{\sqrt{3}}{2}k_2 \cos\theta)} \quad (2.72)$$

For various θ we have the following interfacial result shown in Fig. 2.5.

Our next simulation is based on the fact that the crystals phase under LP model will form shape of two different sizes on $|k| = 1$ and $|k| = q$. We anchor the crystal phase which reaches minima on $|k| = 1$ on the left and $|k| = q$ on the right of the plane. The simulation result is presented in Fig. 2.6 and one observe trilateral bulk in the interfacial region.

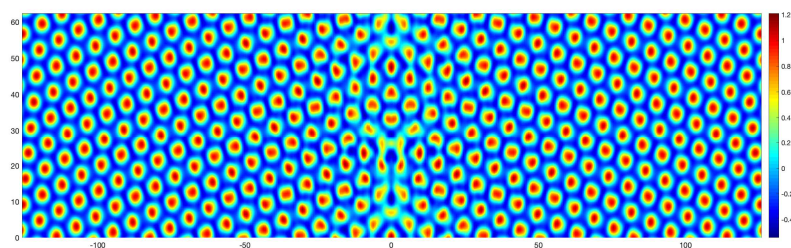
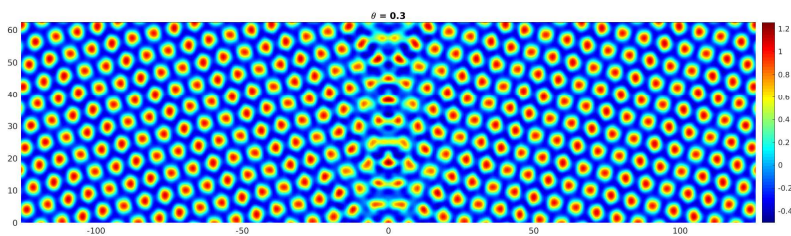
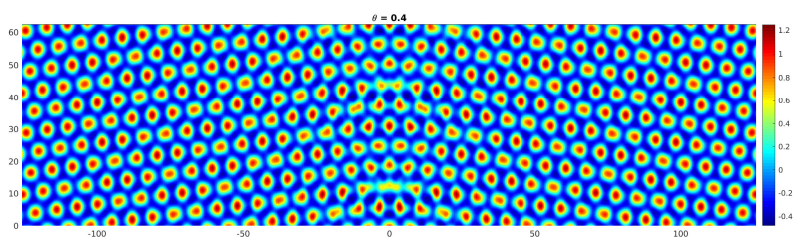
Interface involving the dodecagonal phase

We then simulate the Quasi-crystals with some simplification. After rotation, the eight reciprocal vector have coefficients $\sin\theta, \frac{\sqrt{3}}{2}\sin\theta + \frac{1}{2}\cos\theta, \frac{1}{2}\sin\theta + \frac{\sqrt{3}}{2}\cos\theta, \cos\theta$ and $-\sin\theta, -\frac{\sqrt{3}}{2}\sin\theta + \frac{1}{2}\cos\theta, -\frac{1}{2}\sin\theta + \frac{\sqrt{3}}{2}\cos\theta, \cos\theta$. In general, 6 of these 8 reciprocal

(a) $t = 0$ (b) $t = 5000$ 

(c) Energy dissipation plot

Figure 2.4.: Interfacial transition and energy dissipation of two crystals with $\theta = \arctan \frac{\sqrt{3}}{4}$.

(a) $\theta = 0.17$ (b) $\theta = 0.3$ (c) $\theta = 0.4$ Figure 2.5.: Interfacial transition with various θ

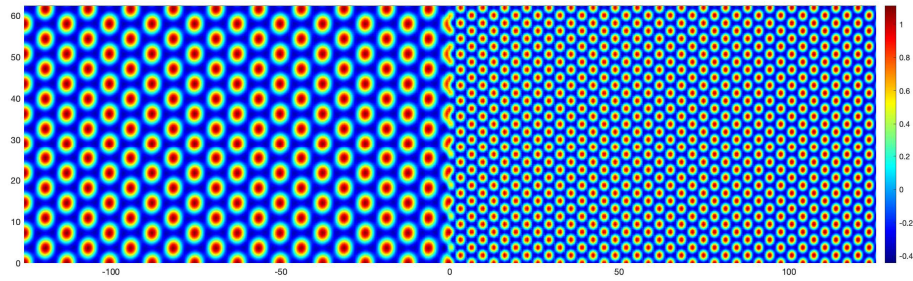
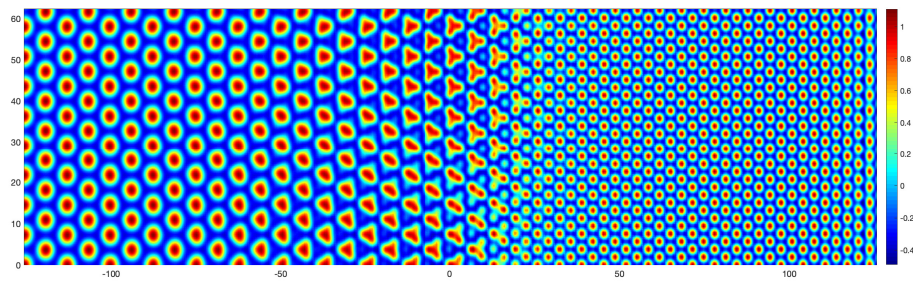
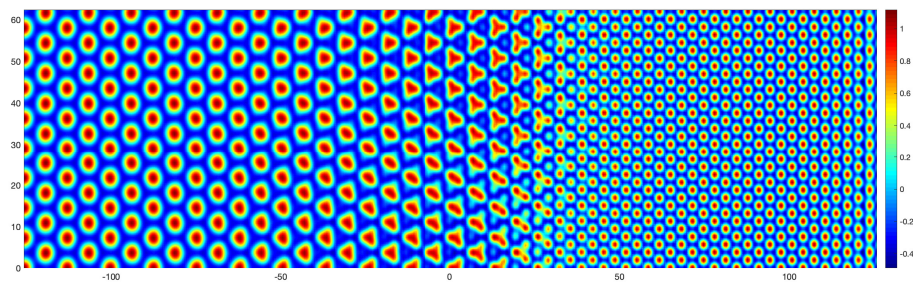
(a) $t = 0$ (b) $t = 10000$ (c) $t = 30000$

Figure 2.6.: Interfacial transition with big-small crystals

vectors are linear independent with rational coefficients. However, by setting θ to be special number, one could reduce the dimension of reciprocal vectors. For integers r and s , we have:

- if $\tan\theta = \frac{r}{s\sqrt{3}}$, we have two independent reciprocal vectors with coefficient $\frac{\sin\theta}{2r}, \frac{\cos\theta}{2s}$;
- if $\theta = \frac{\pi}{4}$, there are three independent reciprocal vectors with coefficient $\frac{\sqrt{2}}{2}, \frac{\sqrt{6}+\sqrt{2}}{4}, \frac{\sqrt{6}-\sqrt{2}}{4}$;
- otherwise, we will have 4 reciprocal vectors $\sin\theta, \frac{\sqrt{3}}{2}\sin\theta + \frac{1}{2}\cos\theta, \frac{1}{2}\sin\theta + \frac{\sqrt{3}}{2}\cos\theta$ and $\cos\theta$.

Due to computation complexity, we here only consider the first two cases, i.e. when $\theta = \frac{\pi}{4}$ and when $\sqrt{3}\tan\theta = r/s$ is a rational number and we have

$$\phi(x, y) = \sum_{k_1, k_2} \hat{\phi}_{k_1, k_2}(x) e^{iyk_1 \frac{\sin\theta}{2r}} e^{iyk_2 \frac{\cos\theta}{2s}} \quad (2.73)$$

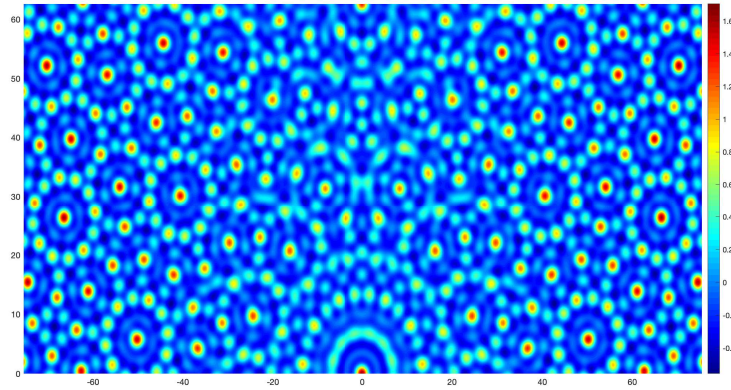
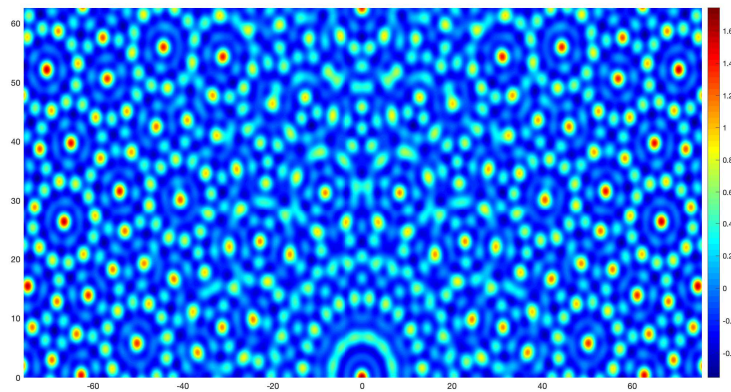
$$\phi(x, y) = \sum_{k_1, k_2, k_3} \hat{\phi}_{k_1, k_2, k_3}(x) e^{iyk_1 \frac{\sqrt{2}}{2}} e^{iyk_2 \frac{\sqrt{6}+\sqrt{2}}{4}} e^{iyk_3 \frac{\sqrt{6}-\sqrt{2}}{4}} \quad (2.74)$$

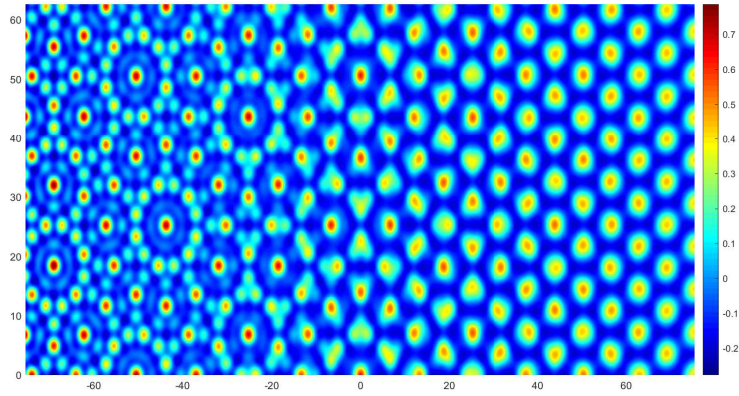
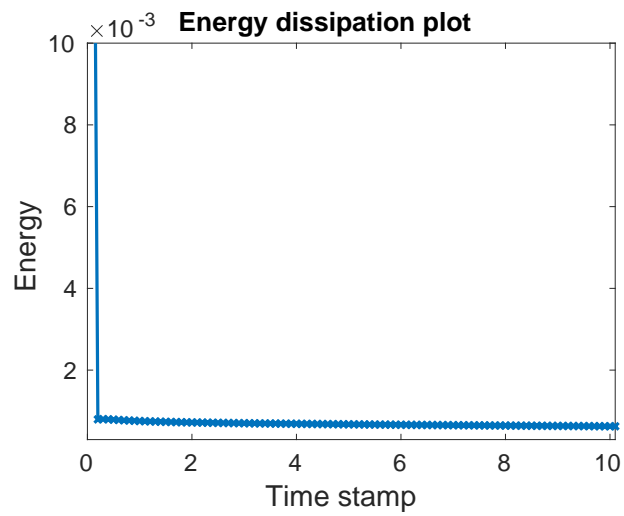
The initial and equilibrium profile is shown in Fig. 2.7. The parameters are chosen as $c = 150, \alpha = 1, \epsilon = 0.015, q$

Our last example is constructed by combining a cylindrical crystal phase with a 12-fold quasicrystal phase. The equilibrium state and energy dissipation are shown in Fig.(2.8). To maintain both phases, we take $\epsilon = 0.00833$ and $\alpha = 0.5$.

2.3.2 Periodic boundary condition

We here list our previous simulations where the phase profile is periodic in x direction. In such situation, the phase function is periodic in both x and y directions and can be solved all in frequency space using pseudo-spectral method.

(a) $t = 0$ (b) $t = 100$ Figure 2.7.: Quasicrystal interfacial transition with $\theta = \arctan\frac{\sqrt{3}}{4}$

(a) $t = 100$ 

(b) Energy dissipation plot

Figure 2.8.: Crystal-Quasicrystal interfacial transition and energy dissipation.

Cylindrical crystal phase

We start our simulation from a crystal phase profile. The phase function could be represented as

$$\phi(x, y) = \sum_{k_1, k_2} \hat{\phi}_{k_1, k_2} e^{ix(k_1 + \frac{1}{2}k_2) + iy \frac{\sqrt{3}}{2}k_2} \quad (2.75)$$

The equilibrium of such crystal has 6-fold symmetry and is shown in Fig. (2.9). The results are calculated with $c = 1, \alpha = 1, \epsilon = 0.15$.

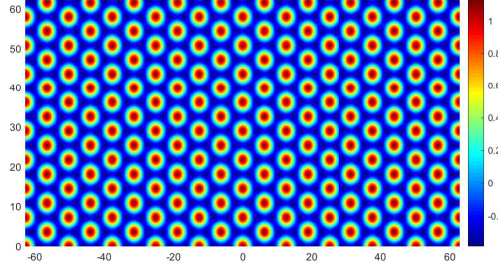


Figure 2.9.: 6-fold symmetry crystal equilibrium state

Quasicrystal

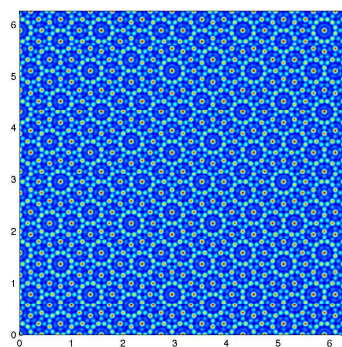
We then demonstrate our algorithm on quasicrystals. For quasicrystal with 12-fold symmetry, we have presented above that the projection matrix has the form:

$$S_{12} = \begin{pmatrix} 1 & \cos \frac{\pi}{6} & \cos \frac{\pi}{3} & 0 \\ 0 & \sin \frac{\pi}{6} & \sin \frac{\pi}{3} & 1 \end{pmatrix}$$

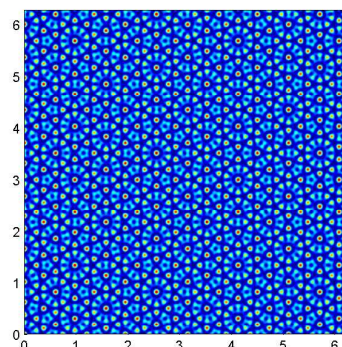
And the 10-fold symmetry quasicrystals have the projection matrix in the following form:

$$S_{10} = \begin{pmatrix} 1 & \cos \frac{\pi}{5} & \cos \frac{2\pi}{5} & \cos \frac{3\pi}{5} \\ 0 & \sin \frac{\pi}{5} & \sin \frac{2\pi}{5} & \sin \frac{3\pi}{5} \end{pmatrix}$$

In this simulations, the parameters are chosen as $q_{12} = 2\cos(\pi/12), q_{10} = 2\cos(\pi/5), c = 1, \alpha = 1, \epsilon = 0.015$. The equilibrium states for both cases are shown in Fig. (2.10).



(a) 12-fold symmetry



(b) 10-fold symmetry

Figure 2.10.: 12-fold and 10-fold symmetry quasicrystal phases

These simulations verify the accuracy of our scheme and we will apply our scheme on the following more complicated cases.

Multi-phase Model

LP model is not only effective on one phase model, one may refer to [76] about multi-phase model. In such Swift-Hohenberg model, the nonlinear part of the free energy is given as:

$$f = \frac{1}{V} \int dr [\tau \phi_2^2 + g_0 \phi_2^3 + \phi_2^4 + t \phi_1^2 + t_0 \phi_1^3 + \phi_1^4 - g_1 \phi_2^2 \phi_1 - g_2 \phi_2 \phi_1^2] \quad (2.76)$$

where t, τ, t_0, g_0, g_1 and g_2 are parameters depending on the interaction between components and the thermodynamic conditions, such as temperature. In order to introduce multiple frequency forcing, the LP model and this Swift-Hohenberg model are combined together by adding two gradient terms into the free energy. The free energy functional now becomes

$$E[\phi_1, \phi_2] = \frac{1}{V} \left\{ \frac{c}{2} \int dr [(\nabla^2 + 1)\phi_2]^2 + [(\nabla^2 + q^2)\phi_1]^2 + E_1[\phi_1, \phi_2] \right\} \quad (2.77)$$

where

$$E_1[\phi_1, \phi_2] = \int dr (\tau \phi_2^2 + g_0 \phi_2^3 + \phi_2^4 + t \phi_1^2 + t_0 \phi_1^3 + \phi_1^4 - g_1 \phi_2^2 \phi_1 - g_2 \phi_2 \phi_1^2)$$

The gradient flow system for the relaxation :

$$\begin{aligned} \frac{\partial \phi_2}{\partial t} &= -\frac{\delta f}{\delta \phi_2} = -c(\nabla^2 + 1)^2 \phi_2 - (2\tau \phi_2 + 3g_0 \phi_2^2 + 4\phi_2^3) + 2g_1 \phi_2 \phi_1 + g_2 \phi_1^2 \\ \frac{\partial \phi_1}{\partial t} &= -\frac{\delta f}{\delta \phi_1} = -c(\nabla^2 + 1)^2 \phi_1 - (2t \phi_1 + 3t_0 \phi_1^2 + 4\phi_1^3) + 2g_2 \phi_2 \phi_1 + g_2 \phi_2^2 \end{aligned}$$

According to [61], we can pose the SAV scheme for gradient flows of multiple functions ϕ_1 and ϕ_2 :

$$\begin{aligned}
\frac{\partial \phi_i}{\partial t} &= \Delta \mu_i \\
\mu_i &= c[(\nabla^2 + 1)^2 \phi_i] + \frac{r(t)}{\sqrt{E_1}} U_i \\
r_t &= \frac{1}{2\sqrt{E_1}} \int_{\Omega} U_i \frac{\partial \phi_i}{\partial t} dx
\end{aligned} \tag{2.78}$$

where $U_i = \delta E_1 / \delta \phi_i$ and $\mu_i = \delta E / \delta \phi_i$.

It is shown in [76] that the effective phase density Φ_A , Φ_B and Φ_C could be recovered from ϕ_1 and ϕ_2 through

$$\Phi_A = \frac{1}{2}(\phi_1 + \phi_2), \Phi_B = \frac{1}{2}(\phi_2 - \phi_1), \Phi_C = -\phi_2$$

And the simulation result is shown in Fig.(2.11).

Modified Non-local model

In the present study, a generic coarse-grained free energy functional is used.

$$E[\phi(\mathbf{r})] = \frac{1}{V} \int \int \frac{c}{2} [\phi(\mathbf{k}) G(\mathbf{k}, \mathbf{k}') \phi(\mathbf{k}')] d\mathbf{k} d\mathbf{k}' \tag{2.79}$$

$$+ \frac{1}{V} \int [-\frac{\epsilon}{2} \phi^2 - \frac{\alpha}{3!} \phi^3 + \frac{1}{4!} \phi^4] d\mathbf{k}, \tag{2.80}$$

where $G(\mathbf{k}, \mathbf{k}') = G(|\mathbf{k} - \mathbf{k}'|)$ is a two-body correlation potential. The term contains $G(\mathbf{k}, \mathbf{k}')$ describes the free energy cost of inhomogeneity of the system and the choice of $G(\mathbf{k}, \mathbf{k}')$ will affect the different dominant modes at particular length scales, thus promoting different ordered structures. In our model, the corresponding pair interaction potential of $G(\mathbf{k}, \mathbf{k}')$ in the Fourier space is given as

$$\widehat{G}(k) = e^{-|k|^2/2\sigma^2} [(1 - |k|^2)^2 (q^2 - |k|^2)^2 - \eta] \tag{2.81}$$

$$= e^{-k^2/2\sigma^2} (d_0 + d_2 k^2 + d_4 k^4 + d_6 k^6 + d_8 k^8) \tag{2.82}$$

The constant η is subtracted to let \widehat{G} not necessarily positive. In our simulation $\eta = 1$. d_i 's are obtained by simplifying the equation and σ is the model parameter. When σ is large, say 1, the result after PM will be similar to the ordinary quasicrystal

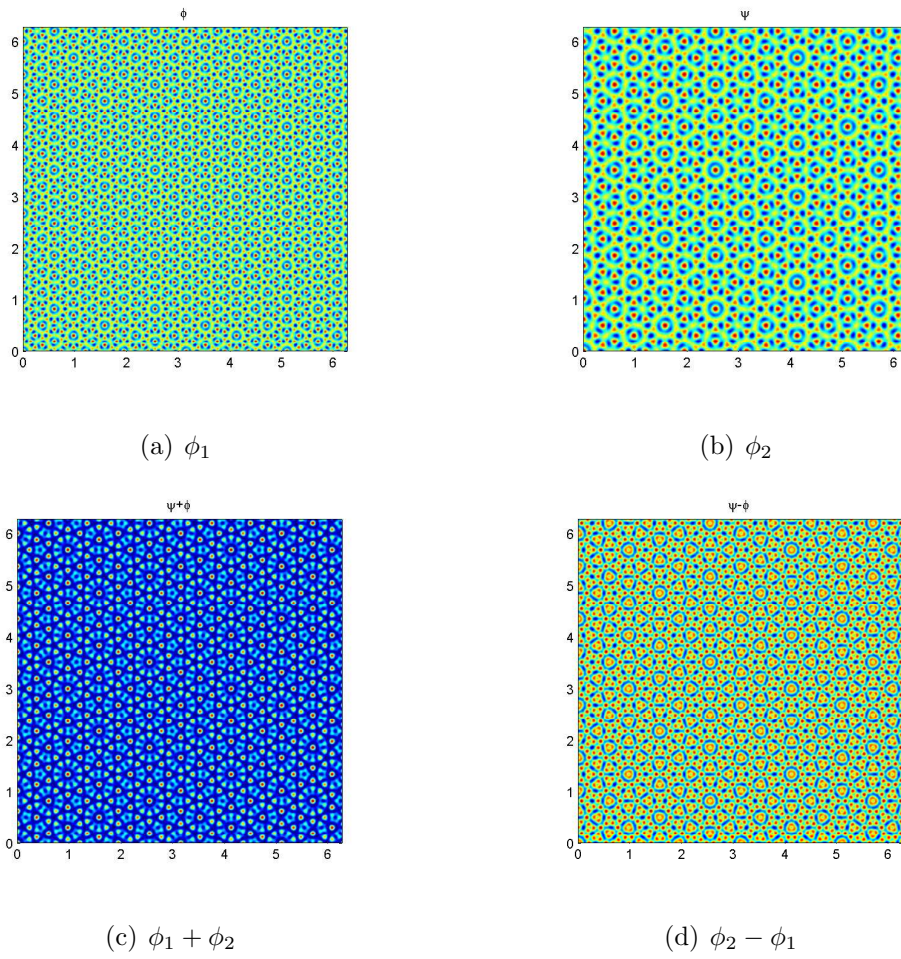


Figure 2.11.: Order parameters obtained from minimization of free energy model

case. For small σ , we observe a Mosaic-like pattern. The equilibrium state is shown in Fig.(2.12).

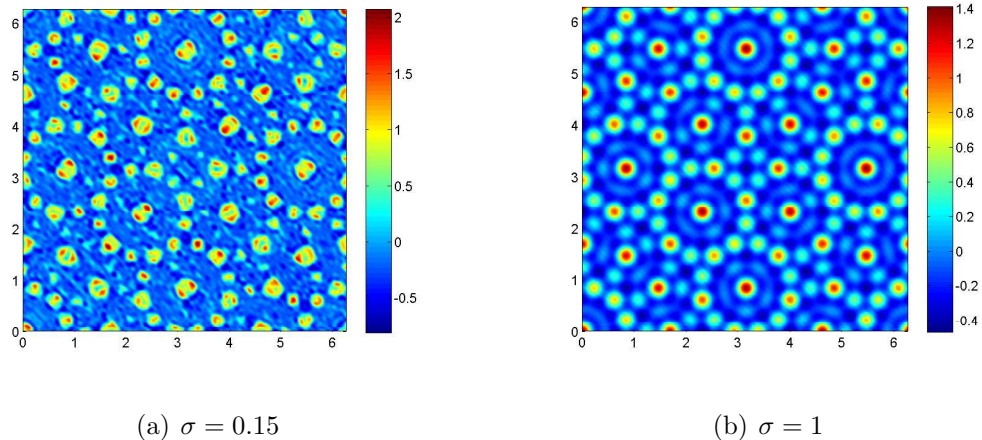


Figure 2.12.: Modified non-local model steady state with different σ

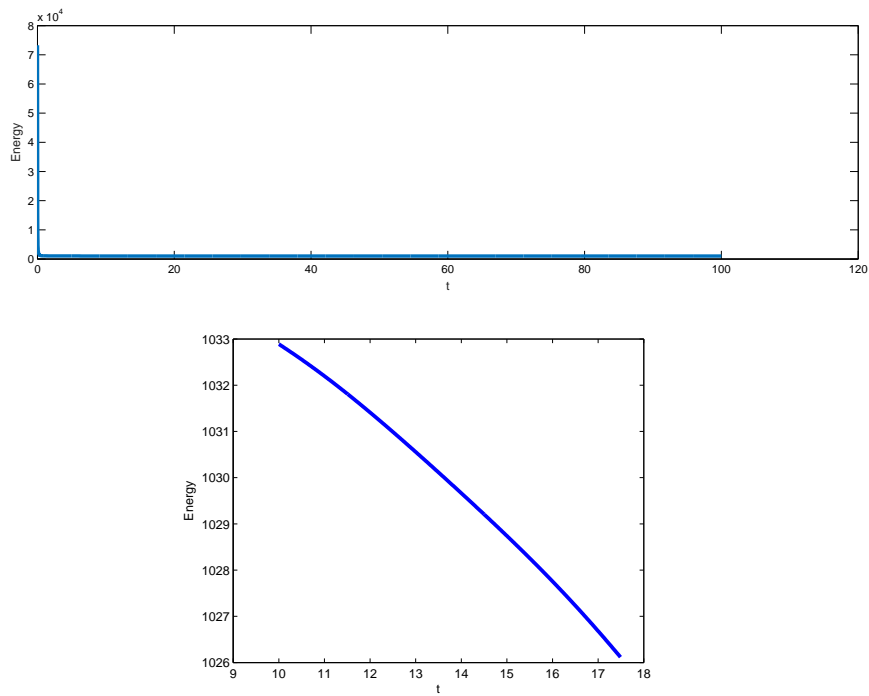
Energy decay

In Fig. (2.13) we plot the modified free energy for the non-local model simulation. The energy decays fast in the beginning of the simulation and goes down smoothly in the later time evolution. The top figure in Fig. (2.13) is the energy for $t \leq 100$ and the bottom figure is a magnified plot in time region $10 \leq t \leq 17$. The energy decay results are pretty similar in other models, thus we only show the energy of this model.

Interface problems

We start presenting our simulation results on interface problems.

Crystals We first place two small fraction of cylindrical crystals each rotated with $\pi/6$ and $-\pi/6$ degree in the center of the domain. The bulk will grow to reach the minima of the free energy. The transition process is shown in Fig. (2.14).



(b) Any time segment with magnifying plot

Figure 2.13.: Energy dissipation plots of non-local model

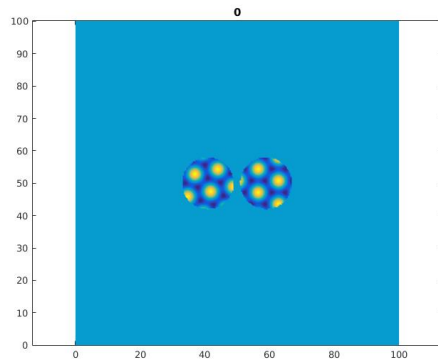
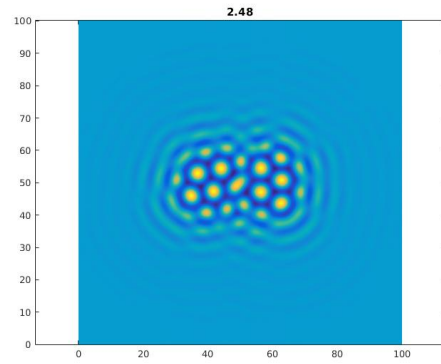
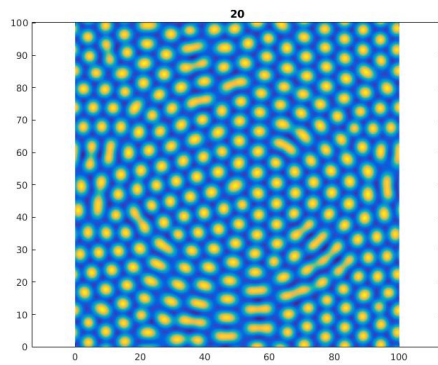
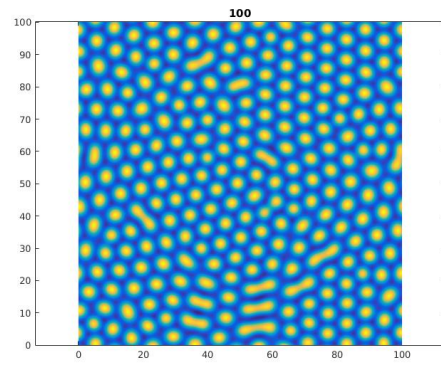
(a) $t = 0$ (b) $t = 2.5$ (c) $t = 20$ (d) $t = 100$

Figure 2.14.: Interface problem for 6-fold symmetry crystal

Quasicrystals We then place two quasicrystal phases in the domain and each are rotated by $\theta = \pm\pi/10$ respectively. In our final result, c is taken as 1 and we noticed that when $c = 150$ the interfacial layer will be transient. The transition process is given in Fig.(2.15). The final stable state is in 12-fold stability.

Similarly we show the result of two 10-fold symmetry quasicrystals. The result is shown in Fig.(2.16).

Under LP model, we could also place two cylindrical crystals in the domain. Under such case, the phase will reach local minima when $|k| = q$ or $|k| = 1$. We thus place on the left a cylindrical crystal with $|k| = q$ and on the right a cylindrical crystal with $|k| = 1$. The transition process is shown in Fig. (2.17). It is interesting to point out that during the transition period, a transient 12-fold quasicrystal phase appears. The six-fold cylindrical phase diffuses to the left and will become the final state in the whole domain.

Multi-phase model We then put two 12-fold (10-fold) symmetry quasicrystals formed by multi-phase model each rotated with angle θ . The result is shown in Fig.(2.18) (and 10-fold result in Fig.(2.19)).

Non-local model Similarly, we could see the pattern of the interfacial problem using nonlocal free energy. The result of 12-fold and 10-fold results are given in Fig.(2.20) and Fig.(2.21) respectively.

2.4 Conclusion

We propose a numerical method for computing the interface between two ordered phases that involves quasiperiodicity. With the properly chosen function space and boundary conditions to fix the relative orientation and displacement, we solve the H^{-1} gradient flow of the Lifschitz–Petrich free energy, to let the interface evolve to its optimal structure. The gradient flow is discretized in time by the SAV approach, and in space by spectral method with a combination of quasiperiodic Fourier series

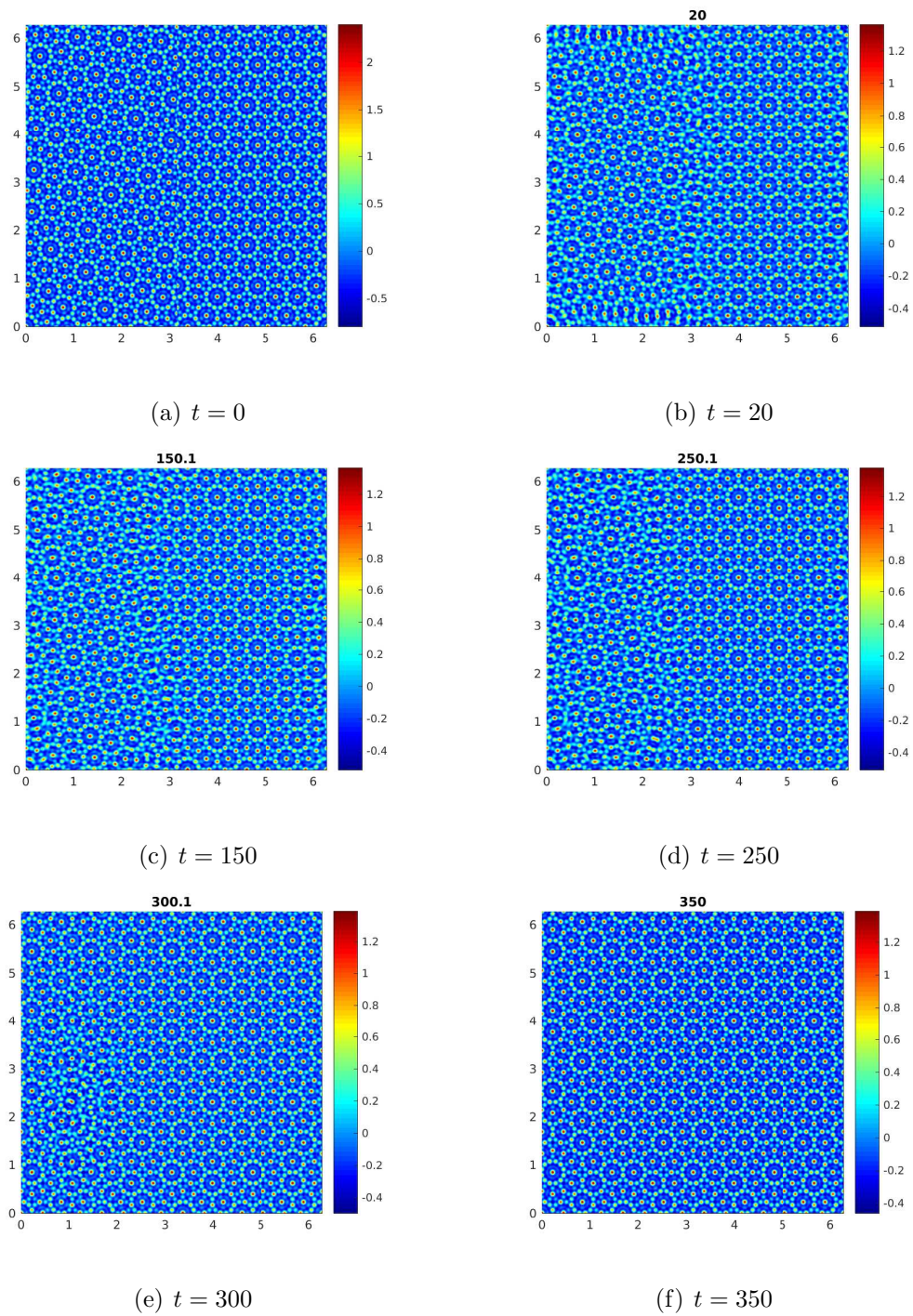


Figure 2.15.: Interface problem for 12-fold symmetry

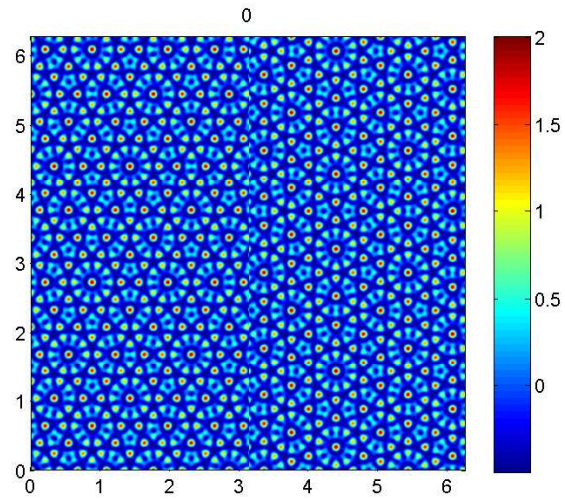
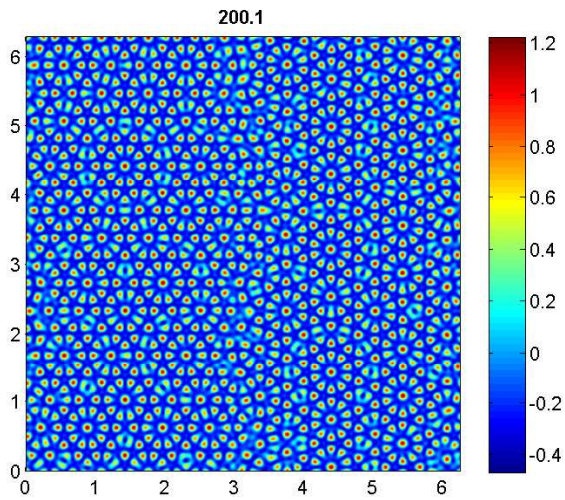
(a) $t = 0$ (b) $t = 200$

Figure 2.16.: Interface problem for 10-fold symmetry

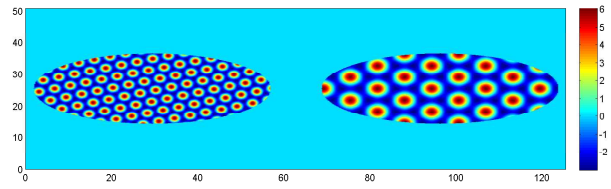
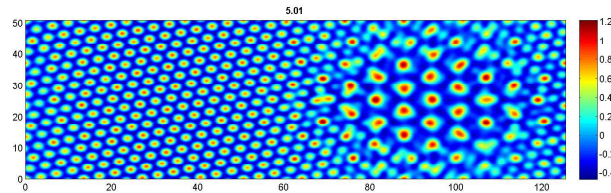
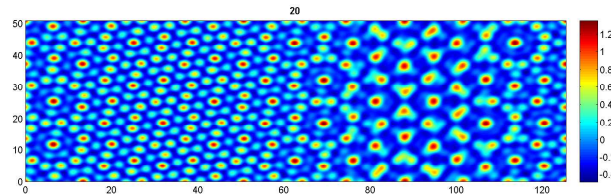
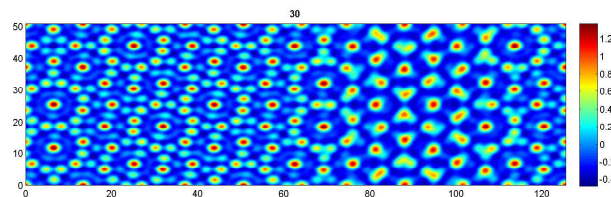
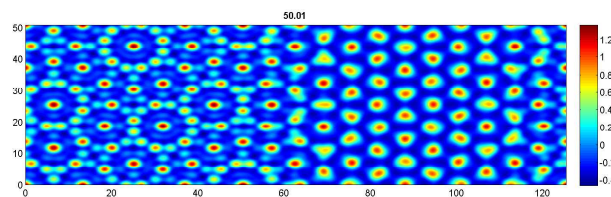
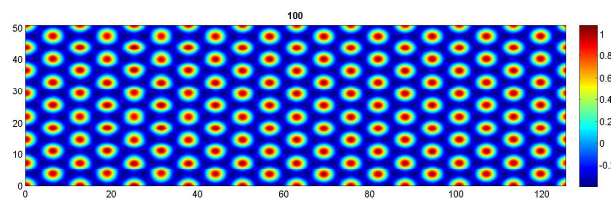
(a) $t = 0$ (b) $t = 5$ (c) $t = 20$ (d) $t = 30$ (e) $t = 50$ (f) $t = 100$

Figure 2.17.: Interface problem for 6-fold symmetry with big-small crystals

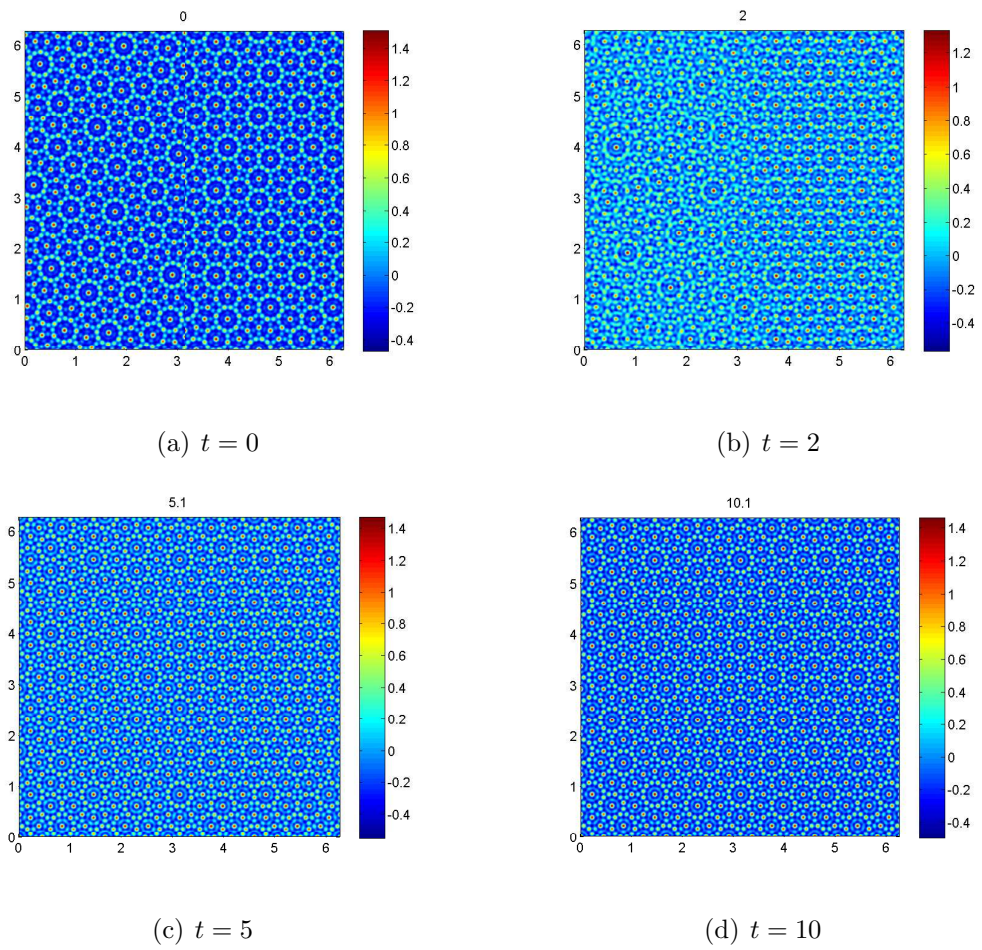


Figure 2.18.: Interface problem for 12-fold symmetry under Multi-phase model

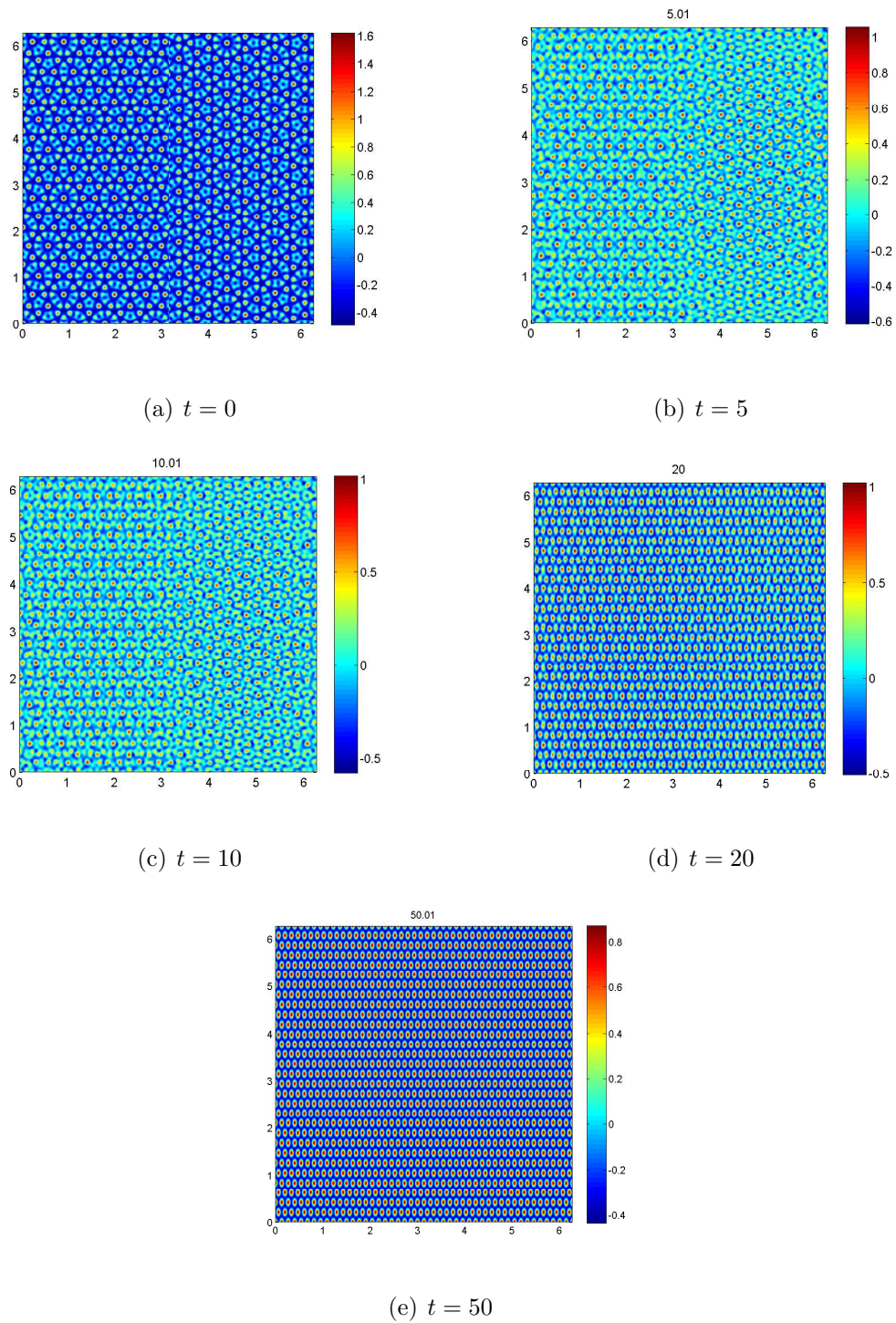


Figure 2.19.: Interface problem for 10-fold symmetry under Multi-phase model

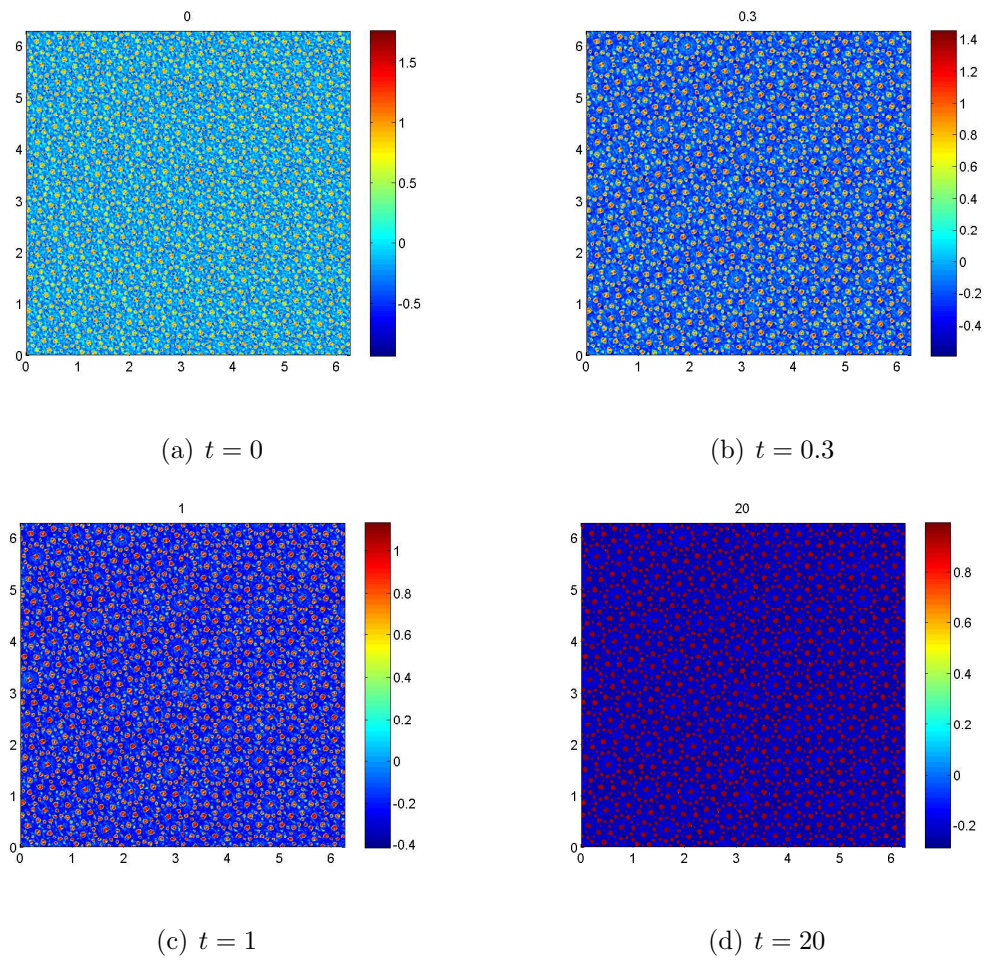


Figure 2.20.: Interface problem for 12-fold symmetry in non-local model

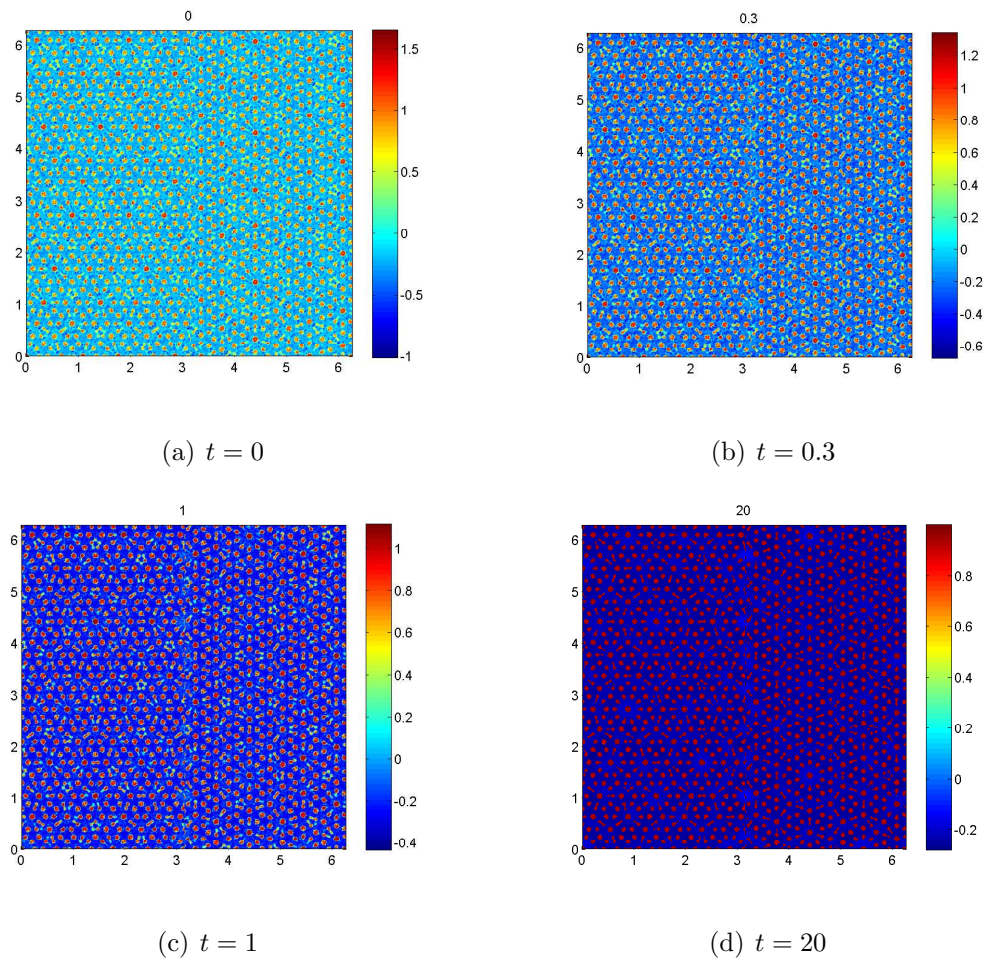


Figure 2.21.: Interface problem for 10-fold symmetry in non-local model

and generalized Jacobi polynomials. We present some typical examples, including the interface of the striped, hexagonal and dodecagonal phases. In particular, we show that our numerical method can successfully capture the interfacial structure in the cases where the interface is quasiperiodic. The method proposed in this work shall be fundamental for systematic simulations of the interface between ordered structures. In the future work, we aim to utilize the method to investigate interface involving other phases, especially the three-dimensional phases, including the bcc/fcc spherical and gyroid that are periodic, and icosahedral quasicrystals.

REFERENCES

- [1] Alfonso Bueno-Orovio, David Kay, and Kevin Burrage. Fourier spectral methods for fractional-in-space reaction-diffusion equations. *BIT*, 54(4):937–954, 2014.
- [2] Shuying Zhai, Dongwei Gui, Jianping Zhao, and Xinlong Feng. High accuracy spectral method for the space-fractional diffusion equations. *J. Math. Study*, 47(3):274–286, 2014.
- [3] Mark Ainsworth and Zhiping Mao. Analysis and approximation of a fractional Cahn–Hilliard equation. *SIAM J. Numer. Anal.*, 55(4):1689–1718, 2017.
- [4] Milos Ilic, Fawang Liu, Ian Turner, and Vo Anh. Numerical approximation of a fractional-in-space diffusion equation, I. *Fract. Calc. Appl. Anal.*, 8(3):323–341, 2005.
- [5] Fangying Song, Chuanju Xu, and George Em Karniadakis. Computing fractional Laplacians on complex-geometry domains: algorithms and simulations. *SIAM J. Sci. Comput.*, 39(4):A1320–A1344, 2017.
- [6] L. Caffarelli and L. Silvestre. An extension problem related to the fractional Laplacian. *Comm. Partial Differential Equations*, 32(8):1245–1260, 2007.
- [7] P.R. Stinga and J.L. Torrea. Extension problem and Harnack’s inequality for some fractional operators. *Comm. Partial Differential Equations*, 35(11):2092–2122, 2010.
- [8] Ricardo H Nochetto, Enrique Otárola, and Abner J Salgado. A PDE approach to fractional diffusion in general domains: a priori error analysis. *Found. Comput. Math.*, 15(3):733–791, 2015.
- [9] Ricardo H Nochetto, Enrique Otarola, and Abner J Salgado. A PDE approach to space-time fractional parabolic problems. *SIAM J. Numer. Anal.*, 54(2):848–873, 2016.
- [10] Lehel Banjai, Jens M Melenk, Ricardo H Nochetto, Enrique Otarola, Abner J Salgado, and Christoph Schwab. Tensor FEM for spectral fractional diffusion. *Found. Comput. Math.*, 19(4):901–962, 2019.
- [11] Sheng Chen and Jie Shen. An efficient and accurate numerical method for the spectral fractional laplacian equation. *Submitted to J. Comput. Phys.*
- [12] Mark Ainsworth and Christian Glusa. Hybrid finite element–spectral method for the fractional Laplacian: approximation theory and efficient solver. *SIAM J. Sci. Comput.*, 40(4):A2383–A2405, 2018.
- [13] Andrea Bonito and Joseph E Pasciak. Numerical approximation of fractional powers of regularly accretive operators. *IMA J. Numer. Anal.*, 37(3):1245–1273, 2016.

- [14] A. Bonito, J. P. Borthagaray, R. H. Nochetto, E. Otárola, and A. J. Salgado. Numerical methods for fractional diffusion. *Comput. Vis. Sci.*, 19:1–28, 2018.
- [15] Anna Lischke, Guofei Pang, Mamikon Gulian, Fangying Song, Christian Glusa, Xiaoning Zheng, Zhiping Mao, Wei Cai, Mark M Meerschaert, Mark Ainsworth, et al. What is the fractional Laplacian? *arXiv preprint arXiv:1801.09767*, 2018.
- [16] Jie Shen. Efficient spectral-galerkin method i. direct solvers of second-and fourth-order equations using legendre polynomials. *SIAM Journal on Scientific Computing*, 15(6):1489–1505, 1994.
- [17] Yiqi Gu. Spectral methods for boundary value problems in complex domains. *Ph.D thesis, Purdue University, 2019*.
- [18] Jie Shen and Lilian Wang. Fourierization of the Legendre–Galerkin method and a new space–time spectral method. *Appl. Numer. Math.*, 57(5-7):710–720, 2007.
- [19] Jie Shen. Efficient Chebyshev-Legendre Galerkin methods for elliptic problems. In *Proceedings of ICOSAHOM*, volume 95, pages 233–240, 1996.
- [20] Jie Shen. A new dual-Petrov-Galerkin method for third and higher odd-order differential equations: application to the KDV equation. *SIAM J. Numer. Anal.*, 41(5):1595–1619, 2003.
- [21] Tosio Kato. Fractional powers of dissipative operators. *J. Math. Soc. Japan*, 13(3):246–274, 1961.
- [22] Weinan E. Convergence of spectral methods for Burgers equation. *SIAM J. Numer. Anal.*, pages 1520–1541, 1992.
- [23] Jacques Louis Lions and Enrico Magenes. *Non-homogeneous boundary value problems and applications*, volume 1. Springer Science & Business Media, 2012.
- [24] Ham Brezis. *Analyse Fonctionnelle. Théorie et Applications. (French)[Functional Analysis. Theory and Applications]*, *Collection Mathématiques Appliquées pour la Maîtrise*. Masson, Paris, 1983.
- [25] Jie Shen, Tao Tang, and Lilian Wang. *Spectral methods: algorithms, analysis and applications*, volume 41. Springer Science & Business Media, 2011.
- [26] Gilbert Strang. Variational crimes in the finite element method. *The mathematical foundations of the finite element method with applications to partial differential equations*, pages 689–710, 1972.
- [27] Benyu Guo, Jie Shen, and Lilian Wang. Optimal spectral-Galerkin methods using generalized Jacobi polynomials. *J. Sci. Comput.*, 27(1-3):305–322, 2006.
- [28] Dana A Knoll and David E Keyes. Jacobian-free Newton–Krylov methods: a survey of approaches and applications. *J. Comput. Phys.*, 193(2):357–397, 2004.
- [29] Kevin Burrage, Nicholas Hale, and David Kay. An efficient implicit FEM scheme for fractional-in-space reaction-diffusion equations. *SIAM J. Sci. Comput.*, 34(4):A2145–A2172, 2012.

- [30] Fangying Song, Chuanju Xu, and George Em Karniadakis. A fractional phase-field model for two-phase flows with tunable sharpness: algorithms and simulations. *Comput. Methods Appl. Mech. Engrg.*, 305:376–404, 2016.
- [31] Long Qing Chen and Jie Shen. Applications of semi-implicit Fourier-spectral method to phase field equations. *Comput. Phys. Commun.*, 108(2-3):147–158, 1998.
- [32] Dongbin Xiu. *Numerical Methods for Stochastic Computations: A Spectral Method Approach*. Princeton University Press, Princeton, NJ, USA, 2010.
- [33] Michael Seul and David Andelman. Domain shapes and patterns: The phenomenology of modulated phases. *Science*, 267(5197):476–483, 1995.
- [34] G. H. Fredrickson. *The equilibrium theory of inhomogeneous polymers*. Clarendon Press, Oxford, 2006.
- [35] P G De Gennes and J Prost. *The physics of liquid crystals*. Oxford science publications. Clarendon Press ; Oxford University Press, Oxford : New York, 2nd edition, 1993.
- [36] D. Shechtman, I. Blech, D. Gratias, and J. W. Cahn. Metallic phase with long-range orientational order and no translational symmetry. *Phys. Rev. Lett.*, 53:1951–1953, Nov 1984.
- [37] Jules Mikhael, Johannes Roth, Laurent Helden, and Clemens Bechinger. Archimedean-like tiling on decagonal quasicrystalline surfaces. *Nature*, 454(7203):501–504, 2008.
- [38] Xiangbing Zeng, Goran Ungar, Yongsong Liu, Virgil Percec, Andres E Dulcey, and Jamie K Hobbs. Supramolecular dendritic liquid quasicrystals. *Nature*, 428(6979):157–160, 2004.
- [39] Kenichi Hayashida, Tomonari Dotera, Atsushi Takano, and Yushu Matsushita. Polymeric quasicrystal: mesoscopic quasicrystalline tiling in abc star polymers. *Physical Review Letters*, 98(19):195502, 2007.
- [40] N D Mermin and Sandra M Troian. Mean-field theory of quasicrystalline order. *Physical Review Letters*, 54(14):1524–1527, 1985.
- [41] T. Dotera. Mean-field theory of archimedean and quasicrystalline tilings. *Philosophical Magazine*, 87(18-21):3011–3019, 2007.
- [42] Andrew J Archer, A M Rucklidge, and Edgar Knobloch. Quasicrystalline order and a crystal-liquid state in a soft-core fluid. *Physical Review Letters*, 111(16):165501, 2013.
- [43] Kobi Barkan, Michael Engel, and Ron Lifshitz. Controlled self-assembly of periodic and aperiodic cluster crystals. *Physical Review Letters*, 113(9):098304, 2014.
- [44] Kai Jiang, Jiajun Tong, Pingwen Zhang, and Anchang Shi. Stability of two-dimensional soft quasicrystals in systems with two length scales. *Physical Review E*, 92(4):042159–042159, 2015.

- [45] Kai Jiang, Pingwen Zhang, and Anchang Shi. Stability of icosahedral quasicrystals in a simple model with two-length scales. *Journal of Physics: Condensed Matter*, 29(12):124003, 2017.
- [46] K R Elder and Martin Grant. Modeling elastic and plastic deformation in nonequilibrium processing using phase field crystals. *Physical Review E*, 70(5):051605, 2004.
- [47] Aldo D Pezzutti, Daniel A Vega, and Marcelo A Villar. Dynamics of dislocations in a two-dimensional block copolymer system with hexagonal symmetry. *Philosophical Transactions of the Royal Society A*, 369(1935):335–350, 2011.
- [48] And Andriy V Kyrylyuk and Johannes G E M Fraaije. Three-dimensional structure and motion of twist grain boundaries in block copolymer melts. *Macromolecules*, 38(20):8546–8553, 2005.
- [49] Jie Xu, Chu Wang, An-Chang Shi, and Pingwen Zhang. Computing optimal interfacial structure of modulated phases. *Communications in Computational Physics*, 21(1):1C15, 2017.
- [50] Ron Lifshitz and Dean M. Petrich. Theoretical model for faraday waves with multiple-frequency forcing. *Phys. Rev. Lett.*, 79:1261–1264, Aug 1997.
- [51] Kai Jiang and Pingwen Zhang. Numerical methods for quasicrystals. *Journal of Computational Physics*, 256:428 – 440, 2014.
- [52] Liangping Qiao, Li Wu, and Tianyou Fan. Dynamic response of an icosahedral quasi-crystalline medium with a griffith crack under mechanical loadings. *Advances in Mechanical Engineering*, 9(2):1687814016688850, 2017.
- [53] Fang Wang, Hui Cheng, Tian-You Fan, and Hai-Yun Hu. A stress analysis of some fundamental specimens of soft-matter quasicrystals with eightfold symmetry based on generalized dynamics. *Advances in Materials Science and Engineering*, 2019, 2019.
- [54] LZ Yang, FM He, and Y Gao. Finite element method for static problems of cubic quasicrystals. *Acta Physica Polonica A*, 126(2):471–473, 2014.
- [55] AN Dongmei. WU Xiangfa, FAN Tianyou. Energy release rate of plane quasicrystals with crack determined by path-independent e-integral. *Chinese Journal of Computational Mechanics*, 17(1):34–42, 1 2000.
- [56] Weizhang. Huang and David M. Sloan. The pseudospectral method for third-order differential equations. *SIAM Journal on Numerical Analysis*, 29(6):1626–1647, 1992.
- [57] Jie. Shen. A new dual-petrov-galerkin method for third and higher odd-order differential equations: Application to the kdv equation. *SIAM Journal on Numerical Analysis*, 41(5):1595–1619, 2003.
- [58] Jie Shen. Efficient spectral-galerkin method i. direct solvers of second and fourth-order equations using legendre polynomials. *Siam Journal on Scientific Computing*, 15, 11 1994.

- [59] Lizhen Chen. Direct solver for the cahn-hilliard equation by legendre-galerkin spectral method. *Journal of Computational and Applied Mathematics*, 358:34–45, 2019.
- [60] Jie Shen, Jie Xu, and Jiang Yang. The scalar auxiliary variable (sav) approach for gradient flows. *Journal of Computational Physics*, 353:407–416, 2018.
- [61] Jie Shen, Jie Xu, and Jiang Yang. A new class of efficient and robust energy stable schemes for gradient flows. *SIAM Review*, 61(3):474–506, 2019.
- [62] Jie Shen and Jie Xu. Convergence and error analysis for the scalar auxiliary variable (sav) schemes to gradient flows. *SIAM Journal on Numerical Analysis*, 56(5):2895–2912, 2018.
- [63] S. A. Brazovskii. Phase transition of an isotropic system to a nonuniform state. *Sov. Phys.-JETP*, 41(1):85–89, 1975.
- [64] J. Swift and P. C. Hohenberg. Hydrodynamic fluctuations at the convective instability. *Phys. Rev. A*, 15:319–328, Jan 1977.
- [65] Glenn H Fredrickson and Eugene Helfand. Fluctuation effects in the theory of microphase separation in block copolymers. *Journal of Chemical Physics*, 87(1):697–705, 1987.
- [66] E I Kats, V V Lebedev, and A R Muratov. Weak crystallization theory. *Physics Reports*, 228:1–91, 1993.
- [67] N. D. Mermin and Sandra M. Troian. Mean-field theory of quasicrystalline order. *Phys. Rev. Lett.*, 54:1524–1527, Apr 1985.
- [68] T. Dotera. Mean-field theory of archimedean and quasicrystalline tilings. *Philosophical Magazine*, 87(18-21):3011–3019, 2007.
- [69] Zhonghua. Qiao, Zhengru. Zhang, and Tao. Tang. An adaptive time-stepping strategy for the molecular beam epitaxy models. *SIAM Journal on Scientific Computing*, 33(3):1395–1414, 2011.
- [70] R Li, WB Liu, and HP Ma. Moving mesh method with error-estimator-based monitor and its applications to static obstacle problem. *Journal of Scientific Computing*, 21(1):31–55, 2004.
- [71] Ben-Yu Guo, Jie Shen, and Li-Lian Wang. Optimal spectral-galerkin methods using generalized jacobi polynomials. *Journal of Scientific Computing*, 27(1):305–322, Jun 2006.
- [72] G. Szegő. *Orthogonal Polynomials*. Number v. 23 in American Mathematical Society colloquium publications. American Mathematical Society, 1959.
- [73] Roland R Netz, David Andelman, and M Schick. Interfaces of modulated phases. *Physical Review Letters*, 79(6):1058–1061, 1997.
- [74] M W Matsen. Kink grain boundaries in a block copolymer lamellar phase. *Journal of Chemical Physics*, 107(19):8110–8119, 1997.

- [75] Yoav Tsori, David Andelman, and M Schick. Defects in lamellar diblock copolymers: Chevron- and ω -shaped tilt boundaries. *Physical Review E*, 61(3):2848–2858, 2000.
- [76] Kai Jiang, Jiajun Tong, and Pingwen Zhang. Stability of soft quasicrystals in a coupled-mode swift-hohenberg model for three-component systems. *Communications in Computational Physics*, 19(3):559C581, Mar 2016.